The Nature of Interactions in Alkylimidazolium Based Ionic Liquids

A Dissertation presented to the
University of Cape Town

in fulfillment of the requirements for the degree of
Master of Science
By

Monde Sinxi
BSc(Hons. University of Cape Town)
Supervisor: Dr. Gerhard A. Venter

Department of Chemistry
University of Cape Town
South Africa
February 2015

The Nature of Interactions in Alkylimidazolium Based Ionic Liquids

Monde Sinxi **February 2015**

Abstract

Ionic liquids are materials that have the ability to be designed for specific tasks. Their properties can be adjusted by changing the molecular constituents of the liquid or the intermolecular interactions between composite ions through functionalisation. Therefore, understanding the nature of the interactions between ions is important. In the thesis, we use density functional theory calculations to obtain conformers of 1-ethyl-3-methylimidazolium ($[emim]^+$)paired with the anions $[Cl]^-$, $[Br]^-$, $[MeCO_2]^-$, $[CF_3CO_2]^-$, $[MeSO_3]^-$, $[CF_3SO_3]^-$, $[BF_4]^-$ and $[PF_6]^-$. We analyse the structures of the pairs and then explore the nature of the electrostatic, dispersion and hydrogen bonding interactions. Electrostatic interactions were the most dominant interactions. The dispersion interaction energies were found to be of the same order as the estimated energy of the hydrogen bond. The non-covalent index (NCI) analysis was used to visualise the non-covalent interactions in real space as enclosed surfaces. The properties of the surfaces were used to characterise interaction types, namely van der Waals interactions and hydrogen bonds. Furthermore, we find that the density enclosed within the hydrogen bonding surfaces can be used to estimate the potential of the hydrogen bond. To our knowledge, a potential for hydrogen bonding from NCI has not been explored for ionic liquids. Finally, the average strength of the hydrogen bond was calculated from structures extracted from molecular dynamics simulations. They reveal that the hydrogen bond strength for $[emim][MeCO_2]$ is approximately two-thirds weaker in the condensed phase than in the gas phase. The effect of the polarising environment is also found to weaken the hydrogen bond slightly.

Acknowledgments

I would like to thank:

- my supervisor Dr. Gerhard Venter for the invaluable support, mentorship and discussions over the period that this work was done.
- Prof. Kevin Naidoo, the director of the research unit.
- Prof. Dr. Barbara Kirchner for accommodating me in her research group in Bonn, Germany.
- Dr. Chris Barnett, Ian Rogers, Alicia Renison and Dr. Krishna Govender for maintaing the computational facilities.
- Kyle Fernandes for the invaluable opinions and technical support with regards to MATLAB.
- Louise Bezuidenhout for her support, warmth and encouragement.
- All group members of the scientific research unit.
- The National Research Foundation and the German Academic Exchange Programme for funding.
- The Centre for High Performance Computing (CHPC) for use of their resources.

I'd like to thank my family for all the love, support and encouragement throughout my years away from home. I extend a special thank you to Ma (my mother), for your kindness, caring and understanding. My brother, Siphosethu, for all the laughter and joy when needed most and my Dad, for all the advice and words of wisdom.

Matete, no words could describe how thankful I am that you've seen me through this difficult period. I could not have done this without you. I love you very much.

Contents

1. Introduction . . . 3

1.1 Ionic Liquids . . . 3

1.1.1 Defining Ionic Liquids . . . 3

1.1.2 Common Properties and Aplications of Ionic Liquids . . . 3

1.1.3 Origin of Physiochemical Properties of Ionic Liquids . . . 5

1.2 Theoretical Studies of Ionic Liquids . . . 7

1.2.1 Ab initio Methods . . . 8

1.2.2 Molecular Dynamics Methods . . . 9

1.2.3 *Ab initio* Molecular Dynamics Methods . . . 11

1.3 The Nature of Interactions in Ionic Liquids . . . 11

1.3.1 Electrostatic Interactions . . . 12

1.3.2 Dispersion Interactions . . . 12

1.3.3 Hydrogen Bonding . . . 14

1.3.4 Effect of Polarisation . . . 15

1.4 Objectives . . . 15

2. Theory . . . 23

2.1 The Basic Principles of the ab initio method . . . 23

2.1.1 The Born-Oppenheimer Approximation . . . 25

2.1.2 The Antisymmetry and Pauli Exclusion Principle . . . 26

2.1.3 Slater Determinants . . . 26

2.1.4 The Energy of a Slater Determinant . . . 27

2.1.5 Derivation of the Hartree-Fock Equations . . . 29

2.1.6 The Roothaan-Hall equations . . . 31

2.1.7 The Basis Set . . . 34

2.2 Density Functional Theory . . . 36

2.2.1 The Hohenberg-Kohn Theorems . . . 36

2.2.2 Kohn-Sham approach 37
2.2.3 Exchange-Correlation Functional 40
2.3 Molecular Mechanics 41
2.3.1 Force Field 41
2.3.2 Molecular Dynamics Simulations 44
2.4 The Quantum Theory of Atoms in Molecules (QTAIM) 50
2.4.1 Properties at the BCP 52
2.5 Non-Covalent Index 53
2.5.1 Using the Reduced Density Gradient in Identifying Interactions 54
2.5.2 Calculating the Reduced Density Gradient 54

3. Analysis of the Gas Phase Ion-Pair 61
3.1 Computational Details 61
3.2 Geometric and Interaction Energy Analysis of Ion-Pairs 63
3.3 Electrostatic Interactions 69
3.3.1 Charge Transfer and Atomic Partial Charges 69
3.3.2 Charge Distribution 73
3.3.3 Calculating the Electrostatic Interaction Energies 78
3.4 Role of Dispersion in the Total Interaction 84
3.5 Hydrogen Bonding 92
3.5.1 NBO Analysis to Describe Hydrogen Bonding 93
3.5.2 Quantum Theory of Atoms in Molecules: Properties at the Bond Critical Points 95
3.6 Non-covalent Index (NCI) analysis 98
3.6.1 The 2D Reduced Density Gradient (RDG) Plots 99
3.6.2 Properties of NCI surfaces 105
3.6.3 Estimated Potential of the Hydrogen Bond 107
3.7 Conclusion 112

4. Analysis From the Condensed Phase 121
4.1 Molecular Dynamics Simulations 121

4.2 Extraction of the Ion-Pair 122
4.3 Average Reduced Density Gradient 124
4.3.1 Strength of the Hydrogen Bond in Bulk [emim][$MeCO_2$] . . . 128
4.3.2 Effect of Polarisation on the Cation 129
4.4 Analysis of a Single Frame 131
4.5 Conclusion 135

5. Closing Remarks 139

1

Introduction

1.1 Ionic Liquids

1.1.1 Defining Ionic Liquids

Ionic liquids (ILs) are composed exclusively or almost exclusively of ions. These include classic molten salts that have high melting temperatures. In recent past (the last two decades or so) the term ionic liquids has been limited to liquids with a melting point or glass-transition temperature below 100°C, which typically contain organic cations and inorganic anions.[1] ILs with melting points around 25°C are termed room-temperature ionic liquids (RTILs).[2] A few common ions are shown in figure 1.1.

1.1.2 Common Properties and Aplications of Ionic Liquids

With over 1500 ionic liquids reported and over one million ionic liquids theoretically possible from mixtures, the scope in applications for ILs range far and wide. Their physical properties can be tuned or tailored by changing the anion or cation, including a specific functionality such as hydrogen bonding or mixing two or more ILs together.[2–8] The large range in properties means that they can be used in many applications, which include being used as reaction media or catalysts for a wide variety of reactions, where some examples are covered in reviews by Welton[9] and Sheldon.[10] ILs can also be used for separation and extraction from aqueous or molecular organic salts.[11,12]

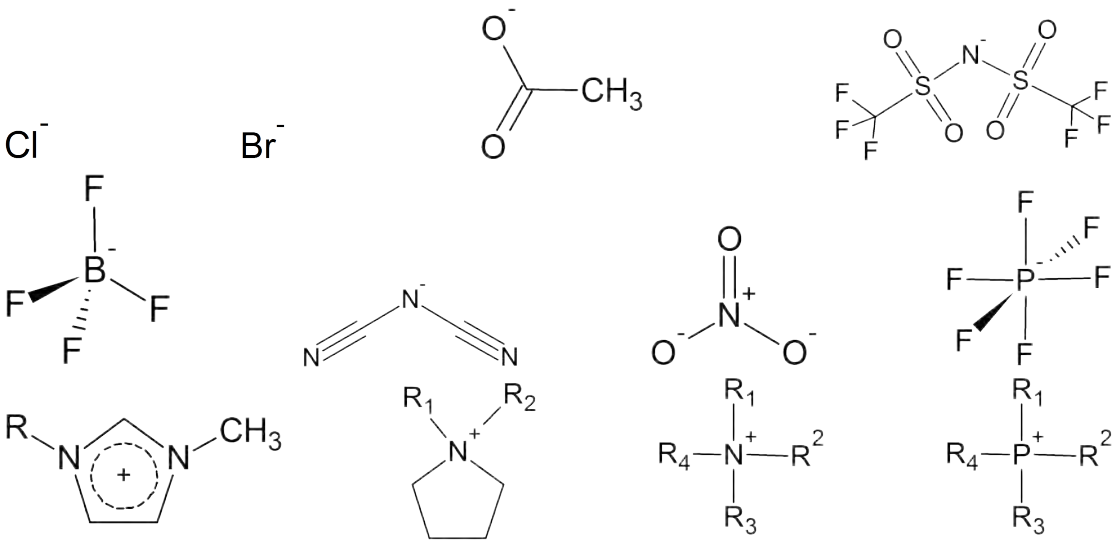

Fig. 1.1: Common ionic liquid ions

Even with so many ILs having been synthesised and yet to be synthesised, a common set of properties are observed that differentiate them from molecular solvents. ILs have a negligible vapour pressure because of the strong electrostatic association between ions, and generally show little or no evidence of distillation.[13] This non-volatility allows them to be used in the extraction of poorly volatile or thermally labile compounds.[14] Strong interactions between ions cause the bulk fluid to be viscous, often 2 to 3 orders of magnitude greater than organic solvents.[15]

An important property of ILs is their liquid range with respect to temperature, which is generally wide. For example, 1-alkyl-3-methylimidazolium salts typically have glass transition temperatures in the range -70 to −90°C and thermal decomposition temperatures ranging from 250 to 450°C with liquid ranges of over 300°C, three times that of water.[13,16] Increasing the liquid range of the liquid focuses on decreasing the melting point, which is influenced by the size and symmetry of the ions.[17] Larger ions cause a lowering in the melting point and higher symmetry in ions cause the melting point to rise. A possibility of ILs to be used for room temperature to high temperature experiments without solvent degradation is attractive. Being solely ions, ILs are conductive and have high electrical stability, which makes them good candidates for use as electrolytes in high energy capacitors.[18]

1.1.3 Origin of Physiochemical Properties of Ionic Liquids

The origin of the physiochemical properties of ionic liquids is driven by the interactions of their molecular components, the size of the ions, symmetry and the presence of hydrogen bonding. ILs are thus considered designer liquids because all of these factors can be changed by rational design. Understanding the nature of interactions is part of the process of property design of ionic liquids. To illustrate the relationship between the molecular structure and interactions in ILs and the properties of the bulk, a brief overview of some properties and their molecular origins is done.

Viscosity

The viscosity of a liquid is its resistance to flow. It is one of the most important properties for the design of industrial processes involving heat, mass or momentum transfer.[19,20] For example, the chemical structure of the cation plays an important role in determining such a property as they introduce certain types of interactions that lead to changes in the viscosity. For example, in a series of 1-alkyl-3-methylimidazolium cations increasing the alkyl chain length from butyl to hexyl to octyl increases the hydrophobicity and the viscosities of ILs, whereas densities and surface tension values decrease.[21] The decrease in the density and surface tensions result from the decrease in charge concentration.

The relationship between the dispersion interactions and the viscosity have been investigated. An increase in the viscosity can be attributed to an increase in the dispersion interactions. Izgorodina et al. have shown that the percentage contribution that the dispersion contributes to the total interaction may determine transport properties of imidazolium based ionic liquids.[22]

Melting Point

Size, symmetry and ionic character of the components of the IL determine the melting point. These properties directly influence the crystal lattice energy, which in turn influences the melting temperature. Lattice energies in ionic solids depend on the product of the net ion charges, the ion-ion separation and the packing efficiency of the ions, thus the introduction of larger ions that delocalise charge and increase charge-charge separation decreases the melting point. Increasing the symmetry of the cation enables for more efficient packing in the crystal cell, which increases the melting point.[13,23]

Solubility and Miscibility

ILs can be used as solvents in liquid-liquid extractions or product separation as the relative solubility of the ILs and the extraction phase can be tuned. A negligible vapour pressure, a density generally higher than water and the tunability of solubility makes ionic liquids more preferable in liquid-liquid extractions. Strong electrostatic interactions between cations and anions, polarisation and the presence of hydrogen bonding influence coordination and solvation properties, thus understanding the structure of ionic liquids in the presence of the solvent or solute is a key feature in predicting selectivity and reactivity of systems involving these compounds.[24]

Using 1-butyl-3-methylimidazolium based ILs as an example in combination with the anions $[Cl]^-$, $[Br]^-$, $[CF_3SO_3]^-$ or $[BF_4]^-$ produce liquids that are miscible with water. However, combinations with $[C(CN)_3]^-$, $[CH_3(OC_2H_4)_2OSO_3]^-$, $[PF_6]^-$ or $[N(SO_2CF_3)_2]^-$ produce ILs that are immiscible with water resulting in mixtures that are phase separated at room temperature. Increasing the alkyl chain length from four to eight carbon atoms on the cation makes the combination with $[BF_4]^-$ immiscible with water.[25]

Intermolecular forces, changes in chemical structure and choice of ions are important in driving properties of ILs, they must be well understood in order to design or predict properties of ILs that have yet to be synthesised. The tools required to do so are available both experimentally and theoretically. The theoretical investigation of properties of ILs will be discussed next.

1.2 Theoretical Studies of Ionic Liquids

Computational methods play a significant role in advancing the knowledge and understanding of molecular interactions in ILs. The three main areas in computational methods used to describe molecular properties and intermolecular interactions are *ab initio* or first-principles methods, classical force fields used in molecular dynamics (MD) simulations and *ab initio* molecular dynamics (AIMD) simulations. They are used to study ILs at different scales, i.e. from the ion-pair to clusters to large simulation boxes, that approximate the behaviour of the bulk. Static electronic structure methods such as Hartree-Fock, second order Møller-Plesset (MP2) or density functional theory (DFT) have generally been used to study ILs at the smaller scales as they are computationally expensive and can thus only be used on a limited scale. *Ab initio* methods are the most accurate and are used to study effects such as polarisation, charge transfer and interaction strength between the ionic components.

Classical MD simulations are used to model a large number of interacting ions that make up the liquid, they provide a basic understanding of the dynamic processes up to the nano scale because they are much cheaper than the electronic methods. The difficulty when simulating ILs using MD is obtaining a force field and parametrising it such that it reproduces both static and dynamic experimental data.[26] As a first-principles method, AIMD simulations do not suffer from the challenges of parametrising. It allows for the propagation of nuclei over time whilst obtaining the electronic structure. AIMD is the most computationally expensive of all methods, which enforces a limitation of the system size and the length of the

simulation. A short review of each of the three methods applied to ionic liquids is discussed next.

1.2.1 Ab initio Methods

Ab initio calculations are usually used to characterise the structure of the gas phase ion-pairs using post Hartree-Fock methods or density functional theory. A wealth of knowledge has been produced from these methods, especially for imidazolium based ionic liquids.[27–31]

A common thread among many publications on the electronic structure of the ion-pairs is the investigation of the possible number of stable conformers in the gas phase, a calculation of the interaction energy and the energetic preference of some conformers over others. Part of describing the electronic structure is calculating and visualising molecular orbitals, which shows the energetic preference for electrons to locate in certain regions in space.[32–34] Structures of the ion-pairs are then usually used to infer how the preferences of some conformers manifests in the structure of the liquid and the possible influences on liquid properties.

Moving beyond ion-pairs, cluster calculations of ionic liquids have been studied. These range from systems containing two pairs to ten pairs.[32,35–37] They are used to understand structure, cooperativity effects for hydrogen bonding, electronic effects such as polarisation and the relative changes in the nature of interactions as the size of the system is increases. An example of this is shown in figure 1.2 produced in a publication by Ludwig that describes a method for calculating thermodynamic properties of ionic liquids by using quantum statistical thermodynamics as characterised by *ab initio* techniques.[38]

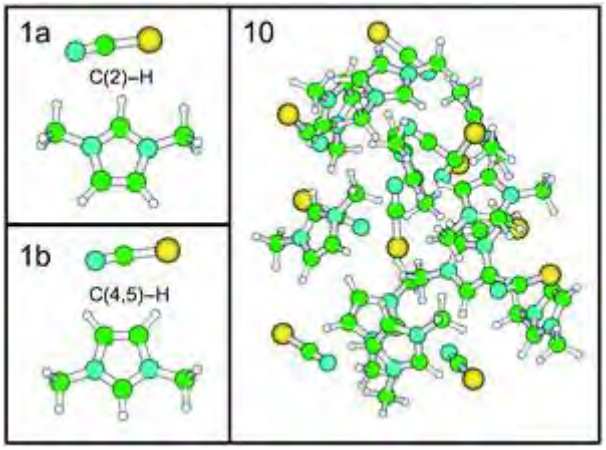

Fig. 1.2: Configurations of monomers (1a) and (1b) denoted as ion-pairs. The 10-mer structure is shown in (10).[38]

1.2.2 Molecular Dynamics Methods

Molecular dynamics simulations have to be used to describe the dynamic and structural properties of ionic liquids in the condensed phase. This has produced a significant amount of publications that have been focused on developing force fields specifically for ionic liquids that are accurate enough to reproduce experimental data.[39–45]

MD studies have found that ILs tend to be highly structured. An example of this order or structure in ILs is shown in figure 1.3, produced by Lopes and Pádua showing a snapshot of a simulation box. It can clearly be seen that there is microphase segregation between polar and non-polar domains in 1-butyl-3-methylimidazolium hexafluorophosphate.[46] Studies of the radial distribution functions of many ILs also show a significant amount of order in the local environment.[42,47–51]

It has become common knowledge that electrostatic interactions dominate all other intermolecular interactions in ionic liquids.[31,52–55] To model structure and dynamics accurately, a proper description of the intermolecular forces is necessary, especially electrostatic interactions. The description of the charge distribution within the molecular ions thus becomes important. The use of point charges on atomic centres is the most common method of describing the distribution, the

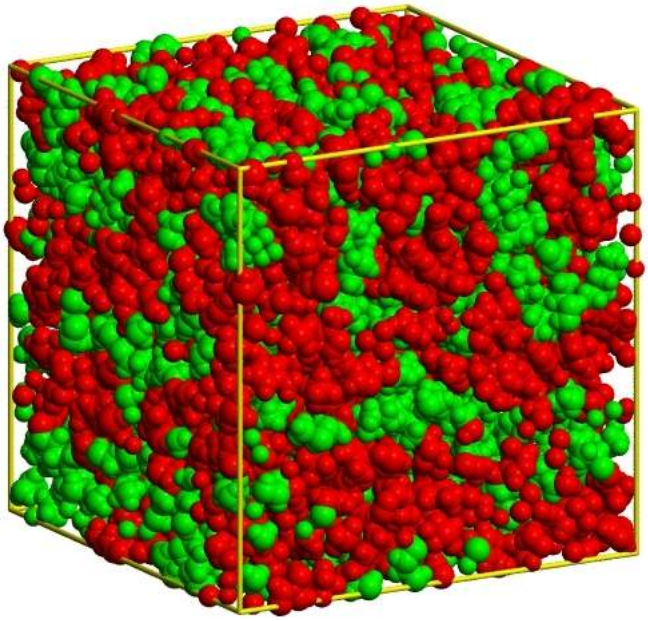

Fig. 1.3: Polar (red) and non-polar (green) domains.[46]

difficulty is in determining charges in the absence of a quantum mechanical charge operator. In practise, partial charges are derived from two major approaches, which are the separation of (i) the one particle density matrix or (ii) electron density.[56] Steinhauser discusses the influence of electrostatic forces on the structure and dynamics of ionic liquids and finds that the charge set has little bearing on the structure of the liquid as was shown by radial distribution functions and orientational correlation functions, but have more of an influence on the dynamics.[57]

With dynamics for simulations generally too slow, charges that improve dynamics become desirable and the development of force fields tend to focus on producing suitable point charges. An example of this is a report by Balasubramanian et al. who introduce a method for parametrising for condensed phase charges derived from the electron density in crystalline ionic liquids.[42] The dynamics of this force field subsequently reproduces experimental measurements for the density, surface tension, enthalpy of vaporisation and ion diffusion coefficients. Acevedo et al. developed a force field for 68 unique ionic liquids and derived charges from the electrostatic potential.[58] Their force field was able to predict heats of vaporisation and they were also able to model the Kemp reaction using mixed quantum and

classical mechanics dynamic simulations to produce the free energy of activation close to the experimental value. One of the most widely used force fields for ionic liquids is the CL&P force field. They fit their point charges from the electron density at an MP2 level of theory using a large basis set.[39–41]

Also important within the description of the intermolecular forces is dispersion. The 12-6 Lennard-Jones potential is widely used and generally believed to model dispersion forces accurately.[59]

1.2.3 *Ab initio* Molecular Dynamics Methods

Ab intio molecular dynamics (AIMD) simulations are computed from first principles. They have the advantage that they do not have to be parametrised and are thus the most accurate model for simulating ionic liquids. A few examples of AIMD simulations have been reported for ionic liquids.[49,60–65] There are a limited amount of these primarily because of the computational cost of running such a simulation, which limits both the size of the system and the time-scale that the system is allowed to progress. Finding dynamic properties becomes difficult but structural and electronic properties can be found. Hydrogen bonding, the effect of polarisation, charge transfer and the determination of partial atomic charges have all been studied using this method.

1.3 The Nature of Interactions in Ionic Liquids

With theoretical and computational tools such as *ab initio* methods and molecular dynamics, the nature of the interactions in ionic liquids can be studied. Additionally, methods that can decompose the total interactions into their individual components allow for probing into the contribution of each interaction type to the total interaction. These methods include Symmetry Adapated Perturbation Theory (SAPT),[66] Morokuma decomposition analysis[67] and the relatively new absolutely localised molecular orbital (ALMO) analysis[68] among many other de-

composition schemes.[69–72] Hydrogen bonding also features as a unique interaction in many reports because of both its prevalence, influence on bulk phase properties and general chemical importance.

1.3.1 Electrostatic Interactions

As discussed earlier, electrostatic interactions are found to be the most dominant of interaction types in ionic liquids. They contribute up to and above 70% of the attractive component of the interactions.[31,52] The sum of the partial atomic charges from quantum mechanical calculations of clusters have shown that the formal charges on the individual anions and cations are not ± 1,[45] they range between ± 0.6 and ± 0.8 e. For non-polarisable force fields the use of scaled atomic charges becomes necessary when describing dynamic properties.[73] This effectively reduces the strength of the electrostatic interactions.

In an energy decomposition analysis by Schmidt et al.,[43] they found that electrostatic interactions in force fields that scale charges are much smaller than those described in the SAPT calculations and also finds little evidence for charge transfer, which results in a reduction of absolute charge. They conclude by stating that the introduction of polarisation is a much more suitable and physically meaningful way to improve the dynamics of a simulation. This leaves open the question to what the best method for calculating electrostatic interactions is; is the use of atomic point charges the most suitable method?

1.3.2 Dispersion Interactions

Although electrostatic interactions dominate all the other interactions, dispersion interactions have been found to be non-negligible in ionic liquids.[43,52,74] It is even suggested by Steinhauser that the charge set used to calculate electrostatic interactions have little influence on structure but instead it is the anisotropic dispersion interactions that determine the local structure of the liquid.[57] Furthermore, Izgoro-

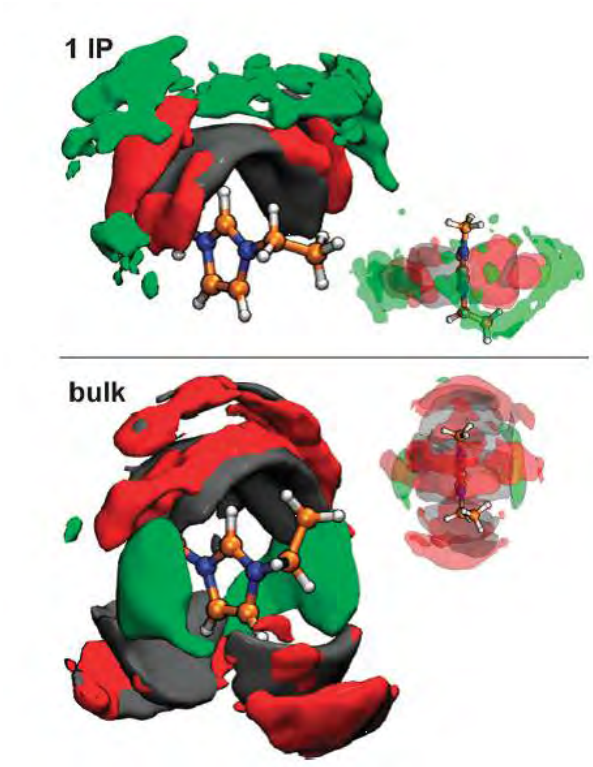

Fig. 1.4: The spatial distribution function of 1-ethyl-methylimidazolium ethylsulfate where the green represents the alkyl chain of the anion. The figure was taken from a publication by Kirchner et al.[76]

dina showed a correlation between the contribution of the dispersion interaction energy and the melting point and some transport properties of imidazolium and pyrrolodinium based ionic liquids.[22] Dispersion interactions were even found to be important in the ability of an ionic liquid to dissolve cellulose.[75] AIMD simulations of 1 ion-pair and 27 ion-pairs of 1-ethyl-3-methylimidazolium ethylsulfate reveal that dispersion interactions change the behaviour of the interaction between pairs significantly. Figure 1.4 shows this by displaying the differences in the spatial distribution functions. Moving from 1 ion-pair to 27 pairs the interaction of the side chain of the anion with the imidazolium ring becomes more pronounced, which is dispersion dominated.[76] A good description of the dispersion interactions is important for both the structure and dynamics of ILs.

1.3.3 Hydrogen Bonding

Hydrogen bonding interactions have been found experimentally in crystal structures of imidazolium based ionic liquids.[77–79] Understanding and characterising these interactions has been a focus of many studies.[31,32,52,80] When focusing on the static nature of the hydrogen bond, the strength or energy of the hydrogen bond tends to be the most sought after property (usually using calculation by first principles) after the geometric indicators of its presence.

These can then be used to determine the geometric parameters for defining hydrogen bonds in force fields, which are classically determined by evaluating the sum of the van der Waals radii of the donor an acceptor atoms. However, there are few studies that separate the hydrogen bond potential from the total interaction making it difficult to judge its energetic contribution to the stabilisation of complexes. Knowledge of the dynamic behaviour of the hydrogen bonds is also important because this will most likely explain the role of hydrogen bonding in the properties of the bulk such as the viscosity and the melting point.

Ludwig stated that hydrogen bonds fluidises the liquid, using FTIR measurements.[81] The reason for this is that the hydrogen bond disrupts the ionic network, reducing the melting point of the liquid.[82] Hydrogen bonds were found to have an influence on melting point, viscosity and enthalpy of vaporisation.[83] A hydrogen bonding network was reported by Zhang et al. that shows the importance of hydrogen bonding in driving structure.[84] Hunger et al. found experimentally a large jump in rotation of the nitrate anion in the ethylammonium nitrate liquid when establishing hydrogen bonds. This behaviour is usually found for strongly hydrogen-bonded liquids like water.[85]

1.3.4 Effect of Polarisation

Molecular dynamics simulations have moved to introduce the effects of polarisation to improve the dynamics within the simulation because "polarisabilities blur the permanent partial charge distribution and thus act like a lubricant between the ions".[86] One of the arguments for scaling charges was to introduce the effects of polarisation, a "poor man's way to include polarizability", but it emerged that scaled charges perform poorly at describing the local structure, mean rotational relaxation time and the diffusion coefficient but are excellent at the long range level.[87] Lynden-Bell et al. found ,from localising the wavefunction from an *ab initio* simulation of dimethylimidazolium, that the local environment polarises the cation by 0.7 D and the amplitude of the fluctuation of the dipole moment of the cation and anion increases.[88] Although the introduction of polarisation forces comes at a computational cost, Schmidt et al. stresses the importance of describing polarisation explicitly in the force field, not effectively via scaling charges.[43]

1.4 Objectives

The objective of the thesis is to describe the nature of interactions in the ion-pairs of ionic liquids, focusing on the electrostatic interactions, the dispersion interactions and hydrogen bonding. The effect of a polarising environment on the hydrogen bond is also to be studied. When discussing electrostatics the representation of charge, charge transfer and charge distribution is presented. The electrostatic interaction energies are to be calculated using charge centres, point charges and distributed multipoles and the values compared. For dispersion interactions, the Lennard-Jones, London, correlation and D3 methods are used and also compared to each other. The relative contribution of the dispersion to the total interaction will be discussed. Hydrogen bonding is to be studied using the theoretical methods highlighted in chapter 2, namely the quantum theory of atoms in molecules, natural bonding orbitals and a non-covalent index analysis. Finally a non-covalent index analysis is conducted for ion-pairs extracted from the condensed phase.

Bibliography

[1] Seddon, K. R.; Rogers, R. D. *Science* **2003**, *302*, 792–793.

[2] Freemantle, M. *An Introduction to Ionic Liquids*; RSC Publishing: Cambridge, 2010.

[3] Seddon, K. R. *J.Chem. Tech. Biotechnol.* **1997**, *68*, 351–356.

[4] Seddon, K. R.; Plechkova, N. *Chem. Soc. Rev.* **2008**, *37*, 123–150.

[5] Liu, J.; Jiang, G.; Jonsson, J. *TrAC* **2005**, *24*, 20–27.

[6] Kubisa, P. *Prog. Polym. Sci.* **2004**, *29*, 3–12.

[7] Zhu, S.; Wu, Y.; Chen, Q.; Yu, Z.; Wang, C.; Jin, S.; Ding, Y.; Wu, G. *Green Chem.* **2006**, *8*, 325–327.

[8] Brennecke, J. F.; Maginn, E. J. *AIChE Journal* **2001**, *47*, 2384–2389.

[9] Welton, T. *Chem. Rev.* **1999**, *99*, 2071–2083.

[10] Sheldon, R. *Chem. Commun.* **2001**, 2399–2407.

[11] G. Huddleston, J.; D. Rogers, R. *Chem. Commun.* **1998**, 1765–1766.

[12] Visser, A. E.; Swatloski, R. P.; Reichert, W. M.; Mayton, R.; Sheff, S.; Wierzbicki, A.; Davis, Jr., J. H.; Rogers, R. D. *Chem. Commun.* **2001**, 135–136.

[13] Welton, T., Wasserscheid, P., Eds. *Ionic Liquids in Synthesis*, second edition ed.; WILEY-VCH Verlags GmbH & Co. KGaA, Weinheim, 2008.

[14] Blanchard, L. A.; Hancu, D.; Beckman, E. J.; Brennecke, J. F. *Nature* **1999**, *399*, 28–29.

[15] Yu, G.; Zhao, D.; Wen, L.; Yang, S.; Chen, X. *AIChE Journal* **2012**, *58*, 2885–2899.

[16] McEwan, A. B.; Ngo, H. L.; LeCompte, L., K.and Hargens *Thermochim. Acta* **2000**, *357–358*, 97–102.

[17] Malvaldi, M.; Chiappe, C. *J. Phys.: Cond. Matter* **2008**, *20*, 035108.

[18] Galiński, M.; Lewandowski, A.; Stpniak, I. *Electrochim. Acta* **2006**, *51*, 5567–5580.

[19] Atilhan, M.; Jacquemin, J.; Rooney, D.; Khraisheh, M.; Aparicio, S. *Ind. Eng. Chem. Res.* **2013**, *52*, 16774–16785.

[20] Nunes, V. M. B.; Loureno, M. J. V.; Santos, F. J. V.; Nieto de Castro, C. A. *J. Chem. Eng. Data* **2003**, *48*, 446–450.

[21] Huddleston, J. G.; Visser, A. E.; Reichert, W. M.; Willauer, H. D.; Broker, G. A.; Rogers, R. D. *Green Chem.* **2001**, *3*, 156–164.

[22] Izgorodina, E. I.; Golze, D.; Maganti, R.; Armel, V.; Taige, T. J. S., M. amd Schubert; MacFarlane, D. R. *Phys. Chem. Chem. Phys.* **2014**, *16*, 7209–7221.

[23] Singer, R. D.; Turner, E. A.; Pye, C. C. *J. Phys. Chem. A.* **2003**, *107*, 2277–2288.

[24] Meindersma, G. W.; Podt, A. J.; de Haan, A. B. *Fuel Processing Technology* **2005**, *87*, 59–70.

[25] Freire, M. G.; Santos, L. M.; Fernandes, A. M.; Coutinho, J. A.; Marrucho, I. M. *Fluid Phase Equilib.* **2007**, *261*, 449–454.

[26] Wendler, K.; Dommert, F.; Zhao, Y. Y.; Berger, R.; Holm, C.; Delle Site, L. *Faraday Discuss.* **2012**, *154*, 111–132.

[27] Hunt, P. A.; Kirchner, B.; Welton, T. *Chem. Eur. J.* **2006**, *12*, 6762–6775.

[28] Hunt, P.; Gould, I.; Kirchner, B. *Aust.J.Chem. 2007* **2006**, *60*, 9–14.

[29] Hunt, P.; Gould, I. *J. Phys. Chem. A* **2006**, *110*, 2269–2282.

[30] Ludwig, R.; Köddermann, T.; Wertz, A., C.and Heintz *ChemPhysChem.* **2006**, *7*, 1944–1949.

[31] Dong, K.; Zhang, S. *Chem. Eur. J.* **2012**, *18*, 2748–2761.

[32] Matthews, R. P.; Ashworth, C.; Welton, T.; Hunt, P. A. *J. Phys.:Condens. Matter* **2014**, *26*.

[33] Hunt, P. A. *J. Phys. Chem. B* **2007**, *111*, 4844–4853.

[34] Li, H.; Lu, Y.; Wu, W.; Liu, Y.; Peng, C.; Liu, H.; Zhu, W. *Phys. Chem. Chem. Phys.* **2013**, *15*, 4405–4414.

[35] Koßmann, S.; Thar, J.; Kirchner, B.; Hunt, P. A.; Welton, T. *J. Chem. Phys.* **2006**, *124*, 1–12.

[36] Izgorodina, E. I.; Rigby, J.; MacFarlane, D. R. *Chem. Commun.* **2012**, *48*, 1493–1495.

[37] Bhargava, B.; Balasubramanian, S. *Chem. Phys. Lett.* **2007**, *444*, 242–246.

[38] Ludwig, R. *Phys. Chem. Chem. Phys.* **2008**, *10*, 4333–4339.

[39] Canongia Lopes, J. N.; Pádua, A. A. H.; Shimizu, K. *J. Phys. Chem. B* **2008**, *112*, 5039–5046.

[40] Lopes, C.; José, N.; Pádua, A. H. *J. Phys. Chem. B* **2004**, *108*, 16893–16898.

[41] Canongia Lopes, J.; Pádua, A. *Theor. Chem. Acc.* **2012**, *131*.

[42] Mondal, A.; Balasubramanian, S. *J. Phys. Chem. B.* **2014**, *118*, 3409–3422.

[43] Schmidt, J. R.; Choi, E.; McDaniel, J. G.; Yethiraj, A. *J. Phys. Chem. Lett.* **2014**, *5*, 2670–2674.

[44] Liu, Z.; Huang, S.; Wang, W. *J. Phys. Chem. B* **2004**, *108*, 12978–12989.

[45] Maginn, E. J. *J. Phys.: Cond. Matter* **2009**, *21*, 373101.

[46] Lopes, J.; Gomes, M.; Pádua, A. A. H. *J.Phys. Chem. B Lett.* **2006**, *110*, 16816–16818.

[47] Cavalcante, A. d. O.; Ribeiro, M. C. C.; Skaf, M. S. *J. Chem. Phys.* **2014**, *140*, 1–10.

[48] Méndez-Morales, T.; Carrete, J.; Cabeza, O.; Gallego, L. J.; Varela, L. M. *J. Phys. Chem. B* **2011**, *115*, 6995–7008.

[49] Zahn, S.; Thar, J.; Kirchner, B. *J. Chem. Phys.* **2010**, *132*, 1–13.

[50] Kowsari, M. H.; Alavi, S.; Ashrafizaadeh, M.; Najafi, B. *J. Chem. Phys.* **2010**, *132*, 1–9.

[51] Borodin, O.; Smith, G. D. *J. Phys. Chem. B* **2006**, *110*, 11481–11490.

[52] Izgorodina, E. I.; MacFarlane, D. R. *J. Phys. Chem. B* **2011**, *115*, 14659–14667.

[53] Kirchner, B.; Zahn, S.; Uhlig, F.; Thar, J.; Spickermann, C. *Angew. Chem. It. Ed.* **2008**, *47*, 3639–3641.

[54] Tsuzuki, S.; Shinoda, W.; Miran, M. S.; Kinoshita, H.; Yasuda, T.; Watanabe, M. *J. Chem. Phys.* **2013**, *139*, 1–9.

[55] Izgorodina, E. *Phys. Chem. Chem. Phys.* **2011**, *13*, 4189–4207.

[56] Izgorodina, E. I.; Rigby, J. *Phys. Chem. Chem. Phys.* **2013**, *15*, 1632–1646.

[57] Schröder, C. S. *J. Chem. Phys.* **2008**, *128*, 1–7.

[58] Sambasivarao, S. V.; Acevedo, O. *J. Chem. Theory Comput.* **2009**, *5*, 1038–1050.

[59] Cramer, C. J. *Essentials of Computational Chemistry*, second edition ed.; John Wiley & Sons: Chichester, 2004.

[60] Del Pópolo, M. G.; Lynden-Bell, R. M.; Kohanoff, J. *J. Phys. Chem. B* **2005**, *109*, 5895–5902.

[61] Bühl, M.; Chaumont, A.; Schurhammer, R.; Wipff, G. *J. Phys. Chem. B* **2005**, *109*, 18591–18599.

[62] Bhargava, B. L.; Balasubramanian, S. *J. Phys. Chem. B* **2007**, *111*, 4477–4487.

[63] Brehm, M.; Weber, H.; Pensado, A. S.; Stark, A.; Kirchner, B. *Phys. Chem. Chem. Phys.* **2012**, *14*, 5030–5044.

[64] Brüssel, M.; Brehm, M.; Voigt, T.; Kirchner, B. *Phys. Chem. Chem. Phys.* **2011**, *13*, 3617–13620.

[65] Wendler, K.; Zhan, S.; Dommert, F.; Berger, R.; Holm, C.; Site, L. D.; Kirchner, B. *J. Comp. Theory Chem.* **2011**, *7*, 3040–3044.

[66] Jeziorski, B.; Moszynski, R.; Szalewicz, K. *Chem. Rev.* **1994**, *94*, 1887–1930.

[67] Kitaura, K.; Morokuma, K. *Int. J. Quantum Chem.* **1976**, *10*, 325–340.

[68] Khaliullin, R. Z.; Bell, A. T.; Head-Gordon, M. *J. Chem. Phys.* **2008**, *128*, 1–16.

[69] Su, P.; Li, H. *J. Chem. Phys.* **2009**, *131*, 1–15.

[70] Glendening, E. D.; Streitwieser, A. *J. Chem. Phys.* **1994**, *100*, 2900–2909.

[71] Mo, Y.; Gao, J.; Peyerimhoff, S. D. *J. Chem. Phys.* **2000**, *112*, 5530–5538.

[72] Glendening, E. D. *J. Phys. Chem. A* **2005**, *109*, 11936–11940.

[73] Beichel, W.; Trapp, N.; Hauf, C.; Kohler, O.; Eickerling, G.; Scherer, W.; Krossing, I. *Angew. Chem. Int. Ed.* **2014**, *53*, 3143–3146.

[74] Zahn, S.; Bruns, G.; Thar, J.; Kirchner, B. *Phys. Chem. Chem. Phys.* **2008**, *10*, 6921–6924.

[75] Rabideau, B. D.; Agarwal, A.; Ismail, A. E. *J. Phys. Chem. B* **2014**, *118*, 1621–1629.

[76] Malberg, F.; Pensado, A. S.; Kirchner, B. *Phys. Chem. Chem. Phys.* **2012**, *14*, 12079–12082.

[77] Abdul-Sada, A. K.; Greenway, A. M.; Hitchcock, P. B.; Mohammed, T. J.; Seddon, K. R.; Zora, J. A. *J. Chem. Soc., Chem. Commun.* **1986**, 1753–1754.

[78] Matsumoto, K.; Hagiwara, R. *J. Fluorine Chem.* **2007**, *128*, 317–331.

[79] Choudhury, A. R.; Winterton, N.; Steiner, A.; Cooper, A. I.; Johnson, K. A. *J. Am. Chem. Soc.* **2005**, *127*, 16792–16793.

[80] Matthews, R. P.; Welton, T.; Hunt, P. A. *Phys. Chem. Chem. Phys.* **2014**, *16*, 3238–3253.

[81] Fumino, K.; Wulf, A.; Ludwig, R. *Angew. Chem. Int. Ed.* **2008**, *47*, 8731–8734.

[82] Köckerling, M.; Ludwig, R.; Roth, C.; Pepperl, T.; Fumino, K.; Paschek, D. *Angew. Chem. Int. Ed.* **2011**, *50*, 6661–6665.

[83] Fumino, K.; Peppel, T.; Geppert-Rybczyńska, M.; Zaitsau, D. H.; Lehman, J.; Verevkin, S. P.; Köckerling, M.; Ludwig, R. *Phys. Chem. Chem. Phys.* **2011**, *13*, 14064–14075.

[84] Dong, K.; Zhang, S.; Wang, D.; Yao, X. *J. Phys. Chem.A* **2006**, *110*, 9775–9782.

[85] Hunger, J.; Sonnleitner, T.; Liu, L.; Buchner, R.; Bonn, M. *J. Phys. Chem. Lett.* **2012**, *3*, 3034–3038.

[86] Bica, K.; Deetlefs, M.; Schroder, C.; Seddon, K. R. *Phys. Chem. Chem. Phys.* **2013**, *15*, 2703–2711.

[87] Schröder, C. *Phys. Chem. Chem. Phys.* **2012**, *14*, 3089–3102.

[88] Prado, C. E.; Del Pópolo, M. G.; Youngs, T. G. A.; Kohanoff, J.; Lynden-Bell, R. M. *Mol. Phys.* **2012**, *104*, 2477–2483.

2

Theory

2.1 The Basic Principles of the ab initio method

The fundamental postulate of quantum mechanics is that there exists a wavefunction, Ψ, for any chemical system and that an operator acts on the wavefunction to return an observable property of the system. In mathematical notation it is represented as

$$\vartheta\Psi = a\Psi \tag{2.1}$$

where ϑ is the operator and a is a scalar value of some property of the system.[1] This is an example of an eigenvalue equation where Ψ is called an eigenfunction and a is called an eigenvalue of the operator. The product of the wavefunction with its complex conjugate ($\Psi^*\Psi$) has the units of probability density. The probability that the chemical system will be within some region of space is given by the integration of $\Psi^*\Psi$ over that region. The integration of $\Psi^*\Psi$ over all space is unity for a bound particle.[1–4]

The operator that returns the energy of the chemical system is called the Hamiltonian operator, $\hat{\mathbf{H}}$, and the eigenvalue equation,

$$\hat{\mathbf{H}}\Psi = E\Psi \tag{2.2}$$

is called the Schrödinger equation.[1] The Hamiltonian operator, expressed in mathematical notation in equation 2.3, is

$$\hat{\mathbf{H}} = -\sum_{i}^{N}\frac{\hbar^2}{2m_e}\nabla_i^2 - \sum_{k}\frac{\hbar^2}{2m_k}\nabla_k^2 - \sum_{i}\sum_{k}\frac{e^2Z_k}{r_{ik}} + \sum_{i<j}\frac{e^2}{r_{ij}} + \sum_{k<l}\frac{e^2Z_kZ_l}{r_{kl}} \tag{2.3}$$

Tab. 2.1: Table of atomic units

Physical qty.	Symbol	value in a.u.	value in S.I. units
Angular momentum	$\hbar$	1	1.055×10^{-34}J
Mass	m_e	1	9.109×10^{-34}kg
Charge	e	1	1.602×10^{14}C
Vacuum permittivity	$4\pi\epsilon_0$	1	1.113×10^{-10}

The first and second term of equation 2.3 are the kinetic energy operators of the electrons and nuclei, respectively. The third term is the expression of the attraction between electrons and the nuclei, the fourth term is the electron-electron repulsion and the last term is the nuclear-nuclear repulsion; these make up the potential energy of the molecular system. The indices i and j run over electrons and k and l run over nuclei, $\hbar$ is Planck's constant, m_e is the mass of the electron, m_k is the mass of the nucleus, ∇^2 is the Laplacian operator, e is the charge of the electron, Z is the atomic number and r_{ab} is the distance between particles a and b. The Laplacian takes the form of equation 2.4

$$\nabla^2 = \frac{\partial^2}{\partial x^2} + \frac{\partial^2}{\partial y^2} + \frac{\partial^2}{\partial z^2} \tag{2.4}$$

The potential energy appears as it would in classical mechanics but the kinetic energy must be returned by the kinetic energy operator shown in equation 2.5

$$\hat{\mathbf{T}} = \frac{\hbar^2}{2m}\nabla^2 \tag{2.5}$$

Most constants in equation 2.3 are made equal to 1 when converted to atomic units, which are displayed in table 2.1.[3,4]

The Hamiltonian in equation (2.3) has many acceptable eigenfunctions each with an associated eigenvalue E_i, i.e. there is a complete set of solutions Ψ_i with eigenvalues E_i.[1] The set of wavefunctions are chosen to be orthonormal (orthogonal and normalised), i.e.

$$\int \Psi_i \Psi_j dr = \delta_{ij} \tag{2.6}$$

where the δ_{ij} is the Kronecker delta function and is defined in equation 2.7

$$\delta_{ij} = \begin{cases} 1 & \text{for } i = j \\ 0 & \text{for } i \neq j \end{cases} \tag{2.7}$$

Taking equation 2.2 and multiplying on the left by the complex conjugate of a specific wavefunction, Ψ_j, and integrating gives

$$\begin{aligned} \int \Psi_j^* \hat{\mathbf{H}} \Psi_i dr &= \int \Psi_j^* E_i \Psi_i dr \\ &= E_i \delta_{ij} \end{aligned} \tag{2.8}$$

which provides the recipe for calculating the molecular energy.

2.1.1 The Born-Oppenheimer Approximation

Since nuclei are much heavier than electrons, they move much more slowly. Electrons are approximated to move in a field of fixed nuclei.[5] The kinetic energy of the nuclei may thus be neglected and the nuclear-nuclear repulsion regarded as a constant when calculating the molecular energy. Any constant added to an operator only adds to the operator eigenvalues and has no effect on the operator eigenfunction.[4] The nuclear-nuclear repulsion energy can be added after calculating the energy of the molecular system in terms of the motion and potential of electrons. The approximation changes the electronic Hamiltonian to equation 2.9,

$$\hat{\mathbf{H}}_{elec} = -\sum_{i=1}^{N} \frac{1}{2} \nabla_i^2 - \sum_{i}^{N} \sum_{k}^{M} \frac{Z_k}{r_{ik}} + \sum_{i=1}^{N} \sum_{j>i}^{N} \frac{1}{r_{ij}} \tag{2.9}$$

and the solution to the electronic Schrödinger equation ($H_{elec}\Psi = \epsilon_{elec}\Psi_{elec}$) is the electronic wavefunction.

$$\Psi_{elec} = \Psi_{elec}(\{r_i\}; \{R_A\}) \tag{2.10}$$

which describes the motion of electrons and explicitly depends on the coordinates of electrons ($\mathbf{r}_i$) but depends parametrically on nuclear coordinates ($\mathbf{R}_A$), as does

the electronic energy.[4]

$$\mathbf{E} = \mathbf{E}(\{\mathbf{R}_A\}) \tag{2.11}$$

2.1.2 The Antisymmetry and Pauli Exclusion Principle

The electronic Hamiltonian depends only on the spatial coordinates of the electrons. To completely describe an electron it is necessary to also specify its spin. Two spin functions $\alpha(\omega)$ and $\beta(\omega)$ are introduced, they are functions of an unspecified spin variable ω.[4] The two spin functions are orthonormal, i.e.

$$\begin{aligned} \int \alpha^*(\omega)\alpha(\omega)d\omega &= \int \beta^*(\omega)\beta(\omega)d\omega = 1 \\ \int \alpha^*(\omega)\beta(\omega)d\omega &= \int \beta^*(\omega)\alpha(\omega)d\omega = 0 \end{aligned}$$

The wavefunction that specifies both spatial distribution and spin is a spin orbital. Each spatial orbital can form two spin orbitals that is a product of the spatial and spin orbitals. Spin orbitals thus completely describe an electron's spatial distribution and spin.

2.1.3 Slater Determinants

The total wavefunction Ψ must be antisymmetric with respect to the interchange of electronic coordinates. The Pauli principle, which states that two or more electrons cannot be in the exact same state, i.e. they cannot share the same set of quantum numbers, is a direct consequence of the antisymmetry principle.[2] The antisymmetry principle can be achieved by building the total wavefunction from Slater determinants.[6] The columns in the Slater determinants are the single-electron wavefunctions and the rows of the Slater determinant are the electron coordinates. The single-electron wavefunctions, for molecules, are called molecular orbitals (MO), which are a product of the spatial orbitals and spin functions.

The Slater determinant for an N-electron system with N MOs is given by 2.12

$$\Psi^{SD} = \frac{1}{\sqrt{N!}} \begin{vmatrix} \psi_1(1) & \psi_2(1) & \cdots & \psi_N(1) \\ \psi_1(2) & \psi_2(2) & \cdots & \psi_N(1) \\ \vdots & \vdots & \ddots & \vdots \\ \psi_1(N) & \psi_2(N) & \cdots & \psi_N(N) \end{vmatrix} \tag{2.12}$$

The Slater determinant can be represented in terms of a "diagonal" product of the determinant Π acted on by the antisymmetry operator $\mathbf{A}$

$$\Psi = \mathbf{A}[\psi_1(1)\psi_2(2)\cdots\psi_N(N)] = \mathbf{A}\Pi \tag{2.13}$$

$$\mathbf{A} = \frac{1}{\sqrt{N!}} \sum_{p=0}^{N-1} (-1)^p \mathbf{P} = \frac{1}{\sqrt{N!}} [\mathbf{1} - \sum_{ij} \mathbf{P}_{ij} + \sum_{ijk} \mathbf{P}_{ijk} - \cdots] \tag{2.14}$$

where $\mathbf{1}$ in the square brackets of 2.14 is the identity operator, $\mathbf{P}_{ij}$ generates all possible permutations of two electron coordinates, $\mathbf{P}_{ijk}$ generates all possible permutations of three electron coordiantes etc. $\mathbf{A}$ commutes with the Hamiltonian and $\mathbf{A}$ acting twice gives the same as $\mathbf{A}$ acting once multiplied by $\sqrt{N!}$.[2]

2.1.4 The Energy of a Slater Determinant

The energy of the Slater determinant wavefunction can now be discussed and Dirac's notation is introduced. In Dirac's notation, the integral is expressed as a set of angle brackets with the left hand side of the bracket called the "bra", $\langle\psi|$, representing the complex conjugate wavefunction and the right hand side the "ket", $|\psi\rangle$, such that $\int \psi^*\psi dr = \langle\psi|\psi\rangle$. Such a bracket is often referred to as a matrix element. The expectation value of the energy given by the Slater

determinant wavefunction in equation (2.13) and can be expressed as:

$$\begin{aligned} E &= \langle\Psi|H|\Psi\rangle \\ &= \langle\mathbf{A}\Pi|H|\mathbf{A}\Pi\rangle \\ &= \sqrt{N!}\langle\Pi|H|\mathbf{A}\Pi\rangle \\ &= \sum_{p}(-1)^{p}\langle\Pi|H|\mathbf{P}\Pi\rangle \end{aligned} \tag{2.15}$$

The terms in the electronic Hamiltonian of equation 2.9 are grouped to give the one-electron operator $\hat{\mathbf{h}}_\mathbf{i}$ and the two electron operator $\hat{\mathbf{g}}_\mathbf{ij}$.

$$\hat{\mathbf{h}}_i = -\frac{1}{2}\nabla_i^2 - \sum_{k}^{M}\frac{Z_k}{r_{ik}} \tag{2.16}$$

$$\hat{\mathbf{g}}_{ij} = \frac{1}{r_{ij}} \tag{2.17}$$

The one electron operator $\hat{\mathbf{h}}_i$ describes the motion of an electron in a field of nuclei and $\hat{\mathbf{g}}_{ij}$ is the two-electron operator giving the electron-electron repulsion. Only the identity operator $\mathbf{1}$ in the antisymmetry operator $\mathbf{A}$ can give a non-zero contribution for the one-electron operator.

$$\begin{aligned} \langle\Pi|\hat{\mathbf{h}}_\mathbf{1}|\Pi\rangle &= \langle\psi_1(1)\psi_2(2)\cdots\psi_N(N)|\hat{\mathbf{h}}_1|\psi_1(1)\psi_2(2)\cdots\psi_N(N)\rangle \\ &= \langle\psi_1(1)|\hat{\mathbf{h}}_1|\psi_1(1)\rangle\langle\psi_2(2)|\psi_2(2)\rangle\cdots\langle\ \psi_N(N)|\psi_N(N)\rangle \\ &= \langle\psi_1(1)|\hat{\mathbf{h}}_1|\psi_1(1)\rangle \\ &= \mathrm{h}_1 \end{aligned}$$

All matrix elements involving a permutation operator give zero because there will be an overlap of two different molecular orbitals that are orthogonal. For the two-electron operator, only the identity operator $\mathbf{1}$ and $\mathbf{P}_{ij}$ can give a non-zero

contribution. The term arising from the identity operator is

$$\begin{aligned}\langle\Pi|\hat{\mathbf{g}}_{12}|\Pi\rangle &= \langle\psi_1(1)\psi_2(2)\cdots\psi_N(N)|\hat{\mathbf{g}}_{12}|\psi_1(1)\psi_2(2)\cdots\psi_N(N)\rangle \\ &= \langle\psi_1(1)\psi_2(2)|\hat{g}_{12}|\psi_1(1)\psi_2(2)\rangle \\ &= J_{12}\end{aligned} \tag{2.18}$$

and is called the Coulomb integral representing the classical repulsion between two charge distributions. The term arising from the P_{ij} operator is

$$\begin{aligned}\langle\Pi|\hat{\mathbf{g}}_{12}|P_{12}\Pi\rangle &= \langle\psi_1(1)\psi_2(2)\cdots\psi_N(N)|\hat{\mathbf{g}}_{12}|\psi_1(2)\psi_2(1)\cdots\psi_N(N)\rangle \\ &= \langle\psi_1(1)\psi_2(2)|\hat{\mathbf{g}}_{12}|\psi_2(1)\psi_2(1)\rangle\cdots\psi_N(N)\rangle \\ &= \langle\psi_1(1)\psi_2(2)|\hat{\mathbf{g}}_{12}|\psi_2(1)\psi_1(2)\rangle \\ &= K_{12}\end{aligned}$$

and is called the exchange integral which has no classical analogue.[2] The total energy can be written as

$$E = \sum_{i=1}^{N} \mathrm{h}_i + \frac{1}{2}\sum_{i=1}^{N}\sum_{j=1}^{N}(J_{ij} - K_{ij}) + V_{nn} \tag{2.19}$$

where the negative sign of the exchange integral comes from $(-1)^p$ in the antisymmetry operator. It is convenient to express the energy in terms of Coulomb and exchange operators, i.e.,

$$E = \sum_{i=0}^{N}\langle\psi_i|\hat{\mathbf{h}}_i|\psi_i\rangle + \frac{1}{2}\sum_{ij}\left(\langle\psi_j|\hat{\mathbf{J}}_i|\psi_j\rangle - \langle\psi_j|\hat{\mathbf{K}}_i|\psi_j\rangle\right) + V_{nn} \tag{2.20}$$

$$\hat{\mathbf{J}}_i|\psi_j(2)\rangle = \langle\psi_i(1)|\hat{\mathbf{g}}_{\mathbf{12}}|\psi_i(1)\rangle|\psi_j(2)\rangle \tag{2.21}$$

$$\hat{\mathbf{K}}_i|\psi_j(2)\rangle = \langle\psi_i(1)|\hat{\mathbf{g}}_{\mathbf{12}}|\psi_j(1)\rangle|\psi_i(2)\rangle \tag{2.22}$$

2.1.5 Derivation of the Hartree-Fock Equations

The objective is to determine a set of molecular orbitals that makes the energy a minimum, or stationary, with respect to a change in the molecular orbitals.[3]

The variations must be done in a manner in which the orbitals remain orthogonal and normalised. Variations subject to constraints are handled by the method of Lagrange multipliers. The Lagrange function, L, must be stationary with respect to an orbital variation

$$\begin{aligned} L &= E - \sum_{ij}^{N} \lambda_{ij}(\langle\psi_i|\psi_j\rangle - \delta_{ij}) \\ \delta L &= \delta E - \sum_{ij}^{N} \langle\delta\psi_i|\psi_j\rangle + \langle\psi_i|\delta\psi_j\rangle = 0 \end{aligned}$$

where λ_{ij} is a Lagrange multiplier.

The electronic energy is varied with respect to the coordinates

$$\begin{aligned} \delta E &= \sum_{i}^{N} \langle\delta\psi_i|\hat{\mathbf{h}}_i|\psi_i\rangle + \sum_{ij}^{N} (\langle\delta\psi_i|\hat{\mathbf{J}}_j - \hat{\mathbf{K}}_j|\psi_i\rangle + \text{complex conjugate} \\ &= \sum_{i}^{N} (\langle\delta\psi_i|\hat{\mathbf{F}}_i|\psi_i\rangle) + \text{complex conjugate} \end{aligned} \tag{2.23}$$

$\hat{\mathbf{F}}_i$ is the one electron Fock-operator, it contains the kinetic energy operator of an electron, the potential that describes attraction of electrons to nuclei and electron-electron repulsion. The Fock-operator is mathematically represented as

$$\hat{\mathbf{F}}_i = \hat{\mathbf{h}}_i + \sum_{j}^{N} (\hat{\mathbf{J}}_j - \hat{\mathbf{K}}_j) \tag{2.24}$$

The variation of the Lagrange function thus yields

$$\delta L = \sum_{i}^{N} (\langle\delta\psi_i|\hat{\mathbf{F}}_i|\psi_i\rangle - \sum_{ij}^{N} \lambda_{ij}\langle\delta\psi_i|\psi_j\rangle) + \text{complex conjugate} \tag{2.25}$$

The variation principle states that the desired orbitals are those that make the variation of the Lagrange function with respect to the orbitals zero,

$$\begin{aligned}\sum_{i}^{N}\langle\delta\psi_i|(\hat{\mathbf{F}}_i|\psi_i\rangle-\sum_{j}^{N}|\lambda_{ij}\psi_j\rangle) &= 0\\ \hat{\mathbf{F}}_i\psi_i-\sum_{j}^{N}\lambda_{ij}\psi_j &= 0\\ \hat{\mathbf{F}}_i\psi_i &= \sum_{j}^{N}\lambda_{ij}\psi_j \end{aligned} \tag{2.26}$$

This equation can be simplified by using a unitary transformation, which makes the matrix of the Lagrange multipliers diagonal,[2] i.e. $\lambda_{ij} \rightarrow 0$ and $\lambda_{ii} \rightarrow \epsilon_i$. A set of molecular orbitals, $\psi^{'}$ called the canonical molecular orbitals transforms equation (2.26) to a set of pseudo-eigenvalue equations

$$\hat{\mathbf{F}}_i\psi_i^{'} = \epsilon_i\psi_i^{'} \tag{2.27}$$

The Lagrange multipliers can be interpreted as molecular orbital energies, i.e. they are the expectation value of the Fock operator in the molecular orbital basis and can be found by multiplying on the left by $\psi_i^{'*}$ and integrating over all space

$$\epsilon_i = \langle\psi_i^{'}|\hat{\mathbf{F}}_i|\psi_i^{'}\rangle \tag{2.28}$$

2.1.6 The Roothaan-Hall equations

The Energy of a Slater Determinant was varied with respect to the molecular orbitals with restraints on the orthonormality of the orbitals to produce a set of equations 2.27, the Hartree-Fock equations. The set of Hartree-Fock equations are not useful for molecular calculations yet as they do not prescribe a mathematically viable procedure of obtaining the initial guess of the molecular orbitals and the wavefunction itself may be so complicated that a qualitative understanding of the electron distribution may be too difficult. However, the Roothaan-Hall method prescribes a procedure for solving such a problem by representing the molecular

orbitals as a linear combination of basis functions,[7,8] which may be written as

$$\begin{aligned} \chi_1 &= \mathrm{c}_{11}\phi_1 + \mathrm{c}_{21}\phi_2 + \cdots + \mathrm{c}_{m1}\phi_m \\ \chi_2 &= \mathrm{c}_{12}\phi_1 + \mathrm{c}_{22}\phi_2 + \cdots + \mathrm{c}_{m1}\phi_m \\ &\vdots \\ \chi_m &= \mathrm{c}_{1m}\phi_1 + \mathrm{c}_{2m}\phi_2 + \cdots + \mathrm{c}_{mm}\phi_m \end{aligned} \tag{2.29}$$

or in a more compact representation may be written as

$$\chi_i = \sum_{s=1}^{M} \mathrm{c}_{si}\phi_s \tag{2.30}$$

where $i = 1, 2, \cdots, M$ for M molecular orbitals. The coefficients c_{si} in equation 2.30 are the coefficients for the s^{th} basis function in the i^{th} molecular orbital. The basis functions are usually centred on the atoms and may be regarded as atomic orbitals. The approach of using a combination of basis functions is thus called the linear combination of atomic orbitals (LCAO) method.

The Hartree-Fock equations may thus be written in terms of the basis functions as:

$$\hat{\mathbf{F}}_i \sum_{s=1}^{M} \mathrm{c}_{si}\phi_s = \epsilon_i \sum_{s=1}^{M} \mathrm{c}_{si}\phi_s \tag{2.31}$$

Multiplying on the left by a specific basis function and integrating produces the Roothaan-Hall equations, which are the Fock equations in the atomic orbital basis. All M equations may be collected in matrix notation,[3]

$$\begin{aligned} \mathbf{FC} &= \mathbf{SC}\epsilon \\ F_{rs} &= \langle \phi_r | F | \phi_s \rangle \\ S_{rs} &= \langle \phi_r | \phi_s \rangle \end{aligned} \tag{2.32}$$

The overlap matrix $\mathbf{S}$ contains all the overlap elements between basis functions, and the Fock matrix $\mathbf{F}$ contains the Fock matrix elements. Each Fock element contains two parts from equation (2.24); integrals involving the one-electron operators and a sum over occupied molecular orbitals of coefficients multiplied with

the two-electron integrals involving the electron-electron repulsion operator:

$$\begin{aligned}
F_{rs} &= \langle\phi_r|\hat{\mathbf{h}}|\phi_s\rangle + \sum_{j}^{occ.MO} \langle\phi_r|\hat{\mathbf{J}}_j - \hat{\mathbf{K}}_j|\phi_s\rangle \\
&= \langle\phi_r|\hat{\mathbf{h}}|\phi_s\rangle + \sum_{j}^{occ.MO} \langle\phi_r\phi_j|\mathbf{g}|\phi_s\phi_j\rangle - \langle\phi_r\phi_j|\mathbf{g}|\phi_s\phi_j\rangle \\
&= \langle\phi_r|\hat{\mathbf{h}}|\phi_s\rangle + \sum_{j}^{occ.MO}\sum_{t}^{AO}\sum_{u}^{AO} \mathrm{c}_{uj}\mathrm{c}_{tj}\langle\phi_r\phi_t|\mathbf{g}|\phi_s\phi_u\rangle - \langle\phi_r\phi_t|\mathbf{g}|\phi_u\phi_s\rangle \\
&= \langle\phi_r|\hat{\mathbf{h}}|\phi_s\rangle + \sum_{t}^{AO}\sum_{u}^{AO} \mathbf{D}_{tu}\langle\phi_r\phi_t|\mathbf{g}|\phi_s\phi_u\rangle - \langle\phi_r\phi_t|\mathbf{g}|\phi_u\phi_s\rangle \\
\mathbf{D}_{tu} &= \sum_{j}^{M} \mathrm{c}_{tj}\mathrm{c}_{uj}
\end{aligned}$$

Note: the physists notatation orders by the electron indeces, i.e. $\langle 12|12\rangle$. $\mathbf{D}_{tu}$ is the density matrix. Finally, the total energy in equation 2.19 can be written fully in terms of the basis functions where $\mathbf{g}$ in the two-electron integrals is implied.

$$\begin{aligned}
E &= \sum_{i}^{N}\langle\psi_i|\mathbf{h}|\psi_i\rangle + \frac{1}{2}\sum_{ij}^{N}(\langle\phi_i\phi_j|\phi_i\phi_j\rangle - \langle\phi_i\phi_j|\phi_j\phi_i\rangle) + V_{nn} \\
&= \sum_{i}^{N}\sum_{rs}^{m} \mathrm{c}_{ri}\mathrm{c}_{si}\langle\phi_r|\mathbf{h}|\phi_s\rangle + \frac{1}{2}\sum_{ij}^{N}\sum_{rstu}^{M} \mathrm{c}_{ri}\mathrm{c}_{si}\mathrm{c}_{uj}\mathrm{c}_{tj}(\langle\phi_r\phi_t|\phi_s\phi_u\rangle - \langle\phi_r\phi_t|\phi_u\phi_s\rangle) + V_{nn} \\
&= \sum_{rs}^{m} \mathbf{D}_{rs}h_{rs} + \frac{1}{2}\sum_{rstu}^{m} \mathbf{D}_{rs}\mathbf{D}_{tu}(\langle\phi_r\phi_t|\phi_s\phi_u\rangle - \langle\phi_r\phi_t|\phi_u\phi_s\rangle) + V_{nn}
\end{aligned}$$

The Roothaan-Hall equation 2.33 show that to calculate the Fock matrix, $\mathbf{F}$, i.e. the matrix elements, F_{rs}, the orbitals, ψ_i, must be known as the Coulomb and exchange operators are defined in terms of the orbitals. To determine the unknown MO coefficients c_{ri}, the Fock matrix must be diagonalised but the Fock matrix is only known if all the MO coefficients $\mathbf{D}_{tu}$ are also known. The procedure begins by guessing the initial coefficients, form the Fock matrix and then diagonalising it. The new set of coefficients is used to form a new Fock matrix and the procedure repeated until the set of coefficients used for calculating the new Fock matrix is equal to those as a result from the diagonalization. This iterative process is called the *self-consistent-field* procedure.

2.1.7 The Basis Set

The basis set is a set of mathematical functions from which the molecular orbitals are built. The form of the basis functions that are the most simple to compute and used for molecular calculations are the Gaussian and Slater functions. Slater functions would be the natural choice if not for the excessive computational cost of evaluating the two-electron integrals. Fortunately, the two-electron integrals are readily calculated using Gaussian functions as the product of two Gaussians is a new Gaussian centred at a new position. However, a single Gaussian function is a poor approximation to the near ideal Slater function. The problem is circumvented by using a combination of Gaussians to approximate a Slater wavefunction.[9] For example, three Gaussian functions, called *primitive Gaussians*, multiplied by respective constants, called the *contraction coefficients*, are added together to form a *contracted Gaussian*, which approximates the Slater function. Such a combination is afforded the nomenclature STO-3G. Increasing the number of primitive Gaussians improves the contracted Gaussians approximation to the Slater function (see figure 2.1).

Single-ζ, multiple-ζ and split valence

The STO-3G basis set is also referred to as a single-ζ basis set; this is as each orbital is described by one basis function, which is composed of a contracted Gaussian e.g, a carbon atom will use 5 functions, one each for the 1s, 2s, 2px, 2py

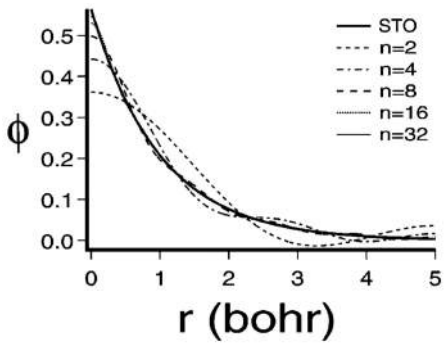

Fig. 2.1: Slater function (solid curve) and the Approximation of Slater Functions by contracted Gaussians where n is the number of primitives used.[10]

and 2pz orbitals.

A greater amount of flexibility may be obtained from decontracting the basis set. Consider a basis set denoted 3-21G, this basis set uses a single basis function to describe each core orbital, the basis functions that describe the core orbitals are contracted Gaussians composed of three primitive Gaussians. Two basis functions are used to describe each valence orbital, the first function is a contracted Gaussian composed of 2 primitive Gaussians and the second is a function represented by one Gaussian. This is the standard nomenclature used for all Pople-type basis sets. Basis sets such as the 3-21G and 6-31G basis sets are referred to as double-ζ basis sets. Basis sets that use three functions to describe each valence orbital are called triple-ζ basis sets.

The decontracted approach of constructing basis sets allows the SCF procedure more flexibility to adjust the contribution of each basis function to the molecular orbitals, thus improving the description of the electron distribution in molecules. Generally, basis sets which use more than one function to describe valence orbitals are called split valence basis sets.

Polarisation and Diffuse Functions

To allow further mathematical flexibility for the description of the molecular orbitals, a set of additional functions may be added to polarise the molecular orbitals, this allows the SCF procedure to establish a more anisotropic electron distribution. For first row elements, d-functions are the most useful polarisation functions (see figure 2.2) and p-functions would be useful in polarizing hydrogen's s-orbital. Polarisation functions thus allow for an improved description of molecular geometry and electron distribution. In the Pople type basis set, the addition of polarisation functions to heavy atoms are denoted by a single asterisk (*) or the function that must be added, e.g 6-31G* or 6-31G(d). Addition of the polarisation functions to hydrogen atoms and heavy atoms is denoted by a double asterisk '**' or the

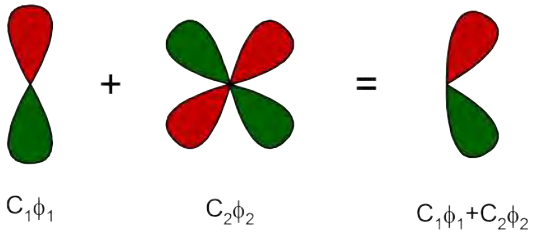

Fig. 2.2: Polarisation of the p-orbital.[11]

function that must be added, e.g 6-31G** or 6-31G(d,p).

To describe the electron distribution further away from the nucleus, which may include electrons in lone-pairs, anions, supermolecular complexes or excited states, diffuse functions must be used. These allow weakly bound electrons to be localised far away from the nuclei. The diffuse functions are Gaussians with small values of α, thus the function falls off very slowly and are able to generate electron density far from the nucleus. Inclusion of a diffuse function on heavy atoms in the Pople type basis sets is denoted by '+' for heavy atoms, e.g 6-31+G(d,p), and '++' for the inclusion on both heavy and hydrogen atoms, e.g 6-31++G(d).

2.2 Density Functional Theory

2.2.1 The Hohenberg-Kohn Theorems

Hohenberg and Kohn showed through a proof by *reductio ad absurdum* that the electron density uniquely determines the Hamilton operator and thus all properties of the molecular system.[12] The first Hohenberg-Kohn theorem states that the external potential $V_{ext}(r)$ is a unique functional of $\rho(r)$; since in turn $V_{ext}(r)$ fixes $\hat{H}$ the full many particle ground state is a unique functional of $\rho(r)$. In other words, any property of a molecule in an electronic ground state is a functional of the ground state electron density function,

$$E_o = F[\rho_o] = E[\rho_o] \tag{2.33}$$

This is merely an existence theorem, which states that the functional F exists, but does not prescribe a method of finding it.[13]

The second theorem states that $F_{HK}[\rho(r)]$, the functional that delivers the ground state energy of the system, delivers the lowest energy if and only if the density is the true ground state density, $\rho_o(r)$, which is the variational principle that can be expressed as

$$E_o[\rho_o] \leq E_\nu[\rho_t] \tag{2.34}$$

where ρ_t is the trial electronic density and E_0 is the true ground state energy corresponding to the true electronic density ρ_0. The trial density must satisfy the conditions $\int \rho_t(r)dr = n$ where n is the number of electrons in the molecule.

2.2.2 Kohn-Sham approach

The Hohenberg-Kohn theorems are put to work by the Kohn-Sham approach. A key idea is the concept of the fictitious non-interacting reference system defined as one in which electrons do not interact and in which the ground state electron density ρ_r of such a system is the same as the ground state density of the real system, i.e.

$$\rho_r = \rho_0 \tag{2.35}$$

Non-interacting electrons are readily treated exactly and the deviations from the behaviour of the real system are swept into a small term involving the unknown functional.[3] The ground state electronic energy of the real molecule is the sum of the electron kinetic energies, the nucleus-electron potential energies and the electron-electron repulsion energies,

$$E_0 = \langle T[\rho_0] \rangle + \langle V_{Ne}[\rho_0] \rangle + \langle V_{ee}[\rho_0] \rangle \tag{2.36}$$

The second term in equation (2.36), the nucleus-electron potential energy, is summed over all 2n electrons for a restricted system and can be expressed as

$$\langle V_{Ne} \rangle = \sum_{i=1}^{2n} \sum_{A} -\frac{Z_A}{r_{iA}} = \sum_{i=1}^{2n} \nu(r_i) \tag{2.37}$$

where $\frac{Z_A}{r_{iA}}$ is the potential energy due to the interactions between electron i and nucleus A at a distance r_{iA}. The double sum can be written more compactly and the electron density function is introduced.

$$\langle V_{Ne} \rangle = \int \psi \sum_{i=1}^{2n} \nu(r_i) \psi dr = \int \rho_0 \nu(r) dr \tag{2.38}$$

The total energy can be written as

$$E_0 = \langle T[\rho_0] \rangle + \int \rho_0(r) \nu(r) dr + \langle V_{ee}[\rho_0] \rangle \tag{2.39}$$

Addressing the electronic kinetic energy, the quantity $\Delta\langle T[\rho_0] \rangle$ is defined as the deviation of the real electronic kinetic energy from that of the reference system of non-interacting particles:

$$\Delta\langle T[\rho_0] \rangle \quad = \quad \langle T[\rho_0] \rangle_{real} - \langle T[\rho_0] \rangle_{ref} \tag{2.40}$$

Addressing next the electronic potential energy, the quantity $\Delta\langle V_{ee} \rangle$ is the deviation of the real electron-electron repulsion energy which is a summation of all energy from a classical charge-cloud coulomb repulsion energies for pairs of infinitesimal volume elements $\rho(r_1)dr_1$ and $\rho(r_2)dr_2$ separated by the distance r_{12}

$$\Delta\langle V_{ee}[\rho_0] \rangle = \langle V_{ee}[\rho_0] \rangle_{real} - \frac{1}{2} \int \int \frac{\rho_0(r_1)\rho_0(r_2)}{r_{12}} dr_1 dr_2 \tag{2.41}$$

substituting equation 2.40 and 2.41 into equation (2.38) the total electronic energy is written as

$$E_0 = \int \rho_0 \nu(r) dr + \langle T[\rho_0] \rangle_{ref} + \frac{1}{2} \int \int \frac{\rho_1(r_1)\rho_2(r_2)}{r_{12}} dr_1 dr_2 + \Delta\langle T[\rho_0] \rangle + \Delta\langle V_{ee}[\rho_0] \rangle \tag{2.42}$$

The last two terms encapsulate the main problem in density functional theory, the sum of the kinetic energy deviation from the reference system and the electron-electron repulsion energy deviation from the classical system. This is the exchange-correlation energy, which is a functional of the electron density

$$E_{XC}[\rho_0] = \Delta\langle T[\rho_0] \rangle + \Delta\langle V_{ee}[\rho_0] \rangle \tag{2.43}$$

Analogous to the derivation of the Hartree-Fock equations, the Kohn-Sham equations are obtained by variation of the electronic energy with respect to the Kohn-Sham molecular orbitals (ψ_i^{KS}) as the electron density is defined as

$$\rho_0 = \rho_r = \sum_{i=1}^{2n} |\psi_i^{KS}|^2 \tag{2.44}$$

Substituting 2.44 into the energy expression and varying E_0 with respect to the ψ_i^{KS}, subject to the constraint that the orbitals remain orthonormal, leads to the Kohn-Sham equations

$$[-\frac{1}{2}\nabla_i^2 - \sum_{nuclei} \frac{Z_A}{r_{iA}} + \int \frac{\rho(r_2)}{r_{12} dr_2} + \nu_{XC}(1)]\psi_i^{KS}(1) = \epsilon_i^{KS}\psi_i^{KS}(1) \tag{2.45}$$

where ϵ_i^{KS}s are the KS energy levels and $\nu_{XC}(1)$ is the exchange correlation potential, which is the functional derivative of the exchange-correlation energy $E_{XC}[\rho_0]$ with respect to the electron density $\rho(r)$, i.e.,

$$\nu_{XC}(1) = \frac{\delta E_{XC}[\rho_0]}{\delta \rho(r)} \tag{2.46}$$

The entire expression in the square brackets in equation (2.45) is the KS operator,

Tab. 2.2: Common functionals in density functional theory

Functional	Type	χ	exchange functional	correlation functional
BLYP	GGA	0	Becke88	Lee–Yang–Parr
B3LYP	H-GGA	20	Becke88	Lee-Yang-Parr
B3PW91	H-GGA	20	Becke88	Perdew–Wang91
BP86	GGA	0	Becke88	Perdew86
M05-2X	HM-GGA	56	M05-2X	M05-2X
M06-2X	HM-GGA	54	M06-2X	M06-2X

$\hat{h}^{KS}(1)$, making the KS equations

$$\hat{h}^{KS}(1)\psi_i^{KS}(1) = \epsilon_i^{KS}\psi_i^{KS}(1) \tag{2.47}$$

The strategy of solving the eigenvalue equation in (2.47) is to expand the KS orbitals in terms of the basis functions ϕ

$$\psi_i^{KS} = \sum_{s=1}^{m} c_{si}\phi_s \tag{2.48}$$

Substituting the basis set expansion into the KS equation and multiplying by $\phi_1, \phi_2, ..., \phi_m$ leads to a set of m equations which are sub-summed into a single matrix equation, analogous to the HF equation $\mathbf{FC} = \mathbf{SC}\epsilon$. In DFT, a guess of the electron density $\rho(r)$ for the explicit expression of the KS operator $\hat{h}^{KS}$ is necessary. The Fock matrix elements must then be calculated and the matrix diagonalized, which gives the initial guesses for the coefficients in the basis set expansion. The new coefficients are used to calculate a set of KS molecular orbitals, which are then used to calculate a better $\rho(r)$ and used to calculate improved matrix elements, which give improved coefficients until convergence of some criteria is reached.

2.2.3 Exchange-Correlation Functional

The quality of the density functional hinges on how accurately the chosen approximation to E_{XC} is. Improving the functional is the main goal in density functional

theory. Methods that try to approximate E_{XC} are mostly based on the Local Density Approximation (LDA), which makes the assumption that at every point in the molecule the energy density (exchange-correlation energy per electron) at that point is the same as that of a homogeneous electron gas with the same density at that point. This is considered "local" as the energy density at a point depends only on the value of the electron density at that point. Functionals that use the gradient and the first derivative of ρ with respect to the position are said to use the Generalized-Gradient Approximation (GGA) and are an improvement on LDA methods. Meta-GGA Functionals are an improvement on GGA functionals and use the second derivative of the electron density to obtain the exchange correlation functionals. Hybrid GGA functionals are those to which Hartree-Fock exchange has been added. The exchange correlation energy is taken as the the weighted sum of the Hartree-Fock exchange energy and the DFT exchange correlation energy. Hybrid Meta-GGA functionals add the Hartree-Fock exchange to the meta-GGA functionals.[3,14] Examples of common functionals are displayed in table 2.2, where χ is the percentage Hartree-Fock exchange energy.

2.3 Molecular Mechanics

Force field methods work on the assumption provided by the Born-Oppenheimer approximation that separates nuclear motion from electronic motion. They ignore electronic motion and calculate the energy of a system using only the position of the nuclei.

Force field methods are used when *ab initio* or DFT methods become too computationally expensive.

2.3.1 Force Field

Force fields in use today are interpreted as a sum of four components of inter and intramolecular forces within the molecular system. The energy given by such a force field may be written as the sum of potentials that describe bond stretching,

angle bending, changes in the torsion angle and non-bonded interactions, i.e

$$V(r^N) = E_{bonds} + E_{angles} + E_{torsions} + E_{non-bonded} \tag{2.49}$$

$V(r^N)$, the potential energy, is a function of the position, r, of N particles.

Bond Stretch

The functional form of the first term in (2.49) is typically written as

$$E_{bonds} = \sum_{bonds} \frac{k_i}{2}(l_i - l_{i,0})^2 \tag{2.50}$$

It describes the interaction between bonded atoms, modeled by a harmonic potential that gives an energy penalty as the bond length l_i deviates from the reference or "equilibrium" value $l_{i,0}$. The force constant k_i describes the strength of the bond. The function is a reasonable approximation to the shape of the Morse potential energy curve of a bond at the bottom of the potential well around distances that correspond to bonding in ground-state molecules.

Angle Bend

The functional form of the second term in (2.49) can be expressed in terms of Hooke's law akin to the potential given for the bond stretch,

$$E_{angles} = \sum_{angles} \frac{k_i}{2}(\theta_i - \theta_{i,0})^2 \tag{2.51}$$

It is a summation over all valence angles in the molecule. The valence angles are the angles between atoms A–B–C with atoms A and C bonded to atom B. The contribution of each angle is characterised by the force constant k_i and the reference angle $\theta_{i,0}$.

Torsion angle

The third term is a torsional potential that models how the energy changes as rotation about chemical bonds occurs. Its functional form is typically given as

$$E_{torsion} = \sum_{torsions} \frac{V_n}{2}(1 + cos(n\omega - \gamma)) \tag{2.52}$$

ω is the torsion angle and V_n describes the relative barriers to rotation around bonds. γ is the phase factor and determines where the torsion angle passes its minimum. The multiplicity, n, gives the number of minima in the function as a bond is rotated through angles 0° to 360°.

Non-bonded interactions

The fourth term in (2.49) is the energy of the non-bonded term calculated between pairs of atoms i and j which are either on different molecules or are within the same molecule but separated by at least three bonds. The functional form of this term is written as

$$\sum_{i=1}^{N} \sum_{j=i+1}^{N} \left(4\epsilon_{ij} \left[(\frac{\sigma_{ij}}{r_{ij}})^{12} - (\frac{\sigma_{ij}}{r_{ij}})^{6} \right] + \frac{q_i q_j}{4\pi\epsilon_0 r_{ij}} \right) \tag{2.53}$$

The non-bonded term is modelled by the Lennard-Jones potential for van der Waals interactions and the Coulomb potential term for the electrostatic interactions. The van der Waals interactions, which are dispersion forces as a result of induced dipole-dipole interactions and repulsive short-range exchange forces that find their roots in the Pauli principle, are modelled by the Lennard-Jones 12-6 function. It contains two parameters, ϵ_{ij} is the well depth of the curve and σ_{ij} is the collision diameter, which is the distance or separation that produces zero energy. The electrostatic interactions between non-bonded atoms are described as a sum of interactions between pairs of point charges q_i and q_j. The charges are restricted to the nuclear centre and are called partial charges

The functional form of the total energy can thus be written as

$$V(r^N) = \sum_{bonds} \frac{k_i}{2}(l_i - l_{i,0})^2 + \sum_{angles} \frac{k_i}{2}(\theta_i - \theta_{i,0})^2 + \sum_{torsions} \frac{V_n}{2}(1 + cos(n\omega - \gamma)) + \sum_{i=1}^{N} \sum_{i=j+1}^{N} \left(4\epsilon_{ij} \left[(\frac{\sigma_{ij}}{r_{ij}})^{12} - (\frac{\sigma_{ij}}{r_{ij}})^{6} \right] + \frac{q_i q_j}{4\pi\epsilon_0 r_{ij}} \right) \quad (2.54)$$

2.3.2 Molecular Dynamics Simulations

Molecular dynamics simulations calculate the real dynamics of a system from which time-averages of properties can be calculated. The sets of atomic positions are derived by solving of the differential equation corresponding to Newton's second law,

$$\frac{d^2 x_i}{dt^2} = \frac{F_{xi}}{m_i} \quad (2.55)$$

which describes the motion of a particle with mass m_i along a coordinate x_i acted upon by a force F_{xi} in the direction of the coordinate x_i. The continuous nature of the potential (and thus the force) described by equation (2.54) requires the equations of motions to be integrated by breaking up the calculations into a series of time steps δt. At each time step t, the forces on each of the atoms are calculated as the sum of interactions with other particles. The forces combined with the current position and velocity of the atoms move the atoms to new positions. The forces on the atoms are again, calculated and the same procedure is repeated. The simulations thus generate a trajectory that describes how the dynamics of the system changes over time.

Finite Difference Methods

One method for integrating the equations of motion is the finite difference method. The Verlet algorithm[15] uses the positions and accelerations at time t and the position at the previous step $r(t - \delta t)$ to calculate the new position at $t + \delta t$,

$r(t+\delta t)$. The relationship between $r(t-\delta t)$ and $r(t+\delta t)$ with the velocities at time t is

$$r(t+\delta t) = r(t) + \delta t v(t) + \frac{1}{2}\delta t^2 a(t) + \cdots \quad (2.56)$$

$$r(t-\delta t) = r(t) - \delta t v(t) + \frac{1}{2}\delta t^2 a(t) + \cdots \quad (2.57)$$

adding the two equations together yields

$$r(t+\delta t) = 2r(t) - r(t-\delta t) + \delta t^2 a(t) \quad (2.58)$$

The velocity can be calculated as the difference between the positions $r(t+\delta t)$ and $r(t-\delta t)$ divided by the time $2\delta t$.

$$v(t) = \frac{r(t+\delta t) - r(t-\delta t)}{2\delta t} \quad (2.59)$$

The disadvantage with using the Verlet algorithm is that it lacks an explicit velocity term and it may lead to a lack of precision as the relatively small term $\delta t^2 a(t)$ is added to the difference between two large terms $2r(t)$ and $r(t-\delta t)$. A variation to the Verlet algorithm is the Leap-frog algorithm that uses the relationships

$$r(t+\delta t) = r(t) + \delta t v(t+\frac{1}{2}\delta t) \quad (2.60)$$

$$v(t+\frac{1}{2}) = v(t-\frac{1}{2}\delta t) + \delta t a(t) \quad (2.61)$$

The velocities $v(t+\frac{1}{2}\delta t)$ must first be calculated by using the velocity at time $t-\frac{1}{2}\delta t$ and the acceleration at time t. The position $r(t+\delta t)$ is then calculated from the new velocities and the position at time t. The velocities at time t can be calculated as the sum of the velocities at times $t+\delta t$ and $t-\delta t$ divided by 2. This method explicitly includes velocity and does not calculate the difference

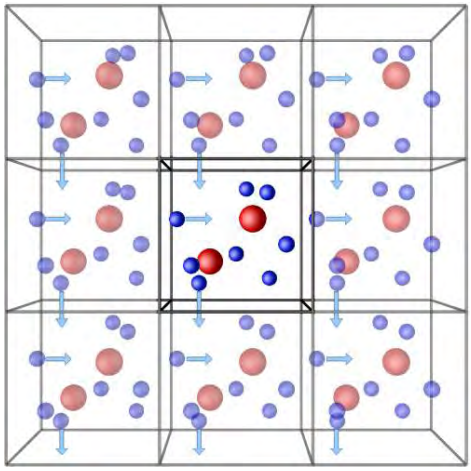

Fig. 2.3: Schematic representation of the periodic boundary conditions.[16]

between two large numbers. The velocity Verlet method calculates the position, velocities and accelerations at the same time and does not compromise precision, it is expressed as

$$r(t+\delta t) = r(t) + \delta t v(t) + \frac{1}{2}\delta t^2 a(t) \tag{2.62}$$

$$v(t+\delta t) = v(t) + \frac{1}{2}\delta t[a(t) + a(t+\delta t)] \tag{2.63}$$

Boundaries

Periodic boundary conditions enable a simulation to be performed using a relatively small amount of particles in such a manner that particles experience forces as if they were in bulk fluid. The particles in the box are replicated in all directions to give a periodic array of the system. Should a particle leave the box during a simulation, it is replaced replaced by its image on the opposite side of the box. The number of particles in the box remains constant. An example of using periodic boundary conditions is shown in figure 2.3.

Truncating Potential and the Minimum Image Convention

The most time consuming part of calculating the forces in a simulation is the evaluation of the non-bonded terms that increase as the square of the number of atoms (N^2). A way to make the calculation of non-bonded interactions more efficient is to introduce the concept of a non-bonded cut-off and apply a minimum image convention. The non-bonded cut-off sets all non-bonded interactions with other particles which are further away than the value of the cut-off to zero, it simplifies non-bonded interactions to being only for the pairs of atoms with "neighbouring" particles or atoms. The value of the cut-off must not be so large such that the atoms or particle experiences a potential with its own image or with the same atom twice. The cut-off should thus, for a system which employs periodic boundary conditions, be half the distance of of the box length. The minimum image convention ensures that every particle experiences the potential as a result of interaction with only one image of every other atom or particle in the system.

To determine whether or not another atom lies within the cut-off value, the distance between an atom and all other atoms must be calculated for each step in the simulation. Fortunately, the atoms within the cut-off distance, called the neighbour list, do not change significantly over short times, which makes it possible to calculate each atom's "neighbour" without calculating the distance between all other atoms. In practise this is done by constructing a list of nearest neighbours that are slightly beyond the cut-off, which is updated at set intervals.

It is useful to use different cut-off values for electrostatic interactions and van der Waals interactions as electrostatic interactions have a much longer range. The use of cut-offs is justified, in most cases, on the grounds of being both practical and convenient.

Ewald Summation[17]

Electrostatic interactions decays slowly over a distance that may be larger than half of the box length and is problematic in molecular dynamics simulations. This is particularly important when simulating charged species and calculating certain properties such as the dielectric constant. In the Ewald summation method, all interacting particles interact with all other particles in the simulation cell and all their images in the infinite periodic cells. The position of each image box is related to that of the central box by specifying a vector that is a multiple of the box length. The neighbouring boxes are at distances nL from the central box. The interactions between the charges in the central box with the charges in the image box is given by

$$V = \frac{1}{2} \sum_{|\mathbf{n}|=0}^{\infty} \sum_{i=1}^{N} \sum_{j=1}^{N} \frac{q_i q_j}{4\pi\epsilon_0 |r_{ij} + \mathbf{n}|} \tag{2.64}$$

where $\mathbf{n}$ is the position at a cubic lattice point ($n_x L, n_y L, n_z L$ with n_x, n_y, n_z being integers). The series does not include the interactions $i = j$ for $\mathbf{n} = 0$, i.e. for interactions in the central box or between interactions within the same cut-off.

The summation in equation (2.64) converges extremely slowly and is *conditionally convergent*. Conditionally convergent series are those that contain positive and negative contributions to the series, these contributions in themselves form a divergent series. Conditionally convergent series also depend on the order in which its terms are considered. To deal with such a problem in the Ewald method, the summation is split into two series, which in themselves converge rapidly.

The first sum considers each charge interacting with a neutralizing charge distribution, it is given as,

$$V = \frac{1}{2} \sum_{|\mathbf{n}|=0}^{\infty} \sum_{i=1}^{N} \sum_{j=1}^{N} \frac{q_i q_j}{4\pi\epsilon_0} \frac{\mathrm{erfc}(\alpha |\mathbf{r}_{ij} + \mathbf{n}|)}{|\mathbf{r}_{ij} + \mathbf{n}|} \tag{2.65}$$

The summation in equation (2.65) is described as the "real space" summation. erfc is the complimentary error function and α specifies the width of the Gaussian. A second charge distribution is added that counteracts exactly the first neutralising distribution,

$$V = \frac{1}{2}\sum_{\mathbf{k}\neq 0}\sum_{i=1}^{N}\sum_{j=1}^{N}\frac{1}{\pi L^3}\frac{q_i q_j}{4\pi\epsilon_0}\frac{4\pi^2}{k^2}\exp\Big(\frac{-\mathbf{k}^2}{4\alpha^2}\Big)\cos(\mathbf{k}\cdot\mathbf{r}_{ij}) \tag{2.66}$$

where vectors $\mathbf{k}$ are reciprocal vectors defined as $\frac{2\pi\mathbf{n}}{L^2}$. The summation in equation (2.66) is performed in reciprocal space. The sum of the Gaussian functions in real space includes interactions of each Gaussian with itself. This self interaction is corrected by

$$V = -\frac{\alpha}{\sqrt{\pi}}\sum_{k=1}^{N}\frac{q_k^2}{4\pi\epsilon_0} \tag{2.67}$$

Finally, a correction term for the medium surrounding the simulation boxes is introduced. If the surrounding medium is a vacuum, the following energy must be added,

$$V = \frac{2\pi}{3L^3}\left|\sum_{i=1}^{N}\frac{q_i}{4\pi\epsilon_0}\mathbf{r}_i\right|^2 \tag{2.68}$$

The final expression given by the Ewald sum is

$$\begin{aligned} V \;=\; & \sum_{i=1}^{N}\sum_{j=1}^{N}\left(\frac{1}{2}\sum_{|\mathbf{n}|=0}^{\infty}\frac{q_i q_j}{4\pi\epsilon_0|r_{ij}+\mathbf{n}|}+\frac{1}{2}\sum_{\mathbf{k}\neq 0}\frac{q_i q_j}{4\pi\epsilon_0}\frac{4\pi^2}{k^2}\exp\Big(\frac{-\mathbf{k}^2}{4\alpha^2}\Big)\cos(\mathbf{k}\cdot\mathbf{r}_{ij})\right. \\ & \left.-\frac{\alpha}{\sqrt{\pi}}\sum_{k=1}^{N}\frac{q_k^2}{4\pi\epsilon_0}+\frac{2\pi}{3L^3}\left|\sum_{k=1}^{N}\frac{q_i}{4\pi\epsilon_0}\mathbf{r}_k\right|^2\right) \end{aligned} \tag{2.69}$$

2.4 The Quantum Theory of Atoms in Molecules (QTAIM)

Each topological feature of the electron density ,ρ, has an associated critical point at r_c where $\nabla\rho(r_c) = 0$ and r_c is the coordinate at the critical point.[18,19] Each component in the derivative is zero and not just the sum of the derivatives. The critical points are evident in the relief map of the electron density in figure 2.4

The behaviour of the the density around the critical point is obtained by a Taylor series expansion, retaining only up to the second-order, the second derivative of the density. The second derivatives of the electron densities are ordered into a three-by-three matrix called the Hessian matrix of $\rho(r)$ ($\mathrm{A(r_c)}$),

$$\mathrm{A(r_c)} = \begin{pmatrix} \frac{\partial^2\rho}{\partial x^2} & \frac{\partial^2\rho}{\partial x\partial y} & \frac{\partial^2\rho}{\partial x\partial z} \\ \frac{\partial^2\rho}{\partial y\partial x} & \frac{\partial^2\rho}{\partial y^2} & \frac{\partial^2\rho}{\partial y\partial z} \\ \frac{\partial^2\rho}{\partial z\partial x} & \frac{\partial^2\rho}{\partial z\partial y} & \frac{\partial^2\rho}{\partial z^2} \end{pmatrix} \tag{2.70}$$

The Hessian matrix is diagonalized to obtain Λ, whose diagonal elements are the three eigenvalues called the principle curvatures and the corresponding eigenvectors.[18]

$$\Lambda = \begin{pmatrix} \lambda_1 & 0 & 0 \\ 0 & \lambda_2 & 0 \\ 0 & 0 & \lambda_3 \end{pmatrix} \tag{2.71}$$

The rank, ω, is the number of non-zero eigenvalues and the signature, σ, is the

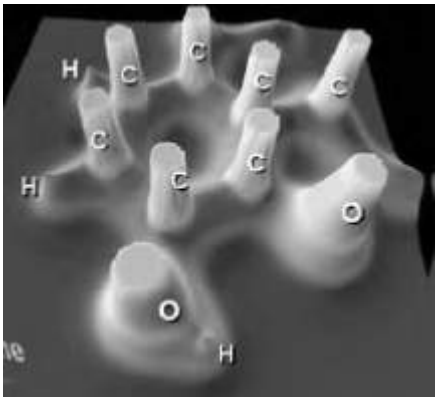

Fig. 2.4: A schematic of the relief map of the electron density.[18]

algebraic sum of the signs of the eigenvalues. The rank and the signature are used to characterise the critical points by (ω, σ). There are four types of critical points:

- (3, -3) are the nuclear critical points topologically described by three negative eigenvalues, i.e. a local maximum of ρ,
- (3, -1) are the bond critical points characterised by two negative curvatures and a single positive curvature,
- (3, +1) are the ring critical points characterised by one negative curvature and a single negative curvature and
- (3, +3) are the cage critical points characterised by three positive curvatures which corresponds to a local minima of ρ.

The topology of the electron density allows for the partitioning of a molecule into spaces of mononuclear regions by a surface of zero flux in the gradient vector field of the electron density i.e.,

$$\nabla\rho(\mathbf{r}) \cdot n(\mathbf{r}) = 0, \text{for r} \in \text{S} \tag{2.72}$$

where r is the position vector and $n(r)$ the unit vector normal to the surface S. These mononuclear regions constitute atoms in molecules. Between two bonded atoms is a surface of zero-flux and a line of locally maximum density that links the nuclei. The point of intersection of the locally maximum line, called the bond path, with the surface of zero-flux is the bond critical point (BCP). The BCP is also the lowest point on the bond path. The bond path is an indicator of chemical bonding and properties at the BCP, such as the density and energy density, are used to characterize chemical bonding.

2.4.1 Properties at the BCP

Electron Density at the Bond Critical Point

The electron density at the bond critical point is an indication of the strength of interaction between bonded atoms. Typically, ρ at r_c is greater than 0.20 a.u. in covalent interactions and is less than 0.10 a.u. in closed-shell interactions.

The Laplacian

The curvatures perpendicular to the bond path, λ_1 and λ_2, are negative whilst the third, λ_3, lies along the bond path. The negative curvatures indicate the extent to which electrons accumulate perpendicular to the bond path and the positive curvature indicates the extent to which the density is depleted along the bond path. The Laplacian is thus negative for covalent interactions and positive for closed-shell bonding, e.g. hydrogen bonding or van der Waals interactions.

Energy Densities

The potential energy density *V(**r**)* is the average effective potential experienced by an electron at the position $\mathbf{r}$ in a many particle system. Once found, using the virial theorem, the kinetic energy density can be calculated. The total energy density can be written as,

$$H(\mathbf{r}) = G(\mathbf{r}) + V(\mathbf{r}) \tag{2.73}$$

where $G(\mathbf{r})$ is the gradient kinetic energy density:

$$G(\mathbf{r}) = \frac{\hbar^2}{2m} N \int \nabla\Psi^* \cdot \nabla\Psi d\tau' \tag{2.74}$$

and V is the potential energy density. The energy density is negative for covalent

interactions and its magnitude reflects the extent to which electrons are shared in interacts.[18]

2.5 Non-Covalent Index

The success of DFT in finding structure, energies and various other properties of atoms and molecules at a much less significant computational cost than wavefunction based methods has made it an integral part of theoretical and computational chemistry.[20] DFT finds its theoretical roots in Hohenberg and Kohn's description of the "Inhomogeneous Electron Gas" following Thomas and Fermi's description of the homogeneous electron gas.[12] The first Hohenberg-Kohn theorem states that the ground-state electron density uniquely determines the ground-state energy and all other ground state electronic properties of atoms or molecular systems. In this theory, the ground-state energy is a functional of the electron density, $\boldsymbol{\rho(r)}$, for a given external potential, $\nu(\mathbf{r})$.

The Kohn-Sham method,[21] which is derived analogous to the Hartree-Fock self-consistent field method, is an application of the Hohengerg-Kohn theory in which the total Kohn-Sham energy of the system is considered as the sum of the kinetic energy of electrons of the reference system of non-interacting electrons, electron-nuclear potential, the electrostatic repulsion of electrons and the exchange-correlation energy. Finding a good exchange-correlation functional is the main problem in DFT research.

Methods that utilize the the electron density and its gradient to obtain an exchange-correlation functional are termed the Generalized Gradient Approximation (GGA) methods. To improve GGA exchange-correlation functionals, the reduced density gradient (RDG), s, shown in equation (2.75), is used; it describes how fast $\boldsymbol{\rho}$ varies on the scales of the local Fermi-wavelength, $2\pi/C_F$.[22,23]

$$s = C_F \frac{|\nabla\rho(r)|}{2\rho(r)^{1/3}} \tag{2.75}$$

$$C_F = \frac{1}{(3\pi^2\rho(r))^{1/3}}$$

2.5.1 Using the Reduced Density Gradient in Identifying Interactions

It was the RDG, a fundamental dimensionless property, that was used by Yang et al. to describe non-covalent interactions for chemical systems.[24] In density tails, which are regions where the electron density is low, the RDG takes up high values and approaches zero in regions where both covalent and non-covalent interactions take place. Regions of non-covalent interactions are characterised by a combination of low density and an RDG that approaches zero. The RDG is thus able to identify the existence of non-covalent interactions and is not subjected to any 'catastrophe' as it is continuous.

The electron density and its gradient can be calculated at points in grid-space, thus the RDG can be found at each grid-point and can be mapped to real space. Yang et al. presented a work-flow for applying the RDG to find non-covalent interactions. The freely available program, NCIPLOT, can be used for doing this analysis.[25]

2.5.2 Calculating the Reduced Density Gradient

$\boldsymbol{\rho}$ and $|\boldsymbol{\nabla\rho}|$ can then be used to find s at each point in the grid-space using equation (2.75). A plot of $\boldsymbol{\rho}$ vs. $\boldsymbol{s}$ is illustrated for a 1-ethyl-3-methylimidazolium chloride ion-pair in figure 2.5 as an example. As covalent bonds are approached, there is an increase in $\rho(r)$ and $\boldsymbol{s} \to 0$, this would be demonstrated in figure 2.5 if the x-axis were extended to the right. Moving into the electron density tails, $\boldsymbol{\rho} \to 0$ much faster than $\boldsymbol{\nabla\rho} \to 0$, s, as a result, tends to very large values as seen in figure 2.5. The peaks, outlined in the figure represent non-covalent interactions. In the case of the ion-pair the peaks are as a result of the weak dispersion type interactions, the stronger hydrogen bond and steric repulsion within the imidazolium ring. At this

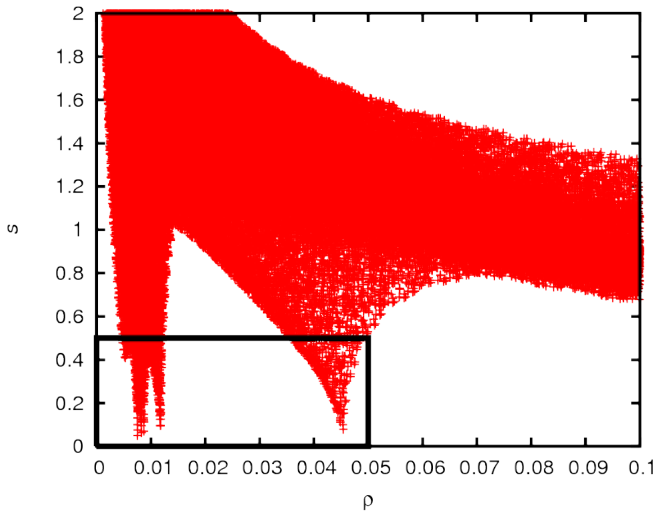

Fig. 2.5: The blocked region represents all non-covalent interactions.

stage, non-covalent interactions can be found but the peaks in figure 2.5 cannot differentiate attractive from repulsive interactions. The quantum theory of atoms in molecules (QTAIM) provides clues which allow for the discernment between attractive and repulsive interactions.[25,26]

In Bader's QTAIM, the second derivative of ρ is structured into the Hessian and allows for the discrimination between local minima, maxima and saddle-points. The eigenvalues of the Hessian can be ordered from the largest to the smallest values, the element in Λ with the smallest numerical value is relabeled λ_1 and the largest, λ_3. The second eigenvalue, λ_2, is negative when there is an accumulation of electron density perpendicular to a bond path and corresponds to an attractive interaction. Depletion of electron density is associated with a positive value of λ_2 and describes a repulsive interaction. The sign of λ_2 thus allows for the differentiation between bonding (attractive) interactions ($\lambda_2 < 0$) and non-bonded (repulsive) interactions ($\lambda_2 > 0$).[24,25]

Multiplying ρ by sign(λ_2) and plotting against s reveals both bonding and non-bonding interactions, shown for an [emim][Cl] ion-pair in figure 2.6 as an example. An isosurface value for s at a value of 0.5 is plotted in real space (see figure 2.7) . The values of $\rho \times sign(\lambda_2)$ are mapped onto the isosurface using a colour scale that ranges from blue, for strong attractive interactions to green, for weak interactions,

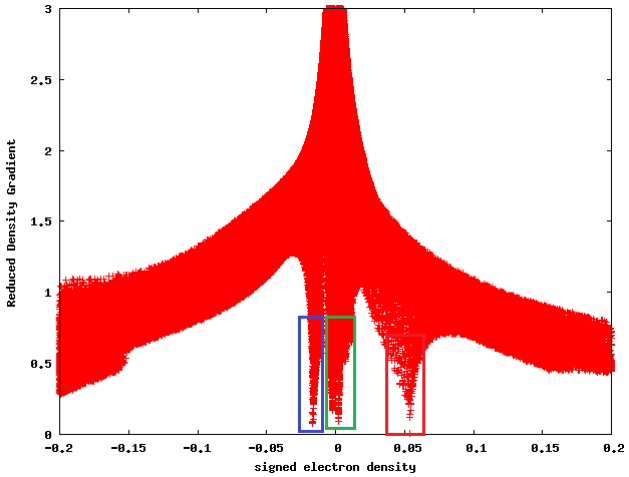

Fig. 2.6: The RDG plotted on the y-axis against $sign(_2)\rho$ on the x-axis revealing attractive and repulsive non-covalent interactions

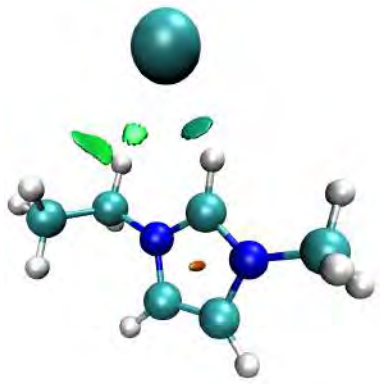

Fig. 2.7: sign(ρ) plotted on the reduced density isosurface

to red, for strong repulsive interactions. The red block in figure 2.6 highlights the repulsive ring strain present in the imidazolium ring , the green block corresponds to the weak van der Waals interactions between $[Cl]^-$ and $[emim]^+$ and finally the hydrogen bond is highlighted in the blue block.

A NCI analysis describes three types of interactions well; hydrogen bonding, steric repulsion and dispersion interactions, classified as type I, type II and type III by Chaudret et. al.[27] The strength of these interactions can be estimated by the position of the peak in the 2-D NCI plots, weak interaction such as dispersion will be found in the centre of the plot with values of ρ close to zero, whilst stronger interactions such as hydrogen bonding will be found at the periphery of the plot. A NCI analysis is not a complete descriptor of all types of interactions, only those that significantly affect the topology of the electron density. This means that

electrostatic interactions might not be clearly quantifiable within the current NCI framework. However, NCI remains a useful tool in analysing non-covalent interactions, particularly because all the information is extracted from the observable electron density, which makes it consistent with a QTAIM approach.

Bibliography

[1] Cramer, C. J. *Essentials of Computational Chemistry*, second edition ed.; John Wiley & Sons: Chichester, 2004.

[2] Jensen, F. *Introduction to Computational Chemistry*; John Wiley & Sons: Chirchester, 1999.

[3] Lewars, E. G. *Computational Chemistry: Introduction to Theory and Applications of Molecular and Quantum Mechanics*, second edition ed.; Springer, 2011.

[4] Szabo, A.; Ostlund, N. S. *Modern Quantum Chemistry: Introduction to Advanced Electronic Structure Theory*, first edition, revised ed.; Dover Publications, Inc., 1996.

[5] Born, M.; Oppenheimer, R. *Annalen der Physik* **1927**, *389*, 457–484.

[6] Slater, J. C. *Phys. Rev.* **1929**, *34*, 1293–1322.

[7] Roothaan, C. C. J. *Rev. Mod. Phys.* **1951**, *23*, 69–89.

[8] Hall, G. G. *Proc. R. Soc. London, Ser. A* **1951**, *205*, 541–552.

[9] Stewart, R. F.; Hehre, W. J.; Pople, J. A. *J. Chem. Phys.* **1969**, *51*.

[10] Slater Function Approximation. `http://rimg.geoscienceworld.org/content/42/1/199/F11.large.jpg`, Accessed: 2014-10-01.

[11] Polarisation of p-orbital. `http://upload.wikimedia.org/wikipedia/commons/thumb/a/a7/D-polarization_function.png/200px-D-polarization_function.png`, Accessed: 2014-10-02.

[12] Hohenberg, P.; Kohn, W. *Phys. Rev.* **1964**, *136*, B864–B871.

[13] Koch, W.; Holthausen, M. C. *Guide to Density Functional Theory*, second edition ed.; Wiley-VCH Verlag GmbH, 2001.

[14] Sousa, S. F.; Fernandes, P. A.; Ramos, M. J. *J. Phys. Chem. A* **2007**, *111*, 10439–10452.

[15] Verlet, L. *Phys. Rev.* **1967**, *159*, 98–103.

[16] Periodic Boundary Conditions. `http://isaacs.sourceforge.net/phys/pbc.html`, Accessed: 2014-10-13.

[17] Leach, A. R. *Molecular Modelling: Principles and Applications*; Addison Wesley Longman Limited, 1996.

[18] Matta, C. F.; Boyd, R. J. *The Quantum Theory of Atoms in Molecules*; WILEY-VCH Verlag GmbH Co., 2007.

[19] Bader, R. F. W. *Atoms in Molecules - A Quantum Theory*; Oxford University Press, 1990.

[20] Geerlings, P.; De Proft, F.; Langenaeker, W. *Chem. Rev.* **2003**, *103*, 1793–1873.

[21] Kohn, W.; Sham, L. J. *Phys. Rev.* **1965**, *140*, A1133–A1138.

[22] Perdew, J. P.; Burke, K.; Ernzerhof, M. *Phys. Rev. Lett.* **1996**, *77*, 3865–3868.

[23] Perdew, J. P.; Burke, K.; Wang, Y. *Phys. Rev. B: Condens. Matter* **1996**, *54*, 16533–16539.

[24] Johnson, E.; Keinan, S.; Paula, M.; Julia, C.; Cohen, A.; Yang, W. *J. Am. Chem. Soc.* **2010**, *132*, 6498–6506.

[25] Julia, C.; Johnson, E.; Keinan, S.; Chaudret, R.; Piquemal, J.; Beratan, D.; Yang, W. *J. Chem. Theory Comput.* **2011**, *7*, 625–632.

[26] Wu, P.; Chaudret, R.; Hu, X.; Yang, W. *J. Chem. Theory Comput.* **2013**, *9*, 2226–2234.

[27] Chaudret, R.; de Courcy, B.; Contreras-Garcia, J.; Gloaguen, E.; Zehnacker-Rentien, A.; Mons, M.; Piquemal, J. *Phys. Chem. Chem. Phys.* **2013**,

3

Analysis of the Gas Phase Ion-Pair

In this chapter, the nature of the intermolecular interactions is investigated in 1-ethyl-3-methylimidazolium based ion-pairs (see figure 3.1 for atom labels). This serves as a precursor to the study of the interactions in ILs in their liquid environment. Evaluating the ion-pair allows for the 'pure' interaction between ions to be investigated and the changes in those interactions by moving into the liquid can be tracked.

The main tool in determining the nature of the interactions between molecular components is through *ab initio* calculations. Static calculations of ion pairs have been useful in the development of the theory of ionic liquids, they have been used to predict melting points and understand the role of specific interactions such as dispersion, hydrogen bonding and electrostatics. It has also been used to explain anomalies such as the increase in viscosity after removing a hydrogen bond donor site.[1–4] The current chapter includes the use of static calculation of the ion-pair to study the strength of electrostatic, dispersion and hydrogen bonding interactions.

3.1 Computational Details

Each of the ion pairs are optimized using the Gaussian09 program.[5] The choice of the functional is important, thus all geometry optimisations and interaction energies are calculated using the highly parametrised empirical exchange-correlation functional, M06-2X.[6] The functional has been shown to describe non-covalent interactions better than many density functionals that are currently in use.[7] The Karlsruhe type basis set def2-TZVP is used. This is recommended by Alrichs and

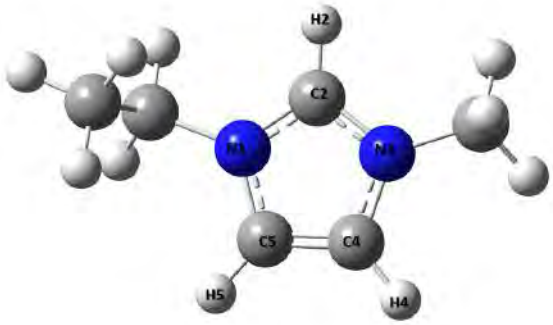

Fig. 3.1: 1-ethyl-3-methylimidazolium cation

Weigend as this basis set produces results that are not far from the DFT basis set limit.[8] It is common practice to use augmented basis sets when describing anions, although this is typically limited to dealing with excited states or small anions. Furthermore Truhlar and Frontera et al. have shown that an augmented Karlruhe basis set does no better at describing non-covalent interactions than the standard def2-TZVP basis set .[9,10] The use of diffuse functions does become important when calculating molecular properties such as the ionisation potential or the polarizability, thus when calculating molecular properties the def2-TZVPD basis set, which was specifically parameterised for this purpose, is utilized.

Previous work has shown that the cation-anion interactions are favoured at the front, top and back of the imidazolium ring.[3,11,12] Rather than an exhaustive potential energy surface scan for ion-pair configurations, the search for the stable conformers is carried out without any geometric constraints by placing the anions around the top, front and back of the cation (see figure 3.2). The converged structures from the geometry optimisations are shown in figure 3.4, where it is evident that most of the structures, no matter where the anions were placed, converge to a single position.

The optimised ion-pairs are then used as input structures for the various methods of analysis i.e., NBO, QTAIM, NCI, electrostatic analyses and dispersion anal-

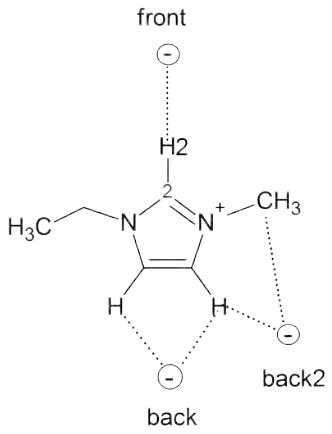

(i) Placing anions

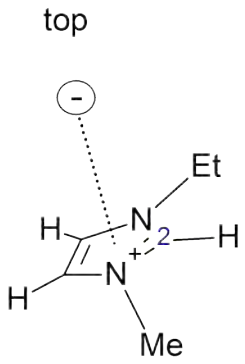

(ii) Placing anion at the top

Fig. 3.2: Placing the anions in different positions around 1-ethyl-3-methylimidazolium

yses. The NBO3.0 routines supplied in Gaussian09 are used for the NBO analysis, whilst the AIMALL package is used for all QTAIM analyses.[13] Distributed multipoles were calculated with Stone's GDMA package[14] and the electrostatic interactions between monomers in dimers was performed using the program MIN16.[15] The NCI analysis is performed using in-house code which generates the 2D and 3D NCI data from cubefiles generated by Gaussian09. All other analyses were performed with in-house Python modules.

3.2 Geometric and Interaction Energy Analysis of Ion-Pairs

The distance between the geometric centre of the imidazolium ring—defined as the origin—and the hydrogen bond acceptor atom X, when X is Cl^- and Br^-, or the atom to which X is bonded for the molecular anions, is measured and reported. The angles measured are those cast in spherical coordinates shown in figure 3.3. φ is the angle between the x-axis and the projection of the vector $\mathbf{r}$ onto the xy-plane. θ is the angle between the z-axis and the vector $\mathbf{r}$. The x-axis is defined as the vector from the $\mathbf{R}_{\text{centre}}$ to C2 and the y-axis is defined as the vector from $\mathbf{R}_{\text{centre}}$ to N1, the y-axis is only needed to define the plane. Results for the geometric description of the ion pairs are shown in table 3.1 and the structures of

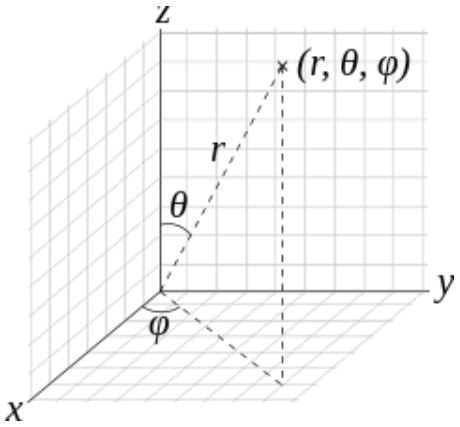

Fig. 3.3: Spherical Coordinates (r, θ, ϕ).[16]

the ion-pairs are shown in figure 3.4.

The interaction energies are calculated and corrected for the basis set superposition error (BSSE) using the Boys and Bernadi counterpoise correction shown in equation 3.1.[17]

$$\Delta \mathrm{E}_{\mathrm{int}}^{\mathrm{CP}} = \mathrm{E}_{\mathrm{AB}}^{\mathrm{AB}} - E_{\mathrm{A}}^{\mathrm{AB}} - E_{\mathrm{B}}^{\mathrm{AB}} \tag{3.1}$$

where the superscript AB denotes a calculation of the energy in the dimer basis. The interaction energies are included in table 3.1

When analysing the results of the geometry optimisations most of the ion-pairs have either their global energy minimum or local energy minimum in the top conformation. For the anions Br^-, Cl^- and $[MeCO_2]^-$, the back (**B** and **B2**) and front (**F**) conformers are found, which are absent for the other ion-pairs. Convergence to the **F** and **B** conformers are the first indications that the hydrogen bonding influences structures of the ion-pairs.

The anions $[BF_4]^-$, $[MeSO_3]^-$ and $[PF_6]^-$ form similar ion-pair structures with respect to their orientation around the cation, shown by θ values of 38.74°, 34.21° and 35.01°, respectively. The θ values for the three orientations indicate that anions are "above" the ring around the carbon atom at the 2-position. The anions

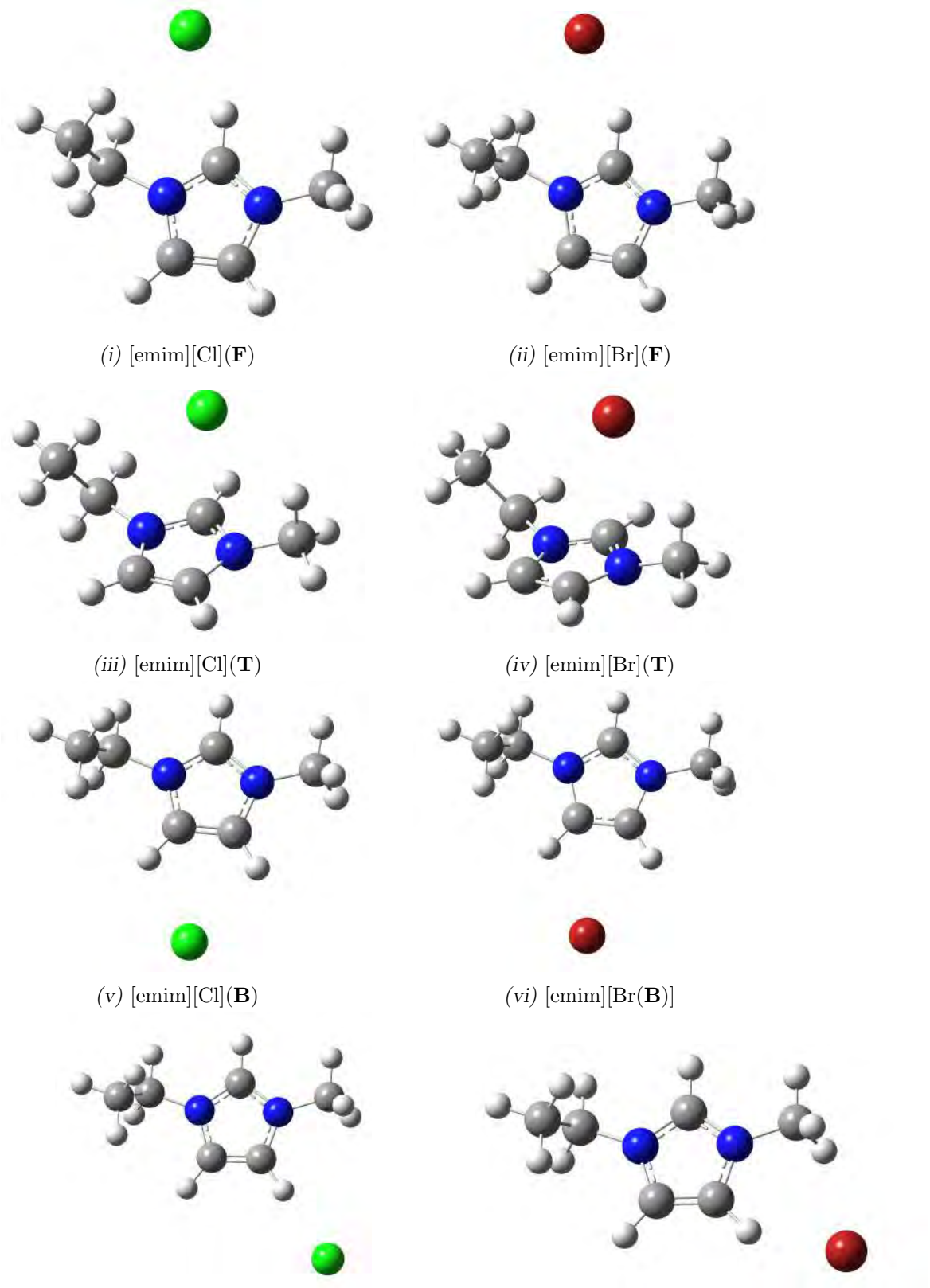

(i) [emim][Cl](**F**) *(ii)* [emim][Br](**F**)

(iii) [emim][Cl](**T**) *(iv)* [emim][Br](**T**)

(v) [emim][Cl](**B**) *(vi)* [emim][Br(**B**)]

(vii) [emim][Cl](**B2**) *(viii)* [emim][Br](**B2**)

Fig. 3.4: Optimised structures of the ion-pairs

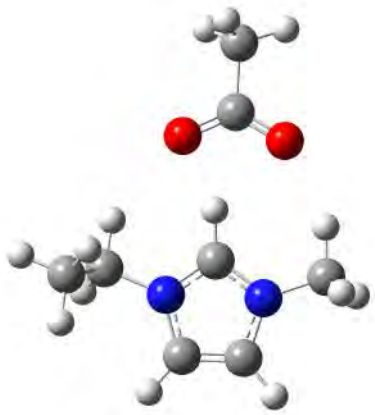

(ix) [emim][$MeCO_2$](**F**)

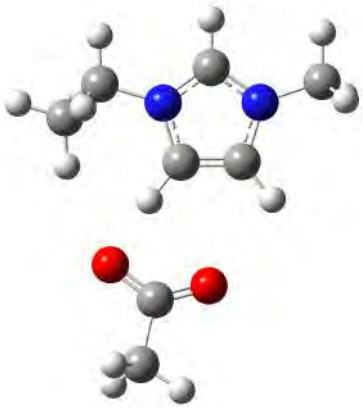

(x) [emim][$MeCO_2$](**B**)

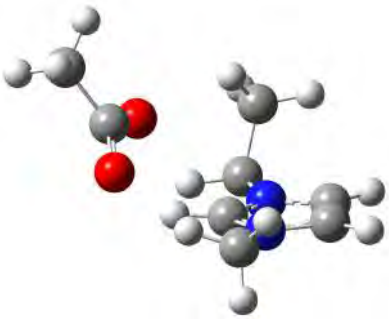

(xi) [emim][$MeCO_2$](**T**)

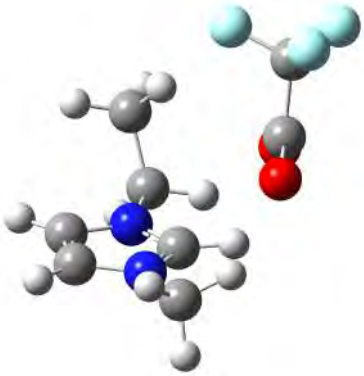

(xii) [emim][CF_3CO_2]

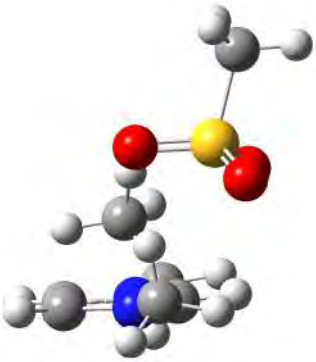

(xiii) [emim][$MeSO_3$]

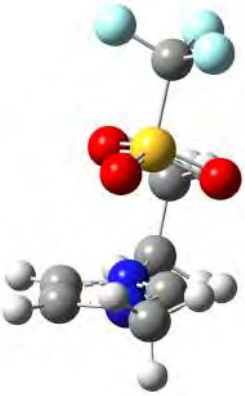

(xiv) [emim][CF_3SO_3]

(xv) [emim][BF_4]

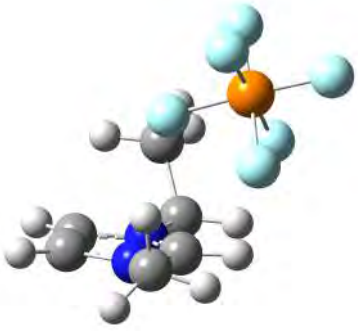

(xvi) [emim][PF_6]

Fig. 3.4: Optimised structures of the ion-pairs

Tab. 3.1: Distances and angles of the anion from the geometric centre of the ring and the interaction energy.

Complex	**r**/[Å]	θ/[°]	ϕ/[°]	ΔE_{int}[kcal · mol^{-1}]
[emim][$MeCO_2$] (**F**)	4.28	94.87	3.69	-105.32
[emim][$MeCO_2$] (**T**)	4.05	59.29	0.15	-105.98
[emim][$MeCO_2$] (**B**)	4.27	80.29	159.74	-89.65
[emim][$MeSO_3$]	3.48	34.21	0.85	-101.02
[emim][Cl] (**F**)	4.12	84.47	14.56	-98.36
[emim][Cl] (**T**)	2.57	13.01	79.70	-99.93
[emim][Cl] (**B**)	3.96	85.36	173.74	-76.55
[emim][Cl] (**B2**)	4.54	89.49	144.39	-79.01
[emim][CF_3CO_2]	3.85	53.62	2.19	-94.95
[emim][BF_4]	4.12	38.74	2.00	-93.25
[emim][Br] (**F**)	4.31	81.33	14.36	-91.96
[emim][Br] (**T**)	3.23	28.13	62.19	-88.19
[emim][Br] (**B**)	4.10	85.24	175.15	-74.24
[emim][Br] (**B2**)	4.34	90.15	121.33	-82.80
[emim][CF_3SO_3]	3.35	22.4	40.26	-88.50
[emim][PF_6]	3.91	35.01	0.76	-87.61

$[CF_3CO_2]^-$ and $[CF_3SO_3]^-$ in their pairs are slightly different to those mentioned above. [emim][CF_3CO_2] has a θ value of 53.62°, maximizing its interaction with the C2-hydrogen whilst [emim][CF_3SO_3] has its θ value at 22.40°, maximizing its interaction with the ring. The distance is shortest for $[CF_3SO_3]^-$and longest for $[BF_4]^-$.

The **F** conformers of the two monoatomic anions, chloride and bromide, have interaction energies of -98.36 kcal · mol^{-1} and -93.25 kcal · mol^{-1}, respectively, a difference of 5.11 kcal · mol^{-1}. The conformers are very similar, i.e both anions are located in the plane of the imidazolium ring situated in front of the hydrogen in the 2-position. As discussed later, the higher charge density of chloride would be the most plausible explanation for the difference in interaction strength of the two pairs, as chloride can locate closer to the acidic hydrogen on the carbon atom, C2,

forming stronger hydrogen bonds. The **B** conformers are the weakest compared to all the other ion-pairs at interaction strengths of -76.55 and -74.24 kcal $\cdot$ mol^{-1} followed by the hydrogen bonded **B2** conformers at -79.01 and 82.80 kcal $\cdot$ mol^{-1} for [emim][Cl] and [emim][Br], respectively. The **B2** conformer of [emim][Br] is more stable than [emim][Cl] with **R** shorter by 0.2 Å.

Comparing the interaction strengths of the top conformers reveals that the [emim][Br] interaction is 11.74 kcal $\cdot$ mol^{-1} weaker than that of [emim][Cl], which again can be attributed to the higher charge density of chloride. There is no clear evidence at this level of theory that there is a preference for the **F** conformer over **T** conformer in both ion-pairs as the differences in interaction energies are very small. [emim][CF_3CO_2] has an interaction energy of -94.95 kcal $\cdot$ mol^{-1}, a difference of approximately 10 kcal $\cdot$ mol^{-1} from its non-fluorinated analogue in the front and top conformer. The effects of fluorinating the anion results in a reduction of interaction strength due to delocalisation of charge within the anion, which results in weaker Coulomb interactions.

[emim][CF_3SO_3] has the second weakest interaction strength of all ion pairs at -88.5 kcal $\cdot$ mol^{-1} and is significantly weaker than its non-fluorinated analogue [emim][$MeSO_3$] with its interaction energy of -101.02 kcal $\cdot$ mol^{-1} , a difference of 12.52 kcal $\cdot$ mol^{-1}. This shows the effect of fluorination, delocalising charge away from the oxygen atoms. This is confirmed by the Merz-Kollman partial charges in which the average charge of the oxygen atom in the fluorinated analogue is -0.55 e, compared to the non-fluorinated at 0.60 e.

[emim][PF_6] has the weakest interaction compared to the other most stable conformers with an interaction energy of -87.61 kcal $\cdot$ mol^{-1}, 5.64 kcal $\cdot$ mol^{-1} weaker than [emim][BF_4], which is the anion most similar to it within the series.

With the stable conformers found and the interaction energies calculated, the role of the most important components of the interactions will be explored namely:

the electrostatics, dispersion and hydrogen bonding (where applicable).

3.3 Electrostatic Interactions

3.3.1 Charge Transfer and Atomic Partial Charges

The total charges on the anion and cation in the ion-pair are calculated using a sum of their atomic partial charges from four popular charge schemes, which are NPA, QTAIM, Mulliken and Merz-Kollman (MK). These charges are used to determine the amount of charge transfer and the feasibility of using any particular scheme for parametrizing charge in a classical force field for molecular dynamics (MD) simulations.

Within this context, charge transfer is defined as the amount of charge less than unity, determined by the sum of all the partial charges on the atoms within the ion shown in equation 3.2

$$\mathrm{CT} = 1 - \left| \sum_{i}^{N} \mathrm{q}_i \right| \tag{3.2}$$

where q_i is the partial charge on atom i in the ion.

Charge transfer is an important concept in the modelling of ionic liquids whose origin may be attributed to the donation of electrons from the anion into the cation, or a result of polarisation.[18–20] Aside from theoretical calculations, evidence of charge transfer has been found experimentally.[21] Whatever the origin of the charge transfer, its inclusion in the development of new force fields for ionic liquids through either charge scaling or the explicit inclusion of polarisation improves the dynamics of MD simulations, reducing over structuring in the liquid and correcting for the overestimation of the intermolecular interactions.[22,23] The charges in figure 3.5 shows the amount of charge transfer when using the four different charge schemes to calculate partial atomic charges.

Chloride and bromide undergo the greatest amount of charge transfer for either the front conformer (NPA, MK) or the top (Mulliken, QTAIM) conformer depending on the charge scheme used. If charge transfer is as a result of the donation of electrons from one species to another, the conformations where hydrogen bonding occur would be the ones that exhibit the greatest amount of charge transfer. This favours the use of the NPA and MK charge schemes. Both **B2** conformations of chloride and bromide undergo a greater amount of charge transfer than their respective **B** conformers for all charge schemes. On the other hand, the **T** conformers exhibit a greater amount of charge transfer than the **B2** conformer, even though hydrogen bonding is absent in the **T** position.

A small difference in charge transfer between the fluorinated and non-fluorinated analogues is found with the non-fluorinated analogue undergoing more charge transfer. $[PF_6]^-$ undergoes the least amount of charge transfer across the series of anions followed by $[BF_4]^-$. Generally, the Mulliken and MK schemes produce larger amounts of charge transfer as compared to NPA and QTAIM charges, which are generally close to unity. Izgorodina et al. found that charges fitted from a restricted electrostatic potential (RESP) perform better as they effectively capture polarisation and charge transfer whilst the NPA and QTAIM charge schemes neglect charge transfer. The Mulliken charge scheme was reported to be unstable with changes in the basis set.[24]

Assuming that the ion-pair is a good descriptor of the liquid state, the most appropriate test to determine how well the ion-pair models charge transfer would be to compare the calculated charge to experimental values. There are distinct differences in the total charge described by the different charge schemes. Charge transfer described by the MK and Mulliken is significantly larger than QTAIM and NPA charges for all ion-pairs. It thus predicts significantly different scaling factors for the same ion-pairs, wich can be determined experimentally by the optical dielectric constant (ϵ_{opt}) given by equation 3.3 below.[20]

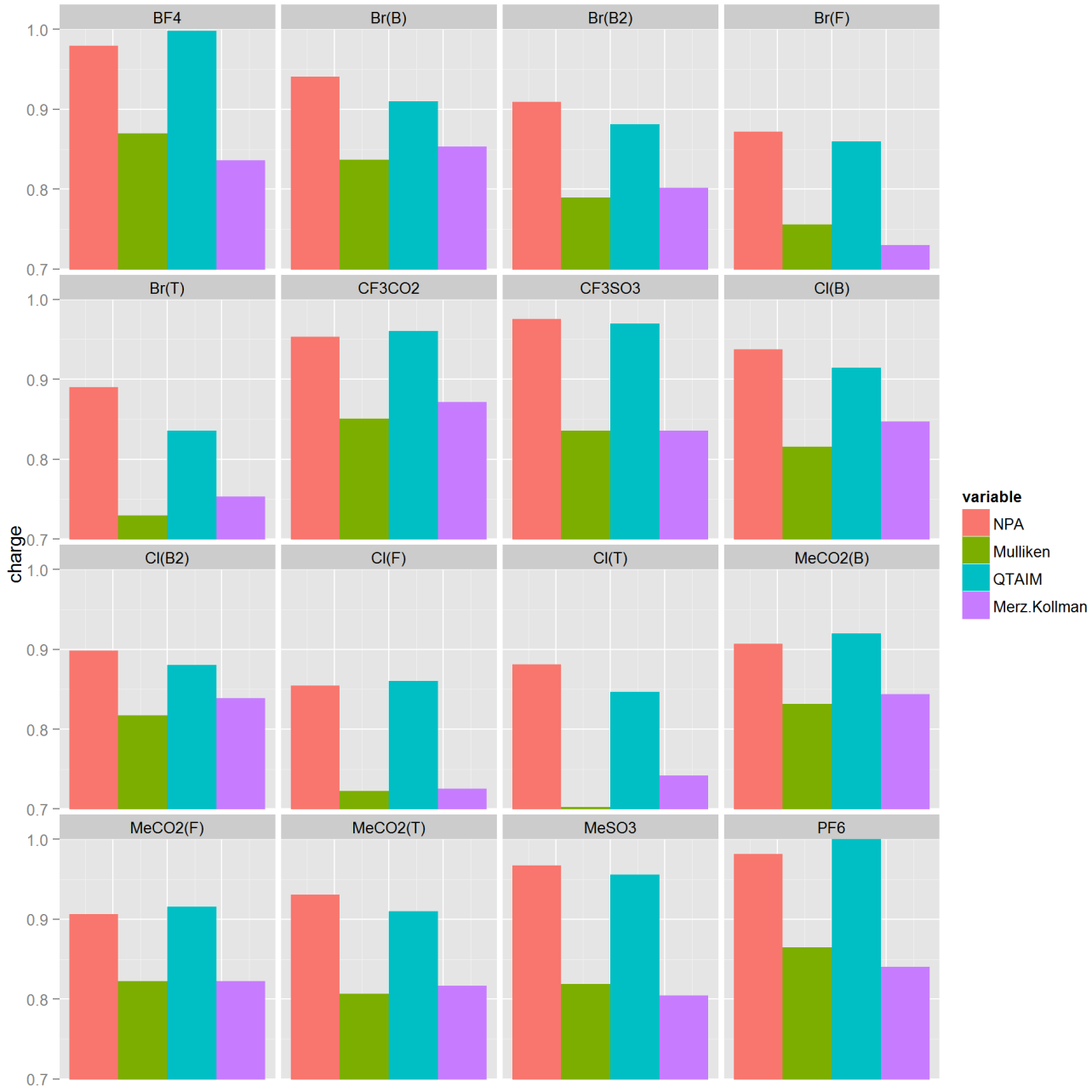

Fig. 3.5: Bar grap of the absolute charges on the ions

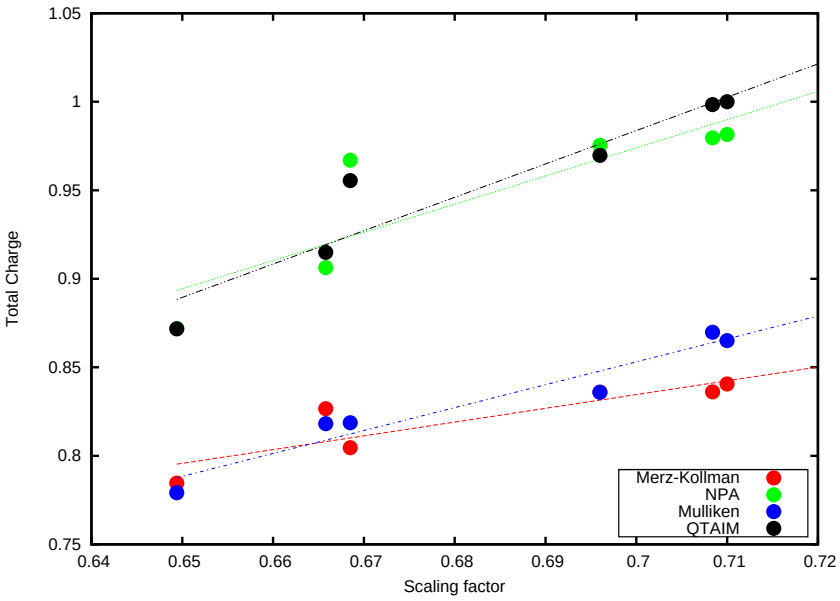

Fig. 3.6: The experimentally determined absolute charge plotted against the absolute charge of the ions in the ion-pair

$$\mathrm{S} = \frac{1}{\sqrt{\varepsilon_{opt}}} \tag{3.3}$$

The optical dielectric constant can be found by measuring the refractive index (n_D) which is related to ε_{opt} by

$$\varepsilon_{opt} = \mathrm{n}_D^2 \tag{3.4}$$

From the experimental data the scaling factors are found, which are: 0.71 (BF_4), 0.65 (Br), 0.70 (CF_3SO_3), 0.67 ($MeCO_2$), 0.67 ($MeSO_3$) and 0.71 (PF_6). The calculated charges in the ion-pairs underestimates the amount of charge transfer in the liquid when compared to the experiment. However, there are relative trends that range from modest to good between the experimental scaling factors and the total charges shown in figure 3.6. Using Mulliken charges produces an R^2 value of 0.93 followed by QTAIM charges with an R^2 of 0.90, MK with an R^2 0.78 and finally NPA charges with an R^2 value of 0.75. Mulliken and QTAIM charges can therefore give a relative description of charge transfer but are not clear in the amount of charge transfer.

Improved methods for calculating charges closer to the ideal scaling value have been found by using clusters of the ion-pairs rather than the pair itself in vacuum.[24] Recently Balasubramanian et al. developed a method for calculating atomic charges in the condensed phase,[25] adapted from Maginn's method for calculating partial charges from known crystal structures of ionic liquids, they use density functional theory based methods to calculate the electron density from which the charges are obtained.[26] Charges for the anions Cl^-, $CF_3SO_3^-$, BF_4^- and PF_6^- total to -0.640, -0.780, -0.790 and -0.775 e, respectively. These values are closer to those that improve dynamics of MD simulations and similar to S.

3.3.2 Charge Distribution

The charge distribution is studied qualitatively by plotting the electrostatic potential of the ion-pairs on an isodensity surface of 0.02 a.u. and are shown in figure 3.8 where the delocalisation of charge in the pair can be visualized. It has been postulated that a more dispersed charge around an ion results in weaker interactions between oppositely charged ions.[27] If the charge is localised or concentrated in one area in the anion the electrostatic interaction becomes more directional and the anion will presents itself to the cation through its more negative end, strengthening the electrostatic interaction. For $[MeSO_3]^-$, $[CF_3SO_3]^-$, $[MeCO_2]^-$ and $[CF_3CO_2]^-$ this is visually evident with the negative (red) parts of the anion in contact with the cation. In the cation the more positive region is around the C2 carbon atom. This can be rationalised by resonance structures, shown in figure 3.7, illustrating the location of the positive charge.[12] The charge is delocalised around the C2, N1 and N3 atoms with the major resonance structures having a formal positive charge on the nitrogen atoms. Predicted pK_a values of 24.90 and 32.97 for the C2-H and C4/5-H hydrogen atoms, respectively, also show that the C2-H hydrogen atom is the most acidic.[28] From an electrostatic perspective, the anions would thus have a preference for conformers where the interaction with the C2 atom are maximized.

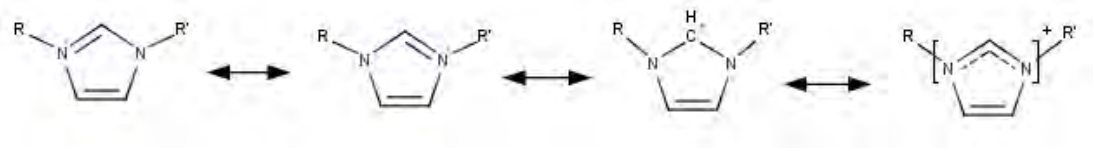

Fig. 3.7: Resonance structures showing delocalisation of the positive charge in the imidazolium ring.

The effect of localising charge becomes clear when comparing the fluorinated and non-fluorinated analogues of the anions. For instance, $[CF_3CO_2]^-$ has a more diffuse charge across the anion when compared to $[MeCO_2]^-$, which is more apparent when comparing $[CF_3SO_3]^-$ to $[MeSO_3]^-$. In $[MeSO_3]^-$ there is a large concentration of charge around the oxygen atoms whereas $[CF_3SO_3]^-$ has the charge more evenly distributed around the anion. The same follows with $[PF_6]^-$ and $[BF_4]^-$ where the charge is more concentrated in $[BF_4]^-$ than in $[PF_6]^-$. The differences in diffusivity of charge around the anions follows the interaction energies; $[CF_3SO_3]^-$ is more weakly interacting with emim than $[MeSO_3]^-$, $[CF_3CO_2]^-$ is more weakly interacting than $[MeCO_2]^-$ and $[PF_6]^-$ is more weakly interacting than $[BF_4]^-$.

The pairs [emim][Br] and [emim][Cl] are very similar for the same conformations but differences between charge concentration on the anion in the different conformations are evident. The stronger interaction sites (**F** and **T**) have the charges on the anions less concentrated than the weaker interaction sites as there is a greater amount of charge transfer in the **F** and the **T** conformations than there is in the **B** and **B2** conformers.

The diffuseness of charge should be quantified to show explicitly the relationship between the charge concentration and the total interaction strength in the ion-pair because a visual analysis can be subjective, relying on the viewer to see what could be subtle differences in colour, rendering it far from ideal. However, the charge distribution is useful in understanding possible reasons for differences in a property of the bulk material such as the melting points. For instance, $[emim][CF_3CO_2]$ has a melting point of -30 to -50°C whilst $[emim][MeCO_2]$ has a melting point of 30°C, $[emim][MeSO_3]$ has a melting point of 35°C with $[emim][CF_3SO_3]$ of -12°C

and [emim][BF_4] has a melting point of 15° whilst [emim][PF_6] has a melting point of 58-62°C. This makes it clear that a more dispersed charge around the anion lowers the melting point of the bulk material.

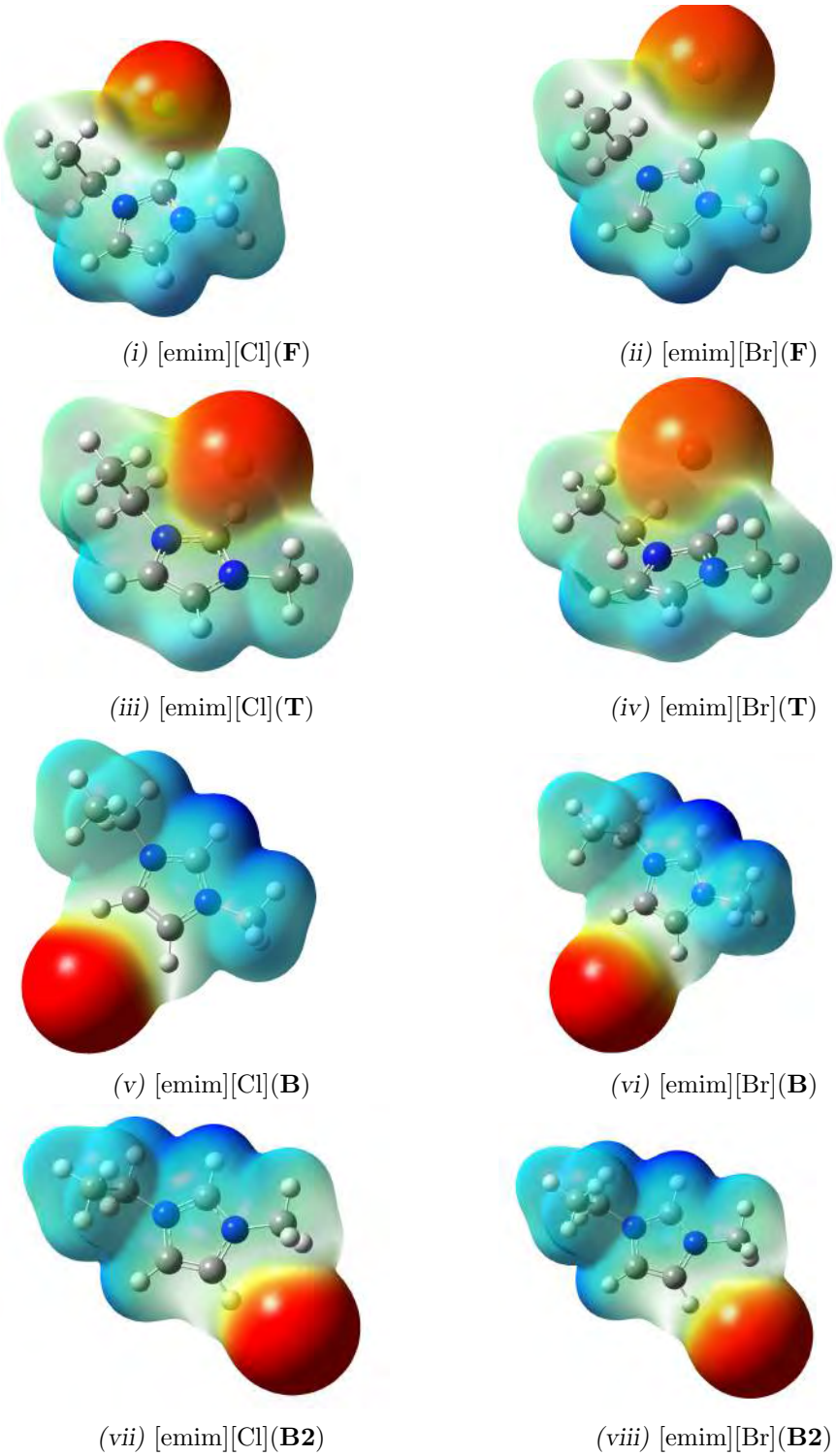

(i) [emim][Cl](**F**) *(ii)* [emim][Br](**F**)

(iii) [emim][Cl](**T**) *(iv)* [emim][Br](**T**)

(v) [emim][Cl](**B**) *(vi)* [emim][Br](**B**)

(vii) [emim][Cl](**B2**) *(viii)* [emim][Br](**B2**)

Fig. 3.8: Structures of the complexes with the electrostatic potential mapped onto the isosurface of the electron density

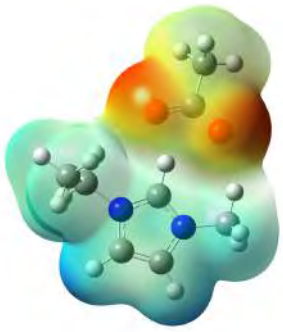

(ix) [emim][$MeCO_2$](**F**)

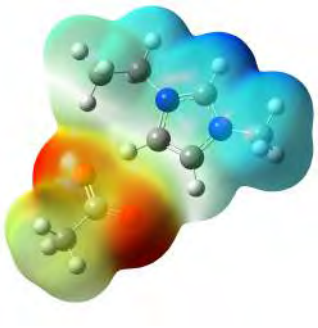

(x) [emim][$MeCO_2$](**B**)

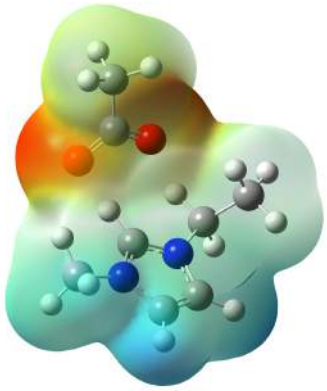

(xi) [emim][$MeCO_2$](**T**)

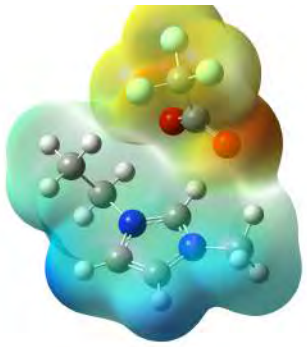

(xii) [emim][CF_3CO_2]

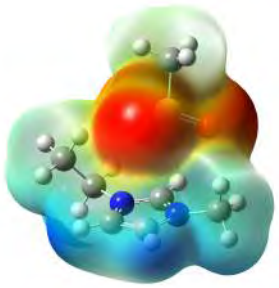

(xiii) [emim][$MeSO_3$]

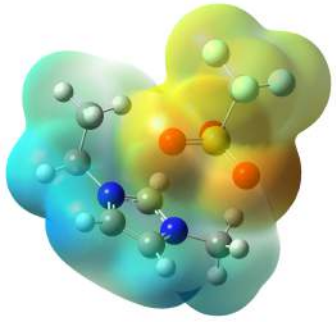

(xiv) [emim][CF_3SO_3]

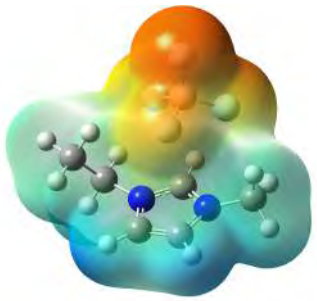

(xv) [emim][BF_4]

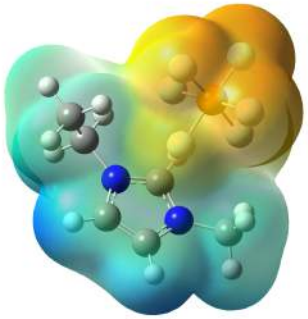

(xvi) [emim][PF_6]

Fig. 3.8: Structures of the complexes with the electrostatic potential mapped onto the isosurface of the electron density

3.3.3 Calculating the Electrostatic Interaction Energies

In this section the electrostatic interaction energies are explicitly calculated. We begin with the interaction energy of the monopole moments then move on to discuss the energy produced from the distributed monopole moments (i.e the interaction between point charges as calculated in the classic force fields) and finally present the electrostatic interactions from distributed multipole moments. The performance of classical force field in calculating the electrostatic interactions is also scrutinized and compared to that calculated from the distributed multipole analysis (DMA), which is regarded here as the most accurate method of representing charge.

The electrostatic energy is given by the expectation value of the Coulomb interaction operator

$$\mathrm{E^{elst}} = \frac{1}{4\pi\epsilon_0}\int \Psi_a^{*(0)}\Psi_b^{*(0)}\sum_{ij}\frac{\mathrm{e}_i^a\mathrm{e}_j^b}{\mathrm{R}_{ij}}\Psi_a^{(0)}\Psi_b^{(0)}d\tau_a d\tau_b \tag{3.5}$$

where $\Psi_a^{(0)}$ and $\Psi_b^{(0)}$ are the unperturbed ground state wavefunctions of molecules **a** and **b** and R_{ij} is the distance between the i^{th} charge $\mathrm{e_i^a}$ in **a** and the $\mathrm{j^{th}}$ charge $\mathrm{e_j^{(b)}}$ in **b** and ϵ_0 is the permittivity of free space. Integration is over the space of each molecule. If the separation of monomers is large relative the size of the monomers, a multipole expansion of the interaction Hamiltonian may be expressed using the permanent multipoles of each monomer. Classically, the multipole moments for an array of charges is given by the Cartesian tensors,

$$\begin{aligned}
\xi^{(0)} &= \mathrm{q} = \sum_j \mathrm{e_j} \\
\xi^{(1)}_{\alpha} &= \mu_\alpha = \sum_{\mathrm{j}} \mathrm{e}_j \mathrm{r}_{\mathrm{j}\alpha} \\
\xi^{(2)}_{\alpha\beta} &= \theta_{\alpha\beta} = \frac{1}{2}\sum_j \mathrm{e_j}(3\mathrm{r}_{jk}\mathrm{r}_{j\beta} - \mathrm{r}_j^2\delta_{\alpha\beta}) \\
\xi^{(\mathrm{n})}_{\alpha\beta\cdots\nu} &= (-1)^{\mathrm{n}}\sum_j \mathrm{r}_j^{2n+1}\nabla_\alpha\nabla_\beta\cdots\nabla_\nu\Big(\frac{1}{\mathrm{r}_j}\Big)
\end{aligned} \tag{3.6}$$

where q is the total charge, μ is the dipole moment, θ is the quadrupole moment, etc. $\mathrm{r_{j\alpha}}$ is the α^{th} component of the $\mathrm{j^{th}}$ position vector, δ's are the Kronecker delta symbols and ∇_α is the α^{th} component of the gradient operator. The electrostatic interaction energy between molecules **a** and **b** is shown in equation 3.7.

$$\begin{aligned}
\mathrm{E} &= \mathrm{Tq^{(a)}q^{(b)}} + \mathrm{T}_\alpha\big(\mathrm{q^{(a)}}\mu^{(\mathrm{b})}_\alpha - \mathrm{q^{(b)}}\mu^{(\mathrm{a})}_\alpha\big) + \mathrm{T}_{\alpha\beta}\big(\frac{1}{3}\mathrm{q^{(a)}}\theta^{(\mathrm{b})}_{\alpha\beta} + \frac{1}{3}\mathrm{q^{(b)}}\theta^{(\mathrm{a})}_{\alpha\beta} - \mu^{(\mathrm{a})}_\alpha\mu^{(\mathrm{b})}_\beta\big) \\
&+ \frac{(-1)^{\mathrm{n}'}}{(2\mathrm{n}-1)!!\,(2\mathrm{n}'-1)!!}\mathrm{T}_{\alpha\beta\cdots\nu\alpha'\beta'\cdots\nu'}\xi^{(\mathrm{n})(\mathrm{a})}_{\alpha\beta\cdots\nu}\xi^{(\mathrm{n})(\mathrm{b})}_{\alpha'\beta'\cdots\nu'}
\end{aligned} \tag{3.7}$$

where the T tensors are the successive derivatives and R is the vector of the origin in molecule a to an origin in molecule b,[29]

$$\begin{aligned}
\mathrm{T} &= \big(4\pi\epsilon_0\big)^{-1}\mathrm{R}^{-1} \\
\mathrm{T}_\alpha &= \big(4\pi\epsilon_0\big)^{-1}\nabla_\alpha\mathrm{R}^{-1} \\
&\vdots \\
\mathrm{T}_{\alpha\beta\cdots\nu} &= \big(4\pi\epsilon_0\big)^{-1}\nabla_\alpha\cdots\nabla_\beta\mathrm{R}^{-1}
\end{aligned} \tag{3.8}$$

The Monopole Moment

To investigate the preference for the top configuration in most of the ion-pairs, the distance between charge centres and the energy associated with the interaction between the charge centres is calculated and shown in table 3.2. The charge centres

are given by

$$R^{centre} = \frac{\sum q_i \cdot x_i}{\sum q_i} + \frac{\sum q_i \cdot y_i}{\sum q_i} + \frac{\sum q_i \cdot z_i}{\sum q_i} \tag{3.9}$$

where q_i is the partial charge on the i^{th} atom and x_i, y_i and z_i are the Cartesian coordinates of the partial charges.

This is the simplest way to look at how electrostatic interactions affect ion-pair formation. From the Coulomb expression, one would expect the distances between the charge centres of the anion and cation to be minimised in order to maximise the interaction strength (E_{CC}^{elst}), subject to Pauli repulsion. To minimize the distance between the charge centres the anion would have to orient itself above or below the ring, i.e the top conformer would be preferred as the centre of charge of the imidazolium lies in the plane of the ring, close to C2.

Through simple monopole moments the orientation of most of the anions can be rationalized through minimisation of the distances between charge centres. Table 3.2 shows that for [emim][Cl], [emim][Br] and [emim][$MeCO_2$] placing the anions above the ring forms the most electrostatically stable conformers. [emim][$MeSO_3$] ranks as the second strongest electrostatic interaction of all the ion-pairs, which would explain why its total interaction energy ranks as the second strongest at -101 kcal $\cdot$ mol^{-1}. The results grossly underestimate the electrostatic interactions because they are very small relative to the total interaction energy. However, the charge centres do explain the geometric preference for the top conformers.

The charge centred electrostatic interactions (E_{CC}^{elst}) are plotted against the total interaction energy and trend lines are shown in figure 3.9. Separate trends are found, the first are for the conformations of Br^- and Cl^- that form the hydrogen bond and a second trend is found for the remaining ion-pairs. Of the 16 ion-pairs formed 2 are excluded from the plot namely, CF_3SO_3 and $MeSO_3$. The simple electrostatic model can thus explain the preference for the top conformation and

Tab. 3.2: Distances between charge centres (R), the electrostatic interaction energy in units kcal·mol^{-1} between charge centres (E^{elst}_{CC}), atomic charges E^{elst}_{AC} and distributed multipole analysis E^{elst}_{DMA}

Complex	R	E^{elst}_{CC}	E^{elst}_{AC}	E^{elst}_{DMA}
[emim][BF_4]	2.74	-16.35	-33.96	-83.68
[emim][Br](**F**)	3.75	-6.66	-23.66	-87.09
[emim][Br] (**T**)	2.70	-13.65	-27.95	-94.13
[emim][Br](**B**)	4.32	-6.86	-30.75	-72.65
[emim][Br](**B2**)	4.56	-5.43	-28.33	-76.78
[emim][CF_3CO_2]	2.81	-16.96	-40.43	-92.85
[emim][CF_3SO_3]	2.64	-17.64	-32.02	-82.22
[emim][Cl] (**F**)	3.45	-7.75	-25.94	-90.65
[emim][Cl] (**T**)	2.45	-16.05	-27.35	-96.26
[emim][Cl] (**B**)	4.10	-7.50	-31.98	-80.76
[emim][Cl] (**B2**)	4.89	-5.18	-26.52	-71.89
[emim][$MeCO_2$] (**F**)	2.55	-18.37	-43.24	-99.92
[emim][$MeCO_2$] (**T**)	2.27	-22.81	-42.17	-104.36
[emim][$MeCO_2$] (**B**)	3.28	-11.66	-39.75	-85.31
[emim][$MeSO_3$]	1.80	-35.15	-35.24	-98.90
[emim][PF_6]	3.10	-12.94	-32.10	-85.14

the differences in interaction energies between similar anions.

Distributed Monopoles

The use of the monopole moments provide the simplest explanation of the electrostatic origin of the preference for the **T** conformer, however it cannot be used to quantify the total electrostatic interaction energy. Calculating electrostatic interactions in the manner used in classic force fields by using derived partial atomic charges can be helpful. Using this model also allows for a critique to be made on the validity of using this partial charge scheme in force fields. The electrostatic interaction for each of the ion-pairs in each conformer is calculated using equation 3.10

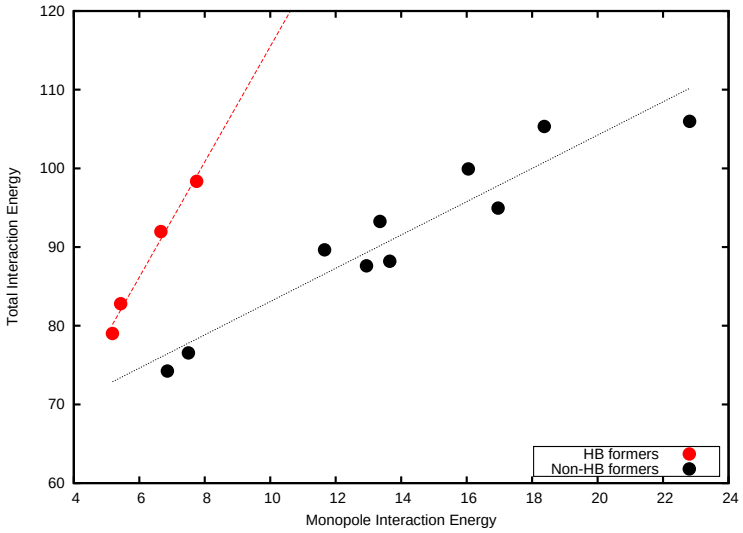

Fig. 3.9: The total interaction energy plotted against the electrostatic interaction energy between charge centres (E_{CC}^{elst})

$$E_{AC}^{elst} = \frac{1}{4\pi\epsilon_0} \sum_{ij} \frac{q_i^{(a)} q_{(j)}^{b}}{R_{ij}} \tag{3.10}$$

where $q_i^{(a)}$ is the atomic charge on the i^{th} atom in the a molecule, $q_j^{(b)}$ is the charge on the j^{th} atom in the b molecule and R_{ij} is the distance between them. The results are shown in table 3.2. Using atomic charges, the electrostatic interactions range from approximately -20 to -45 kcal $\cdot$ mol^{-1}, which significantly stronger than the charge centre interactions. However, these electrostatic interactions are still less than half of the total interaction energy. It suggests that the electrostatic interaction is still being underestimated.

Distributed Multipole Analysis

If the separation of the monomers is large the interaction Hamiltonian may be expressed as the permanent multipole of the monomers. However, at shorter distances the conventional multipole describes electrostatic interactions poorly. The distributed multipole analysis (DMA) gives a more accurate description of the charge distribution and the interaction energy at all accessible distances.

The starting point is the one-electron density matrix over a basis of Gaussian type orbitals together with the nuclear charge and their positions. An overlap distribution of Gaussian orbitals can be represented by a terminating multipole expansion. The multipole expansion at some point **P** can be represented at any other point **S** making the sites for the expansions of multipoles arbitrary. The sites, **S**, are chosen to be at the position of the nuclei as the basis functions are centred at the nuclei and the nuclei themselves carry charge.[30] The electrostatic interactions produced from the DMA up to the hexadecapole moments are shown in table 3.2

Figure 3.10 is a correlation plot produced in order to investigate the presence of trends between the total interaction energies and the electrostatic interactions. It is produced using the statistical program R[31] and the corrplot package.[32] The half below the diagonal in the figure are ellipses coloured by the value of the correlation coefficient given in the colour bar and the eccentricity of those ellipses is also determined by the correlation coefficient. The upper half of the diagonal is the correlation coefficient, R. It shows that the monopole and distributed monopoles result in poor correlation with the electrostatic interactions showing virtually no trend with R^2 values of 0.47 and 0.21, respectively. The DMA interactions however, with an R^2 value of 0.83, shows promise with a relatively good trend with the total interaction energy. There is also a weak trend between the distributed multipoles and the charge centres.

It can be preliminarily concluded that the use of partial charges to describe electrostatic interactions may be inadequate and that other parameters such as those used in calculating dispersion may be adjusted to improve on the inadequacies of the description of the electrostatics. Using distributed multipoles centred on the nuclei is therefore found to be a much more accurate method that can be used to explicitly describe electrostatic interactions.

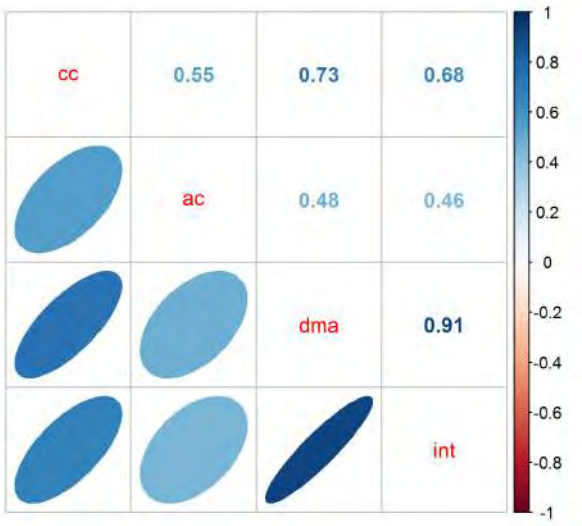

Fig. 3.10: Correlation plot of the electrostatic interaction interaction energies and the total interaction energy

3.4 Role of Dispersion in the Total Interaction

Dispersion is an attractive interaction that is a quantum-mechanical phenomenon, originating from the interaction of fluctuating dipoles. Dispersion is not as easily expressed as electrostatics, particularly in the region of the van der Waals minimum and is essential to modelling the interaction between molecules. In Hartree-Fock theory, dispersion interactions are completely absent and in DFT have to be included in by parametrizing using dispersion bound complexes in a training set for non-local functionals, an example would be M06-2X.[6]

Dispersion interactions have been found to be important in describing the structure and properties of ionic liquids. Grimme et al. showed that dispersion is important for calculating non-covalent interaction energies for ion-pairs.[33] In this section, the dispersion interaction energy is calculated explicitly using the molecular London expression, Grimme's D3 dispersion and the attractive part of the Lennard-Jones potential. In addition we compare these results to the overall interaction and correlation energy.

London Dispersion

The London expression for the dispersion interaction is given in equation 3.11

$$E_{AB}^{disp} = -\frac{3}{2}\frac{I_A I_B}{I_A + I_B}\frac{\alpha^A \alpha^B}{R^6} \tag{3.11}$$

where I_A and I_B are the ionisation potentials of atoms or molecules A and B. α^A and α^B are the dipole polarizability volume of the respective atoms or molecules and R is the distance between the centres of mass of the anions and cations when A and B are molecules.

The dipole polarisability of the anion and cation are explicitly calculated and their ionisation potentials are estimated using the energy of the highest occupied molecular orbitals (HOMO) as stated by Koopmans' theorem.[34] The values of the dipole polarisability of the anions, α^A, the ionisation potential of the anions and the estimate of the dispersion interactions in the ion-pairs are shown in table 3.3. [emim] has an ionisation potential of 306.5 kcal $\cdot$ mol^{-1} and a polarizability volume of 76.29 a_0^3. With the dispersion calculated using molecular properties of the cation and anion rather than their atomic properties, it becomes more simple to interpret which molecular properties affect dispersion most.

The London dispersion energies range between -0.21 kcal $\cdot$ mol^{-1} and -7.18 kcal $\cdot$ mol^{-1} at an average of -2.64 kcal $\cdot$ mol^{-1}. Small deviations in the distance between centres of mass results in relatively large differences in the dispersion interaction energies, which is most evident for the same anion in different conformations. The **T** conformers of the ion-pairs [emim][Cl], [emim][Br] and [emim][$MeCO_2$] show stronger dispersion interactions than the other conformers, it can thus be deduced that the formation of this conformer is favored for all ion-pairs when considering dispersion interactions. The **B** and **B2** conformers, which have the greatest distance between their centres of mass, have the weakest dispersion interactions of all the ion-pairs.

Tab. 3.3: The anion polarizability volume (α^A) in a_0^3, ionisation potential (I^A) in kcal $\cdot$ mol^{-1}, dispersion interaction energy (E^{disp}) in kcal $\cdot$ mol^{-1} and the distance between anion and cation in Angstrom(Å)

Complex	R	I^A	α^A	E^{DISP}_{London}	E^{COR}_{MP2}	E^{DISP}_{D3}	E^{DISP}_{LJ}
[emim][BF_4]	3.16	161.96	23.33	-6.23	-8.91	-8.49	-13.44
[emim][Br](**F**)	3.85	50.39	41.73	-1.39	-7.53	-3.57	-11.42
[emim][Br] (**T**)	3.04	50.39	41.73	-5.74	-10.35	-5.35	-16.92
[emim][Br](**B**)	4.38	50.39	41.73	-0.64	-8.74	-5.56	-5.78
[emim][Br](**B2**)	4.84	50.39	41.73	-0.35	-8.78	-3.01	-9.97
[emim][CF_3CO_2]	4.20	93.60	41.44	-1.36	-7.66	-6.49	-12.64
[emim][CF_3SO_3]	4.00	110.55	50.01	-2.49	-11.07	-11.49	-16.99
[emim][Cl] (**F**)	3.65	51.45	29.36	-1.37	-7.92	-3.09	-12.31
[emim][Cl] (**T**)	2.85	51.45	29.36	-6.05	-9.95	-4.66	-17.48
[emim][Cl] (**B**)	4.20	51.45	29.36	-0.59	-8.43	-1.98	-6.02
[emim][Cl] (**B2**)	5.01	51.45	29.36	-0.21	-5.33	-1.36	-4.16
[emim][$MeCO_2$] (**F**)	4.12	66.50	43.01	-1.21	-3.53	-4.51	-11.46
[emim][$MeCO_2$] (**T**)	3.78	66.50	43.01	-2.02	-5.03	-5.53	-12.31
[emim][$MeCO_2$] (**B**)	4.43	66.50	43.01	-0.78	-7.84	-3.99	-9.36
[emim][$MeSO_3$]	3.26	88.30	50.14	-7.18	-9.83	-11.51	-18.12
[emim][PF_6]	3.55	178.06	32.60	-4.60	-10.01	-10.10	-14.29

The molecular London expression returns the smallest values for the dispersion interactions when compared to the other methods below. Although the expression can give accurate values for interactions in a vacuum, they are known to be lower than more rigorously determined dispersion energies.[35] It is thus the lower bound to dispersion due to the reduction of the ions to two points making it a poorer descriptor as the ions become larger.

Correlation Energy

The intermolecular correlation energy can be considered as an estimate of the upper-bound to the dispersion energy. Correlation is calculated as the difference between the MP2 and HF energies. The intermolecular correlation energy is calculated as difference between the correlation energies of the ion-pair and the

monomers that make up the ion-pair, this is shown in equation 3.12

$$\mathrm{E}_{\mathrm{MP2}}^{\mathrm{COR}} = \mathrm{E}_{\mathrm{AB}}^{\mathrm{COR}} - \mathrm{E}_{\mathrm{A}}^{\mathrm{COR}} - \mathrm{E}_{\mathrm{B}}^{\mathrm{COR}} \tag{3.12}$$

where $\mathrm{E}_{\mathrm{MP2}}^{COR}$ is the intermolecular correlation energy, the subscript AB denotes the dimer and A and B denotes the monomers. The correlation energies are shown in table 3.3.

Values of the electron correlation energies of the ion-pairs are closely spaced with a standard deviation of 2.07 kcal $\cdot$ mol^{-1} and an average of -8.91 kcal $\cdot$ mol^{-1}. These values are significantly larger than that given by the London expression. For [emim][Cl] and [emim][Br], the **T** conformers show stronger dispersion compared to the other conformers. [emim][$MeCO_2$] differs in that the **B** conformer has stronger dispersion than the other conformers. [emim][PF_6] has a larger upper-bound to dispersion than [emim][BF_4], a reversal from the dispersion interactions given by the London expression.

Although calculating the upper-bound to the dispersion interaction is helpful, it is not an explicit expression of the dispersion. With the London expression giving dispersion interactions that are too low, explicit atom-atom pairwise expressions for calculating dispersion must be utilized.

Lennard-Jones Dispersion

The Lennard-Jones (LJ) expression used to describe dispersion interactions is frequently used in classical force fields. It is an atom-atom pairwise expression given by equation 3.13

$$\mathrm{E}^{LJ} = 4\varepsilon_{ij}\left[\left(\frac{\sigma_{ij}^{\mathrm{vdW}}}{r}\right)^{12} - \left(\frac{\sigma_{ij}^{\mathrm{vdW}}}{r}\right)^{6}\right] \tag{3.13}$$

where ε_{ij} is the well-depth , r is the distance between nuclei, σ_{ij}^{vdW} is the distance

Tab. 3.4: References from which the Lennard-Jones parameters were obtained.

Ion	Reference
$[BF_4]^-$	Liu et al.[36]
Br^-	GAFF[37]
$[CF_3CO_2]^-$	GAFF[37]
$[CF_3SO_3]^-$	Lopes et al.[38]
Cl^-	Liu et al.[36]
$[MeCO_2]^-$	GAFF[37]
$[MeSO_3]^-$	Lopes et al.[39]
$[PF_6]^-$	Liu et al.[36]
emim	Liu et al.[36]

at which the LJ potential is zero. The potential is composed of two terms, the first is a repulsive term that is used to model steric repulsion and the second is an attractive term used to model dispersion. Dispersion is calculated using parameters from force fields listed in table 3.4, the results are shown in table 3.3.

With an average of -12.04 kcal·mol^{-1} and a standard deviation of 4.26 kcal·mol^{-1} overall, the Lennard-Jones dispersion interactions are found to be significantly larger than the correlation energies. [emim][$MeSO_3$] has the largest dispersion interaction at -18.12 kcal·mol^{-1} followed closely by [emim][Cl] at -17.48 kcal·mol^{-1}, [emim][CF_3SO_3] at -16.99 kcal $\cdot$ mol^{-1} and [emim][Br] at -16.92 kcal $\cdot$ mol^{-1}. The dispersion interactions for the monoatomic anions are unexpectedly strong with fewer atom-atom interactions than all the other anions. For $[MeCO_2]^-$, Cl^- and Br^- the **T** conformers are favoured more than the other conformers, followed by the **F** conformers. The differences between fluorinated and non-fluorinated analogues is small. The difference between dispersion interactions in ion-pairs [emim][PF_6] and [emim][BF_4] is also small at 0.85 kcal $\cdot$ mol^{-1}.

Comparing the upper-bound to the dispersion interaction (E_{MP2}^{COR}) to the Lennard-Jones dispersion interactions, the LJ dispersion seems to overestimate the strength of dispersion. It was shown that partial charge electrostatic interactions were

grossly underestimated and could possibly be compensated partly by the overestimated dispersion interactions.

D3 Dispersion

The dispersion energy between a pair of spherical atoms at long range may be written as an infinite series in the form

$$\mathrm{E}^{\mathrm{DISP}} = \sum_{n=6}^{\infty} C_n^{AB} R_{AB}^{-n} \tag{3.14}$$

where C_n^{AB} denotes the average isotropic n^{th}-order dispersion co-efficients for atom pair AB and R_{AB} is the internuclear distance between atoms. At short range, the behaviour can be modified with a damping function so that the dispersion does not become infinite at $R = 0$. DFT-D , one of the most successful and widely used methods to correct for dispersion uses the expression in 3.15,[40]

$$\mathrm{E}^{\mathrm{DISP}} = \sum_{n=6,8,10,\ldots}^{\infty} s_n \frac{C_n^{AB}}{R_{AB}^n} D_n(R_{AB}) \tag{3.15}$$

where s_n is a scaling factor, which is density functional (DF) dependent, $D_n(R)$ is the damping function, which is unity at long range and falls to zero at $R = 0$. In Grimme's DFT-D3, $s_6 = 1$ and the series in equation 3.15 is truncated after $n = 8$. In this section the dispersion correction parametrised for HF is used. HF does not account for any dispersion as it totally neglects the correlated movement of electrons, which is ideal for the calculation of dispersion. More specifically, the intermolecular dispersion interaction is calculated; the dispersion correction of the monomers is subtracted from the dimer. No damping function is used and results are shown in table 3.3

The dispersion interaction energies generally fall within the upper-bounds given by the correlation energy. The variation is small with a standard deviation of 3.18 $\mathrm{kcal} \cdot \mathrm{mol}^{-1}$ and an average of -5.67 $\mathrm{kcal} \cdot \mathrm{mol}^{-1}$. Unlike the LJ dispersion, Cl^-,

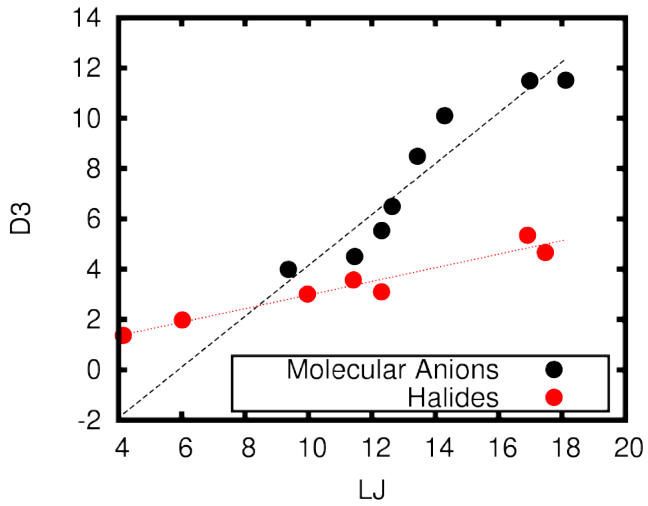

Fig. 3.11: The Lennard-Jones potential plotted against the D3 dispersion interaction energies

Br^- have weaker dispersion interactions than the other ions with the strongest dispersion interaction occurring, again, in the **T** conformation. Having these ions form the weakest dispersion interactions is expected as there are fewer atom-atom interactions. There is only a small difference between the fluorinated and non-fluorinated anions. Finally, $[PF_6]^-$ has a stronger dispersion interaction with the cation when compared to $[BF_4]^-$. To compare the two pairwise methods in calculating the interaction, the D3 dispersion energy is plotted against the Lennard-Jones dispersion in figure 3.11.

The trend between D3 and LJ has to be separated into molecular anions and monoatomic anions as the LJ dispersion interaction energies seem to be overestimated. With an R^2 value of 0.85 for the monoatomic anions and 0.96 for the molecular anions, a general trend is found between the two methods. Calculating the dispersion using the LJ expression thus seems appropriate when parametrised correctly.

The plot in figure 3.12 provides an overall view of the correlation between methods. The molecular properties and the overall interaction energy are also included. There is no significant trend between the overall interaction (IE) and dispersion interaction energies, this confirms that the ion-pairs are dominated by electrostatic interactions. When considering the molecular properties, only the D3 dispersion

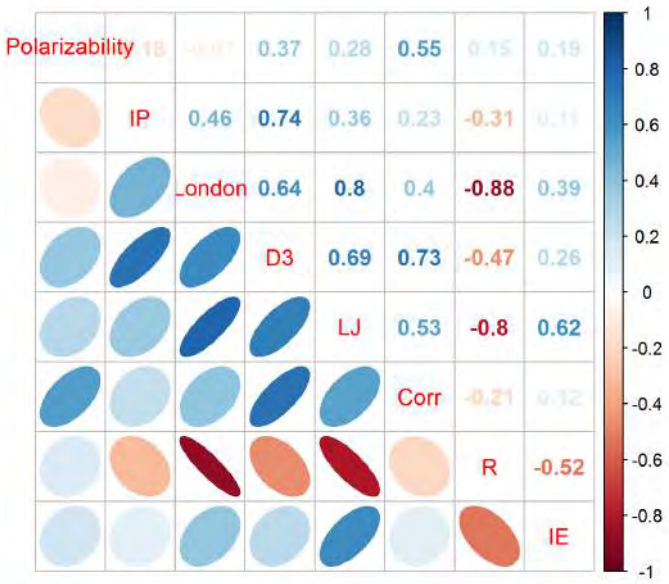

Fig. 3.12: The correlation matrix of the dispersion interactions, interaction energies (IE), ionisation potential (IP) and dipole polarisability (Polarizability) of anions. LJ = Lennard-Jones potential, R = centre of mass distances, Corr = upper-bound to dispersion energy.

and the ionisation potential show a significant trend more so when the outliers $[MeSO_3]^-$ and $[CF_3SO_3]^-$ are removed, which improves R from 0.74 to 0.86. A fairly strong centre of mass distance dependence is found with the Lennard-Jones and London dispersion with R values of 0.8 and 0.88, respectively. Conversely, the D3 dispersion does not exhibit the same behaviour.

Concluding the discussion on dispersion interactions, we find that the London expression is inappropriate for calculating the dispersion energy, because of it is grossly underestimated. The correlation energy is a reasonable guide for gauging the upper-bound to the dispersion energy and is used to judge how well the explicit atom-atom dispersion interaction indicators perform. The D3 dispersion falls within the upper-bound of the correlation when the damping functions are not utilised and the Lennard-Jones dispersion interactions are overestimated. The dispersion interactions favour the **T** conformers. The values of the dispersion interactions are much smaller than those of the electrostatic interaction energies, but remain significant, particularly as the size of the anion increases.

3.5 Hydrogen Bonding

Hydrogen bonding has featured as an important characteristic when studying ionic liquids and has been observed both theoretically and experimentally.[3,41–44] Wang et al. found, through an NMR experiment, hydrogen bonding for $[BF_4]^-$ and $[PF_6]^-$ by analysing the ^{13}C dipole-dipole relaxation rates and suggested that it might contribute to a higher viscosity of the bulk material.[41]

Kirchner et al. reported that hydrogen bonding is not the most important interaction type with regards to the total interaction, although hydrogen bonds were found in many of their systems.[42] Köckerling and Ludwig showed that hydrogen bonding has a significant effect on structure and properties such as the melting point, viscosity and enthalpies of vaporisation.[43] Izgorodina showed that the total interaction energy and the charge transfer are not good criteria for distinguishing hydrogen bonding from ion-ion interactions and that experimentally, a red-shift is a good indicator for hydrogen bonding whereas a blue-shift is more indicative of ion-ion interactions.[3]

The charges on hydrogen and carbon atoms at the 2-position were modified by Kirchner et al. to see the effect of the hydrogen bond. Making the charges zero was shown to not affect dynamics but affects the local structure in the liquid. Making the charge on the hydrogen negative or enhancing hydrogen bonding by making the charge positive strongly influences the structure and the diffusion coefficients.[45]

In this section, the strength and character of the hydrogen bond is investigated using natural bonding orbitals (NBO) and the quantum theory of atoms in molecules (QTAIM) as well as the non-covalent index (NCI).

3.5.1 NBO Analysis to Describe Hydrogen Bonding

The natural bond orbital (NBO) approach produces a maximal localisation of orbitals and describes stabilisation as a result of orbital overlap between orbitals of different atoms, giving a Lewis-type interpretation of "shared-electrons", a language familiar to many chemists.[46] In this particular context hydrogen bonding is characterised as electron donation from the lone pair (n_B) of the hydrogen bond acceptor into the empty sigma anti-bonding orbital (σ^*_{AH}) of the hydrogen bond donor. The estimate of the stabilisation energy is given by equation 3.16

$$\mathrm{E}_{i\to j^*} = -n_i^{(0)} \frac{\langle \phi_i^{(0)} | \hat{\mathrm{F}} | \phi_j^{*(0)} \rangle^2}{\epsilon_j^{*(0)} - \epsilon_i^{(0)}} \tag{3.16}$$

where $n_i^{(0)}$ is the occupation number of the donor orbital, $\phi_i^{(0)}$ and $\phi_j^{*(0)}$ are the donor and acceptor orbitals with orbital energies $\epsilon_i^{(0)}$ and $\epsilon_j^{*(0)}$, respectively and $\hat{\mathrm{F}}$ is the Fock operator.

NBO analysis is performed on the optimised ion-pairs. All pairs were analysed and only data showing significant stabilisation from the lone-pair of the acceptor atom, X, into the anti-bonding orbital of the C2-H (**F** conformer) and C4-H (**F** conformer) bond are reported in table 3.5. Note: the $\mathrm{C5-H\cdots X}$ hydrogen bond was not analysed as the conformers that would have such an interaction were not obtained.

The **F** conformer of Br^- would be expected to form the strongest hydrogen bond because the donor and acceptor orbitals are closer in energy with a gap of 0.70 a.u. However, Cl^- forms the strongest hydrogen bond in the **F** conformer because the anion's smaller size, allows the lone pair to better overlap with the anti-bonding (σ^*_{C2H}) orbital. The hydrogen bond distance and angle of the chloride are, respectively, shorter and more linear than the bromide. This leads to both the largest occupation of the anti-bond and the largest stabilisation energy of all the ion-pairs. Br^- then follows with a stabilisation energy of 35.28 $\mathrm{kcal \cdot mol^{-1}}$.

Tab. 3.5: NBO delocalisation energies in kcal·mol^{-1} for hydrogen bond forming ion-pairs, $\epsilon_j - \epsilon_i$ and F(i,j) are in atomic units

Complex	X	$r_{H\cdots X}$	Angle	$\epsilon_j - \epsilon_i$	F(i,j)	$n_{occ}(\sigma^*)$	$\Delta E(n_X \rightarrow \sigma^*_{AH})$
[emim][Br](**F**)	Br	2.20	152.21	0.70	0.135	0.09439	32.86 (35.28)
[emim][Cl](**F**)	Cl	1.98	154.02	0.72	0.161	0.11073	44.85 (48.1)
[emim][$MeCO_2$](**F**)	O1	1.77	156.45	0.75	0.113	0.07347	20.55 (24.34)
[emim][$MeCO_2$](**F**)	O2	2.14	133.37	0.73	0.039	0.07347	2.60 (3.26)
[emim][Br](**B2**)	Br	2.31	147.62	0.72	0.106	0.06224	19.57 (20.84)
[emim][Cl](**B2**)	Cl	2.11	146.85	0.75	0.112	0.07011	24.82 (26.44)
[emim][$MeCO_2$](**B**)	O1	1.71	167.13	0.78	0.135	0.07514	28.48 (33.47)
[emim][$MeCO_2$](**B**)	O2	2.32	106.09	0.74	0.014	0.07514	0.19 (0.40)

The values in the bracket for $\Delta E(n_X \rightarrow \sigma^*_{AH})$ are the total energies from all lone pairs of X whereas the values outside the bracket is the largest contribution of a single lone pair. F(i,j) is the Fock matrix element, $n_{occ}(\sigma^*)$ is the occupation number of the σ^* anti-bond orbital.

$[MeCO_2]^-$ in the **F** conformer forms a weaker hydrogen bond than the halides with a total hydrogen bond stabilisation energy of 24.34 kcal·mol^{-1}, a surprising result when considering that the hydrogen bond distance is shorter at 1.77 Å and more linear with an angle of 156.45°. The second oxygen atom of the acetate makes a negligible contribution to the stabilisation due to poor overlap of the lone pair with the σ^*_{C2H}.

The **B2** conformer of the halides and the **B** conformer of the acetate also form hydrogen bonds. Acetate forms the strongest hydrogen bond of these conformers with a hydrogen bond distance of 1.71 Å and angle of 167.13° and stabilisation energy of 33.47 kcal·mol^{-1}. The **B** conformer forms a stronger hydrogen bond than the **F** conformer because the lone-pair has a greater overlap with the anti-bonding orbital as the hydrogen bond distance is shorter and the angle more linear. The second oxygen makes a negligible contribution to the stabilisation.

Acetate prefers to maximise the stabilisation of a single hydrogen bond rather than form a bifurcated hydrogen bond, which would consist of two interactions of similar strength. This appears to be due to a secondary interaction with the

ethyl chain, which is negligible in the NBO analysis. For the **B2** conformers of the halides, a combination of smaller orbital overlap and larger orbital energy differences produce weaker hydrogen bonds than their respective **F** conformers. Each of the **B2** conformers have longer hydrogen bond distances and hydrogen bond angles further from linearity than their respective **F** conformers. They also have smaller occupation numbers for the anti-bonding orbital.

The estimates of the stabilisation energies given by NBO for hydrogen bonding are useful in providing information to assess the presence of hydrogen bonds but not in providing good quantitative energies for the contribution to the total interaction energies as they are much higher than typical hydrogen bond energies.

3.5.2 Quantum Theory of Atoms in Molecules: Properties at the Bond Critical Points

QTAIM allows for interrogation of the nature of atom-atom interactions.[47] A QTAIM analysis is conducted on the ion-pairs and properties at the bond critical points associated with hydrogen bonding are tabulated in table 3.6, these include the potential energy density (V_C), kinetic energy density (G_C), electron density (ρ) and the Laplacian ($\nabla^2\rho_C$) at the bond critical points.

Hydrogen bonds can be identified in QTAIM according to certain criteria highlighted by Koch and Popelier,[48] amongst the criteria based on atomic volumes, charges and energies is evidence of a bond path between a hydrogen atom and an acceptor, an electron density at the bond critical point of 0.002-0.034 a.u. and a Laplacian of 0.024-0.130 a.u. The critical points reported in table 3.6 fulfill these criteria for the hydrogen bonding and in the cases of [emim][Cl](**F**), [emim][$MeCO_2$](**F**) and [emim][$MeCO_2$](**B**) the values of the electron density exceed the above mentioned reference range for the electron density at the bond critical point.

Tab. 3.6: QTAIM properties in atomic units for hydrogen bond forming ion-pairs. The electron density ρ, potential energy density (V_C), kinetic energy density (G_C), total potential energy density (H_C) and the Laplacian $\nabla^2\rho_C$ are all reported in atomic units and the estimated potential energy of the hydrogen bond (E_{HB}) is reported in kcal $\cdot$ mol^{-1}

Complex	ρ	V_C	G_C	H_C	$\nabla^2\rho_C$	E_{HB}
[emim][Br](**F**)	0.0336	-0.0228	0.0201	-0.0003	0.0700	-7.15
[emim][Cl](**F**)	0.0454	-0.0377	0.0295	-0.0082	0.0850	-11.89
[emim][$MeCO_2$](**F**)	0.0427	-0.0417	0.0361	-0.0055	0.1224	-13.10
[emim][Br](**B2**)	0.0272	-0.0181	0.0167	-0.0014	0.0611	-5.68
[emim][Cl](**B2**)	0.0345	-0.0268	0.0229	-0.0038	0.0763	-8.42
[emim][$MeCO_2$](**B**)	0.0483	-0.0463	0.0396	-0.0067	0.1311	-14.54

Rozas et al. used the Laplacian ($\nabla^2\rho_C$) and the energy density (H_C) to characterise the hydrogen bond.[49] A "medium" strength hydrogen bond is characterised by $\nabla^2\rho_C > 0$ and $H_C < 0$ where H is the total electron energy density and is defined in equation 3.17.

$$H_C = V_C + G_C \tag{3.17}$$

They also identify weak hydrogen bonds by $\nabla^2\rho_C$ and $H_C > 0$ and strong hydrogen bonds by $\nabla^2\rho_C$ and $H_C < 0$. The hydrogen bonds identified in table 3.6 could thus all be considered as medium strength hydrogen bonds

Classification of the strength of hydrogen bonds was also investigated by Sathyamurthy et al. where the stabilisation energy of a number of hydrogen bond complexes was calculated and the electron density at the hydrogen bond critical point determined. They then used the information to classify hydrogen bonds into four categories of strength, which are the weak van der Waals limit, moderate, strong and covalent limit hydrogen bonds.[50] The border of the moderate and strong hydrogen bond has ρ_C at 0.05 a.u. [emim][$MeCO_2$](**F**), [emim][Cl](**F**) and [emim][$MeCO_2$](**B**) thus form moderate to strong hydrogen bonds, comparable to the hydrogen bond strengths of the complexes $NH_4^+ \cdots H_2O$, $NH_3 \cdots HF$ and $NH_3 \cdots HCl$. The border of the weak and moderate strength hydrogen bonds

has ρ_C of 0.02 a.u., classifying [emim][Cl](**B2**) and [emim][Br](**F**) as moderate strength hydrogen bonds and [emim][Br](**B2**) as a weak to moderate strength hydrogen bond former.

The energy of the hydrogen bond is next found from the potential energy density ($E_{HB} = 314V_C$). This relationship is proposed in a study by Espinosa et al.,[51] which was a topological analysis of 83 experimentally observed hydrogen bonds (X–H$\cdots$O where X= C,O,N). Katsyuba et al.[52] use this relationship to describes intermolecular hydrogen bond energies of O–H$\cdots$F and C–H$\cdots$F. The hydrogen bond energies for the ion-pairs are calculated and shown in table 3.6. [emim][$MeCO_2$] forms the most stable hydrogen bond in the **B** conformation, followed by the same ion-pair in the **F** conformation. Chloride forms stronger hydrogen bonds than bromide in both the **F** and **B2** conformations. If the electron density alone at the bond critical point were an indicator, [emim][Cl](**F**) would form a stronger hydrogen bond than [emim][$MeCO_2$](**F**). However, the small inconsistencies do not change the quantitative conclusion of the overall trend.

The properties from the QTAIM analysis are plotted against each other and the NBO stabilisation energies in figure 3.13. There is no strong correlation between the NBO energy and any of the QTAIM parameters. There is a strong correlation between V_C and ρ_C, ρ_C and H_C and finally V_C and $\nabla^2\rho_C$. Any parameter that correlates to the potential energy density can be used to also estimate the hydrogen bond strength. The use of the electron density is attractive because of the ease with which it can be calculated in a typical quantum mechanical calculation.

All other interactions from the QTAIM analysis of the remaining ion-pairs are characterised by low values of ρ_C, positive values of H_C and $\nabla^2\rho_C$. By Cremer and Kraka's suggestion these represent non-covalent, closed shell van der Waals interactions. Coupled with the results from the NBO analysis, the QTAIM results show that no other hydrogen bonds form in the ion-pairs in the configurations found.

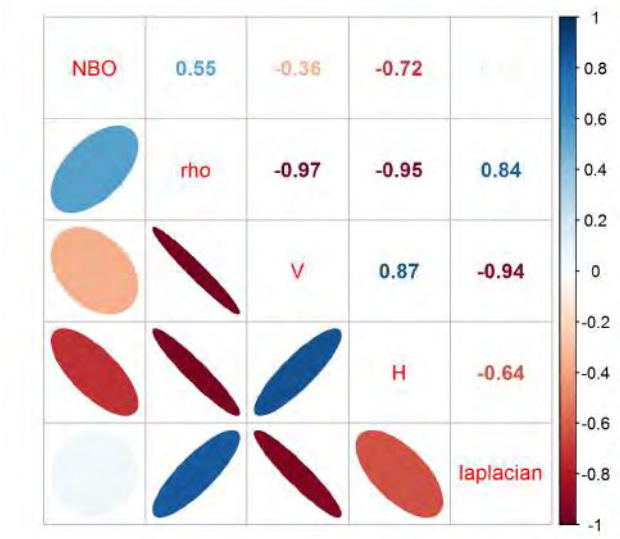

Fig. 3.13: Correlation matrix of NBO and QTAIM properties. rho = ρ_C and Laplacian = $\nabla^2\rho_C$

There is a strong indication that electrostatic interactions are dominant but that hydrogen bonding and dispersion interactions are also important. Hydrogen bonding and dispersion energies are within the same order of each other but the electrostatic interactions are approximately an order of magnitude greater than these. A more general descriptor for the overall interaction between ions that uses the electron density as the basis for all analysis can be used to reveal non-covalent interactions visually.[53]

3.6 Non-covalent Index (NCI) analysis

An NCI analysis was done for all optimised geometries of the ion-pairs. The electron density and the density gradient are used to find the reduced density gradients (**s**), which in turn allows for non-covalent interactions to be found. The sign of the second eigenvalue of the Hessian matrix ($sign(\lambda_2)\rho$) is used to distinguish between attractive and repulsive interactions; when $\lambda_2 < 0$ the interaction is attractive and when $\lambda_2 > 0$ the interaction is repulsive. A plot of the reduced density gradient against $sign(\lambda_2)\rho$ reveals non-covalent interactions by a peak in the graph. Peaks in the negative region of the graph denote attractive interactions whilst peaks in the positive region of the graph denote repulsive interactions.

NCI is a useful tool in analysing non-covalent interactions, particularly because all the information is extracted from the observable electron density (see section 2.5), which makes it consistent with a QTAIM approach.

3.6.1 The 2D Reduced Density Gradient (RDG) Plots

The reduced density gradient is plotted against $sign(\lambda_2)\rho$ for all ion-pairs in figure 3.14 alongside the 3-dimensional isosurface of **s**, which is mapped by the values of $sign(\lambda_2)\rho$. Blue represents strong attractive interactions, red represents strong repulsive interactions and green represents weak interactions. In some of the figures, the bond paths and the bond critical points are plotted and show embedded in the surfaces.

With peaks clearly present in all the graphs and isosurfaces visible in real space, non-covalent interactions are present in all ion-pairs. $[MeSO_3]^-$, $[CF_3SO_3]^-$, $[BF_4]^-$ and $[PF_6]^-$ fall within a single category with broad peaks close to $\text{sign}(\lambda_2)\rho = 0$ in both the attractive and repulsive domains. Figures 3.14i and 3.14ii typify these interaction types, the peaks in the attractive region are partnered with a peaks in the repulsive region. The NCI surfaces in real space are large flat surfaces between the anion and cation spread across the face of the imidazolium ring. These indicate weak van der Waals interactions.

The ion-pairs that undergo hydrogen bonding can be easily separated from those that do not, they exhibit peaks in the attractive region at -0.04 to -0.05 a.u. with the partnering short peak. Hydrogen bonding is visible for the emim conformers with $[Cl]^-$(**F**), $[Cl]^-$(**B2**), $[Br]^-$(**F**), $[Br]^-$(**B2**), $[MeCO_2]^-$(**F**) and $[MeCO_2]^-$(**B**). They are characterised by small blue pellet-like surfaces between the hydrogen bond acceptor and the hydrogen. These are the same ion-pairs that were found to undergo hydrogen bonding using NBO and QTAIM indicators.

When forming hydrogen bonds in the front and the back, the halides interact with one of the side chains via dispersion interactions as well. In the **T** conformer, the dispersion interactions with the ethyl side chains are evident for both halides. Chloride also interacts with the methyl side chain. The blue colour of the surface above C2 indicates that the interaction between the anion and the carbon atom is relatively strong, greater than the van der Waals interactions with the side chains but weaker than the hydrogen bonds formed in the other conformers. The 2D NCI profiles are similar to the hydrogen bonding profiles of the halides.

It becomes apparent why it is difficult to form stable/strong hydrogen bonds in the gas phase where the anion has multiple atoms that can interact with the cation. In the case of $[CF_3CO_2]^-$, the oxygen atoms interact with the C2-hydrogen above the plane of the ring and the fluorine atoms interact with the side chain hydrogen atoms, which is significantly different from $[MeCO_2]^-$. In the latter case, the methyl group is oriented away from the anion. The interaction between the fluorine atoms and the side chain would hinder the formation of a stable conformer that undergoes hydrogen bonding, which could explain why all geometry optimisations started in the **F** position converge to the **T**.

$[MeCO_2]^-$ in the **T** conformer forms relatively strong interactions with the hydrogen in the 2-position and weak dispersion interactions with the carbon atom in the ethyl chain. The 2-D and 3-D plots of these two anions are markedly different. $[CF_3CO_2]^-$ forms multiple localised interactions with hydrogen atoms, which result in multiple overlapping peaks that form a broad peak in the attractive region and two peaks in the repulsive region.

The isosurfaces give a qualitative description of the type of interactions in the ion-pairs. From the shape of the surfaces and the position of the peaks, weak dispersion interactions can be differentiated from hydrogen bonds. To quantify any of the information provided by the reduced density gradient, integration of some surface properties are done.

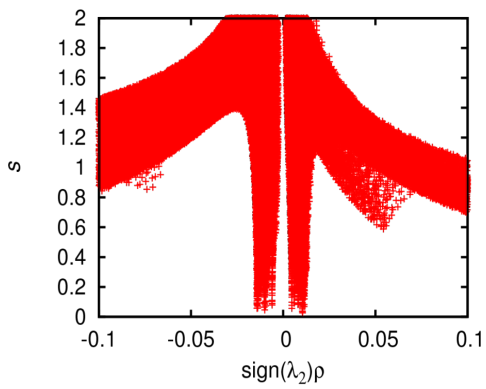

(i) [emim][BF_4]

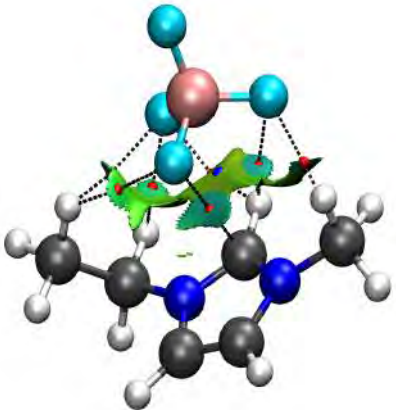

(ii) [emim][BF_4]

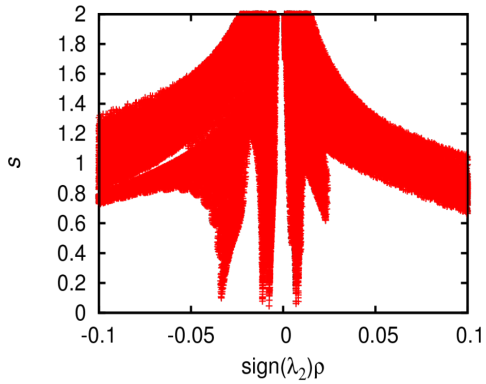

(iii) [emim][Br](**F**)

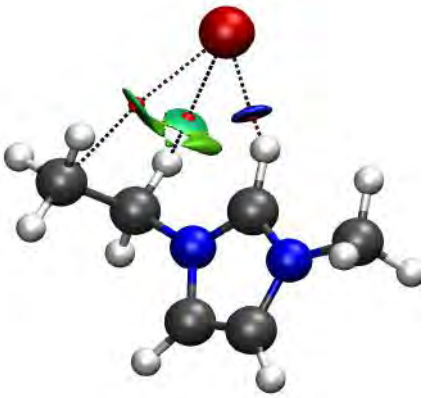

(iv) [emim][Br]

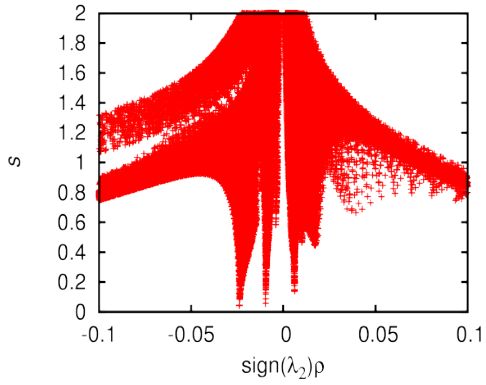

(v) [emim][Br](**T**)

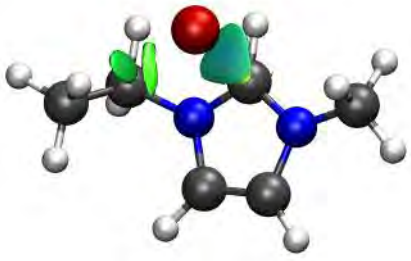

(vi) [emim][Br](**T**)

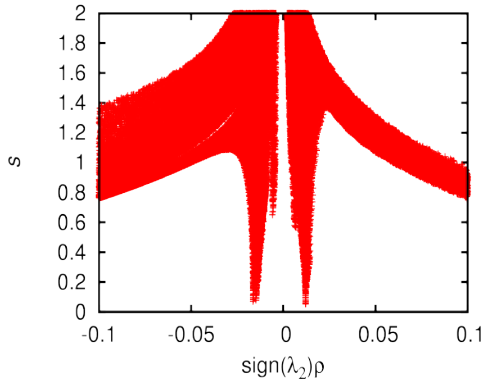

(vii) [emim][Br](**B**)

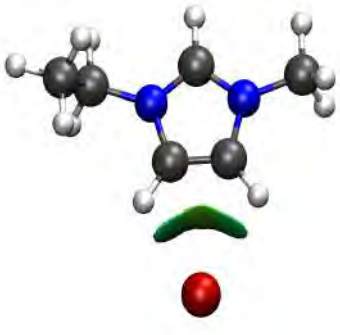

(viii) [emim][Br](**B**)

Fig. 3.14: Plot of the reduced density gradient against $sign(\lambda_2)\rho$ and their corresponding surfaces in real space at an isourface value of 0.5

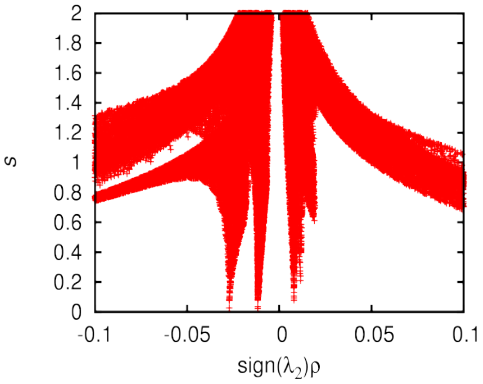

(ix) [emim][Br](**B2**)

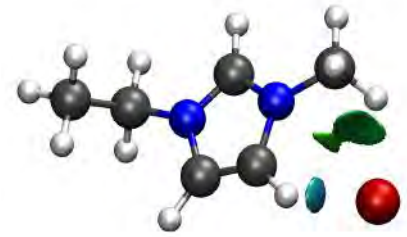

(x) [emim][Br](**B2**)

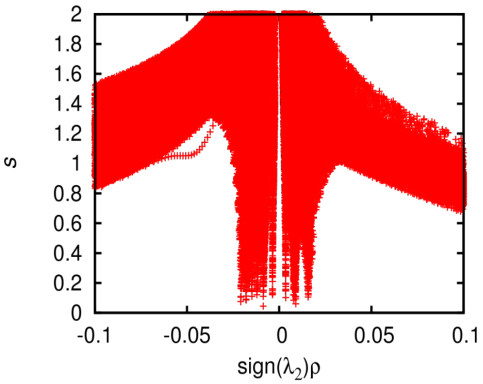

(xi) [emim][CF_3CO_2]

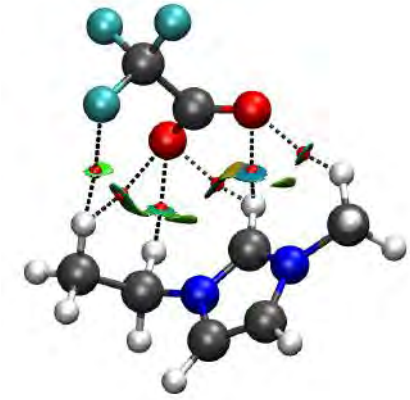

(xii) [emim][CF_3CO_2]

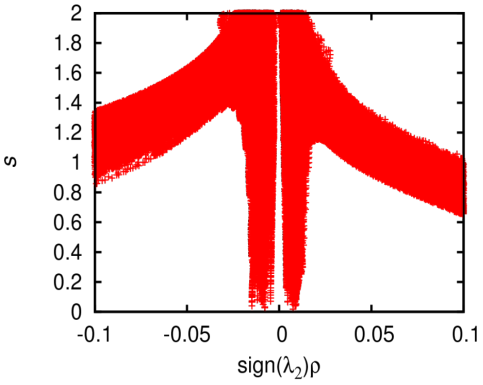

(xiii) [emim][CF_3SO_3]

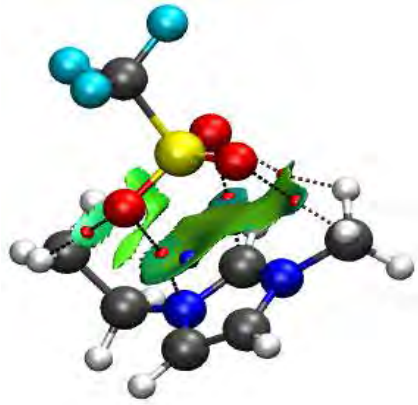

(xiv) [emim][CF_3SO_3]

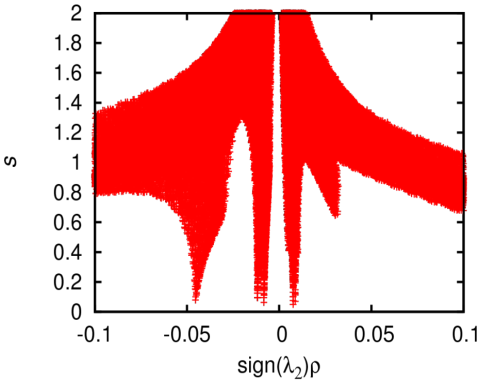

(xv) [emim][Cl](**F**)

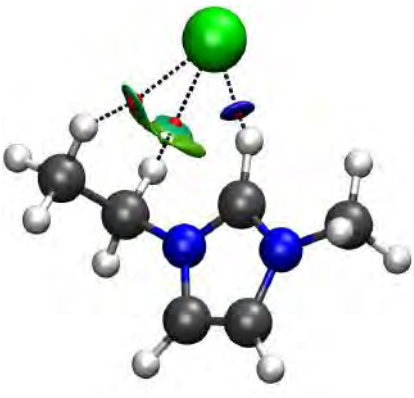

(xvi) [emim][Cl](**F**)

Fig. 3.14: Plot of the reduced density gradient against $sign(\lambda_2)\rho$ and their corresponding surfaces in real space at an isosurface value of 0.5

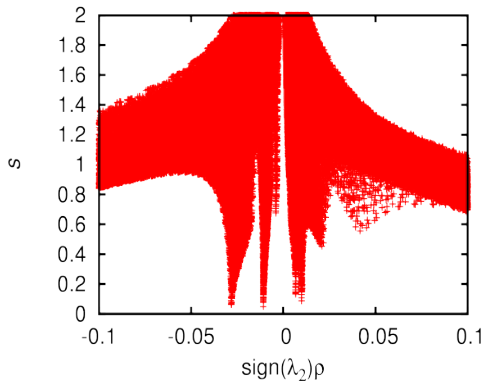

(xvii) [emim][Cl](**T**)

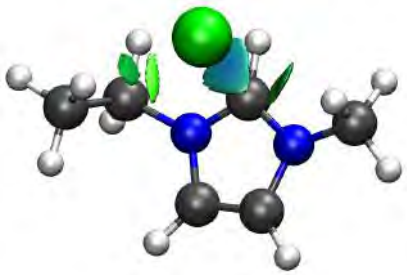

(xviii) [emim][Cl](**T**)

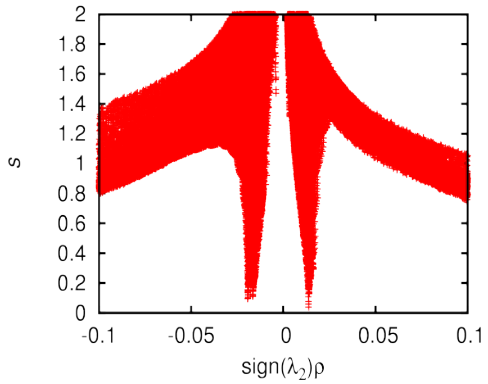

(xix) [emim][Cl](**B**)

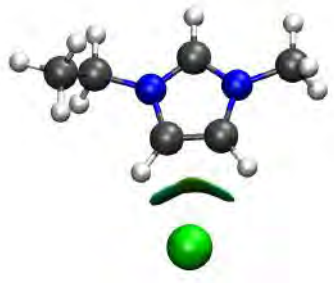

(xx) [emim][Cl](**B**)

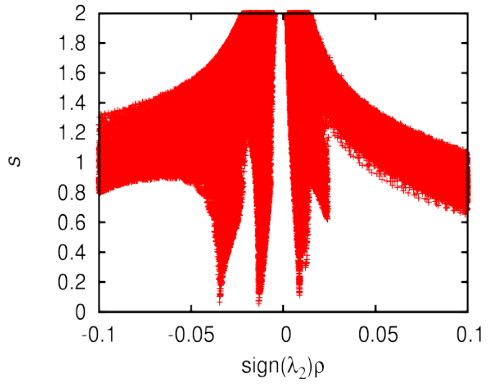

(xxi) [emim][Cl](**B2**)

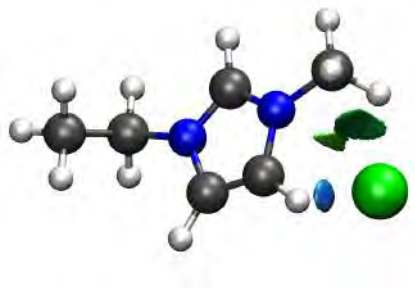

(xxii) [emim][Cl](**B2**)

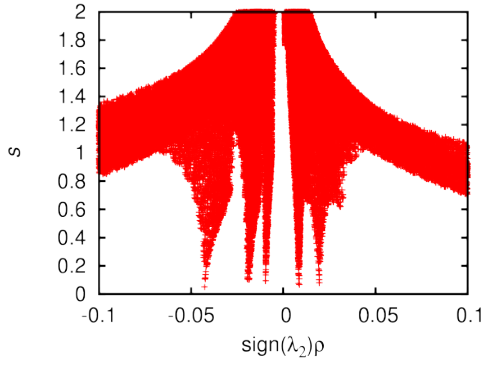

(xxiii) [emim][$MeCO_2$](**F**)

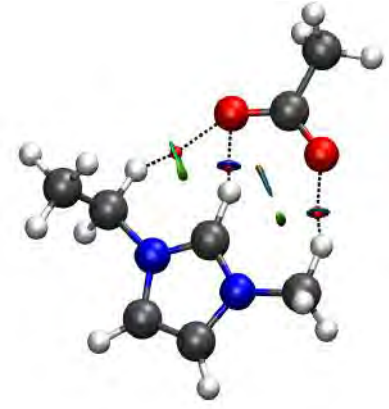

(xxiv) [emim][$MeCO_2$](**F**)

Fig. 3.14: Plot of the reduced density gradient against $sign(\lambda_2)\rho$ and their corresponding surfaces in real space at an isosurface value of 0.5

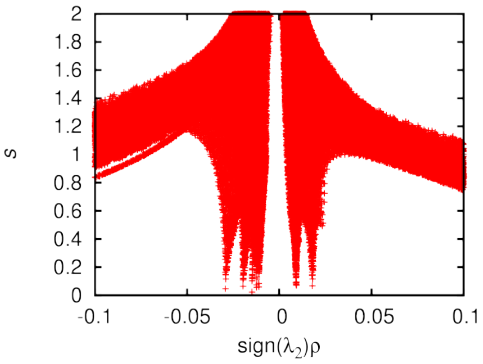

(xxv) [emim][$MeCO_2$(**T**)]

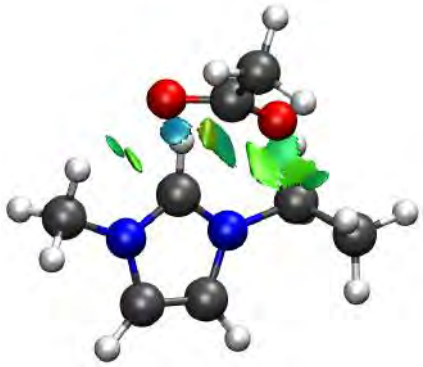

(xxvi) [emim][$MeCO_2$](**T**)

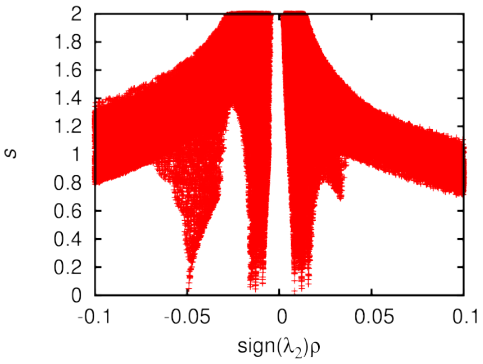

(xxvii) [emim][$MeCO_2$(**B**)]

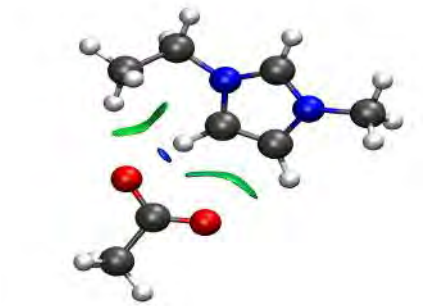

(xxviii) [emim][$MeCO_2$](**B**)

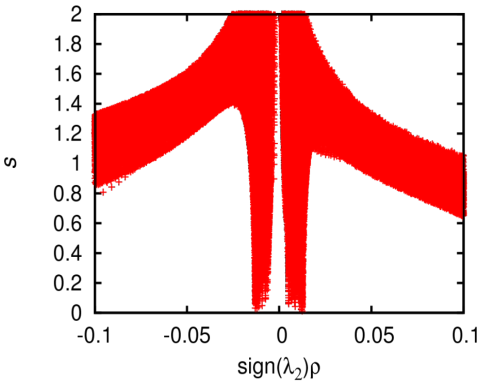

(xxix) [emim][$MeSO_3$]

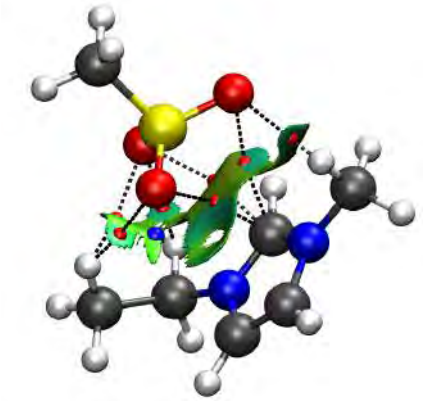

(xxx) [emim][$MeSO_3$]

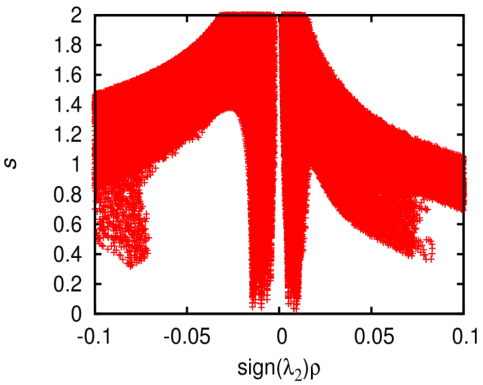

(xxxi) [emim][PF_6]

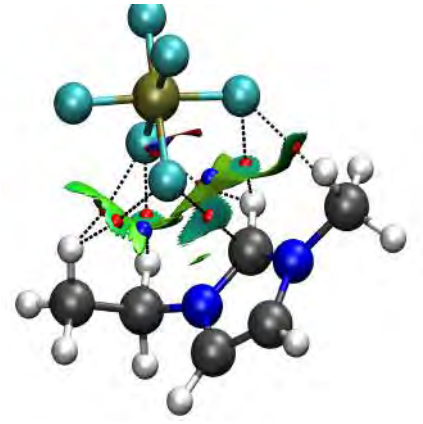

(xxxii) [emim][PF_6]

Fig. 3.14: Plot of the reduced density gradient against $sign(\lambda_2)\rho$ and their corresponding surfaces in real space at an isosurface value of 0.5

Tab. 3.7: NCI Properties at an isosurface of 0.5. The volume is reported in $\mathring{A}^3$, and the densities ρ_{att}, ρ_{rep} and ρ_{bind} are in the atomic units $\frac{e}{a_0^3}$

Complex	Volume	ρ_{att}	ρ_{rep}	ρ_{bind}
[emim][BF_4]	3.07	-15.42	18.22	2.80
[emim][Br](**F**)	0.13	-15.63	3.67	-11.97
[emim][Br](**T**)	1.24	-20.20	1.83	-18.38
[emim][Br](**B**)	0.12	-10.55	6.71	-3.84
[emim][Br](**B2**)	0.27	-30.85	5.17	-25.68
[emim][CF_3CO_2]	1.54	-12.77	8.30	-4.47
[emim][CF_3SO_3]	4.35	-16.36	25.80	9.45
[emim][Cl](**F**)	1.17	-35.43	8.72	-26.70
[emim][Cl](**T**)	1.36	-41.29	13.03	-28.26
[emim][Cl](**B**)	1.03	-18.58	12.30	-6.28
[emim][Cl](**B2**)	1.02	-31.27	5.38	-25.89
[emim][$MeCO_2$](**F**)	0.06	-23.54	7.91	-15.63
[emim][$MeCO_2$](**T**)	1.40	-26.94	19.15	-7.80
[emim][$MeCO_2$](**B**)	0.09	-26.32	13.57	-12.75
[emim][$MeSO_3$]	4.64	-22.77	26.18	3.41
[emim][PF_6]	3.28	-23.20	25.56	2.35

3.6.2 Properties of NCI surfaces

The properties include the volume of the surface, the sum of $sign(\lambda_2)\rho$ when $sign(\lambda_2)<0$, which is defined as ρ_{att} and the sum of sign$(\lambda_2)\rho$ when $sign(\lambda_2) >0$, which is ρ_{rep}. The sum of ρ_{att} and ρ_{rep} is ρ_{bind} and is estimated as an indicator of interaction strength with the most negative values indicating strong stabilizing interactions.[54] All properties are calculated using an isosurface value for **s** of 0.5. The properties of the surfaces are calculated are shown in table 3.7.

Results show that the ion-pairs that form the large flat interaction surfaces above the ring have positive ρ_{bind} values; they are the only ion-pairs that display this behaviour. This initially suggests that the interactions in these particular positions for the anions are repulsive within this NCI framework, which is not

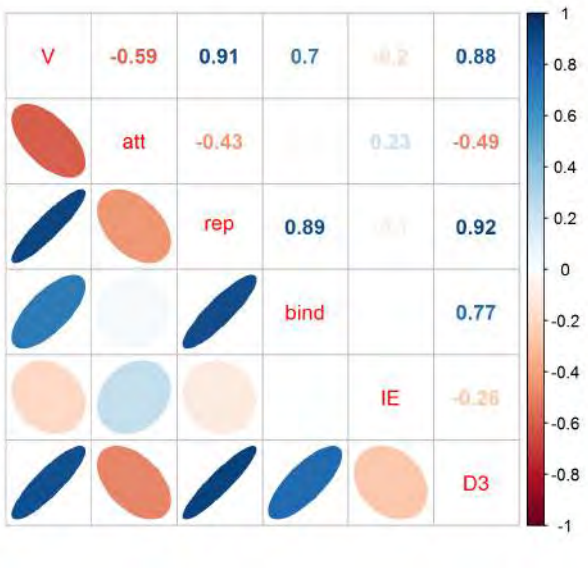

Fig. 3.15: Correlation matrix plots for NCI properties

necessarily the case. Positive values of ρ_{bind} could probably be the result of errors in the numerical calculation of $sign(\lambda_2)$ as the sign would fluctuate when $\lambda_2 \approx 0$. Thus the interpretation of the strength of interaction in these regions would be inaccurate and imprecise, this problem has been noted before by Chaudret et al.[55] On the other hand, the ion-pairs that exhibit more directional interactions have negative ρ_{bind} values owing to peaks lying more deeply in the attractive region of the 2-dimensional plots.

The properties are plotted against each other, the total interaction energy and the D3 dispersion energy in figure 3.15. The correlation coefficients are also shown in the plot. There is no correlation between the total interaction energy and ρ_{bind}. However, a positive linear correlation between ρ_{rep} and the volume of the enclosed surface is found; ρ_{bind} is positive for larger values of the volume. The D3 dispersion is included in the correlation plot to investigate its relationship with the volume. With an R value of 0.88, a weak trend between the dispersion interaction and the size of the enclosed surface is found. Although these integrated 'dispersion' surfaces have their ρ_{bind} values as positive, the size of the surface is more likely to determine how strong the dispersion interactions are within the dimer.

In general, the NCI plots and figures qualitatively describe interactions. They show that hydrogen bonds are strong and directional where they are present, and that the top position shows no directionality in the interactions (having flat disperse NCI surfaces) for anions $[BF_4]^-$, $[PF_6]^-$, $[MeSO_3]^-$, $[CF_3SO_3]^-$. $[CF_3CO_2]^-$ shows distinct atom to atom interactions with the cation (shown by the localised NCI surfaces), with the interaction of its fluorine atoms with the side chain of the cation stabilizing the interaction further, preventing the formation of the hydrogen bond in the gas phase ion-pair. Overall, the properties calculated do not provide any insight into the strength of the interactions because of the instability of the sign of λ_2.

3.6.3 Estimated Potential of the Hydrogen Bond

An attempt to quantify the strength of the hydrogen bond by integrating the density within the enclosed isosurface of the reduced density gradient is done. Although having been done for water, this has not been investigated using NCI for ionic liquids. To do this, the isosurfaces that describe the hydrogen bonding must be isolated by only calculating the reduced density gradient for regions around the surface describing hydrogen bonding. These are shown in the 2-D and 3-D NCI diagrams in figure 3.16 . The integrated properties from the isosurfaces are reported in table 3.8

The volume, ρ_{att}, ρ_{rep}, ρ_{bind} and $\overline{\rho}_{\text{bind}}$ are shown in table 3.8 with all properties calculated using an isovalue of the reduced density gradient of 0.5. $\overline{\rho}_{\text{bind}}$ is the average binding density per grid point calculated as shown in equation 3.18

$$\overline{\rho}_{\text{bind}} = \frac{\sum_{i}^{N} \rho_{\text{att}} + \sum_{i}^{N} \rho_{\text{rep}}}{\text{N}} \tag{3.18}$$

where N is the number of points in enclosed within the enclosed surface. The new properties of the hydrogen bonds are compared to some of the QTAIM parameters in figure 3.17. ρ_{rep} is negligible when compared to ρ_{att} making ρ_{bind} solely depen-

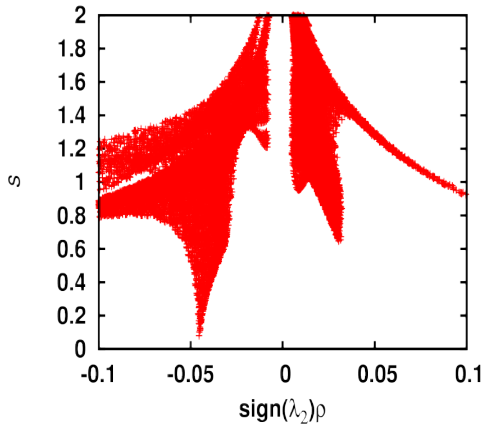

(i) 2D NCI [emim][Cl](**F**)

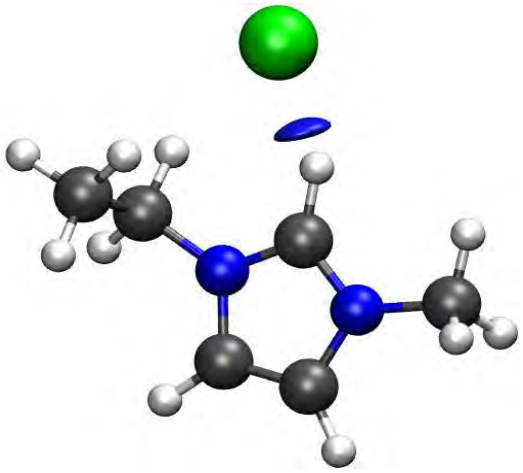

(ii) 3D NCI [emim][Cl](**F**)

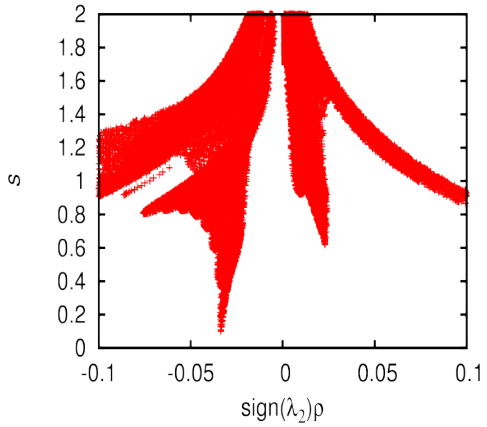

(iii) [emim][Br](**F**)

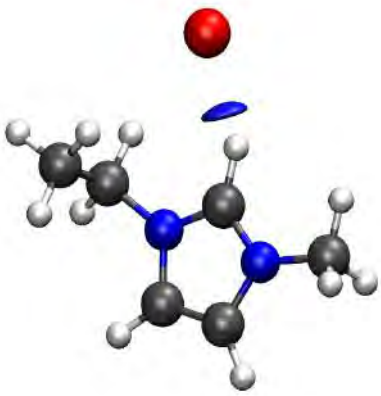

(iv) [emim][Br](**F**)

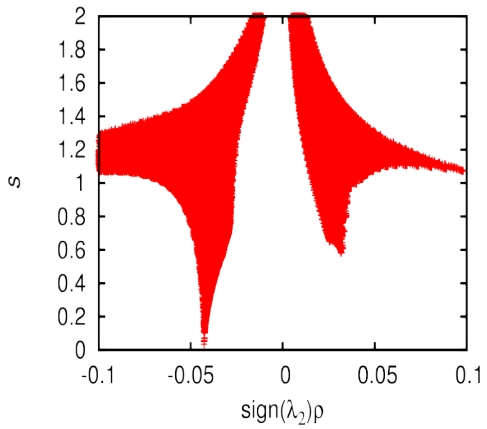

(v) [emim][$MeCO_2$](**F**)

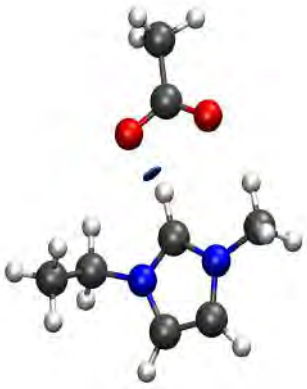

(vi) [emim][$MeCO_2$](**F**)

Fig. 3.16: The 2D and 3D NCI diagrams of the isolated hydrogen surfaces

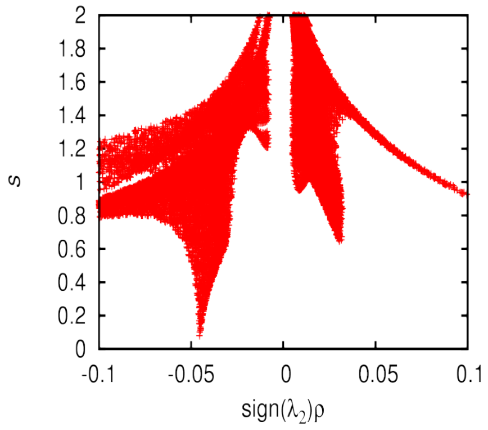

(vii) [emim][Cl](**B2**)

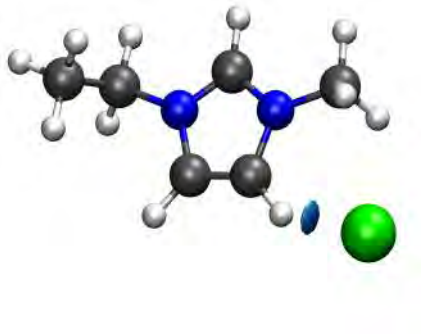

(viii) [emim][Cl](**B2**)

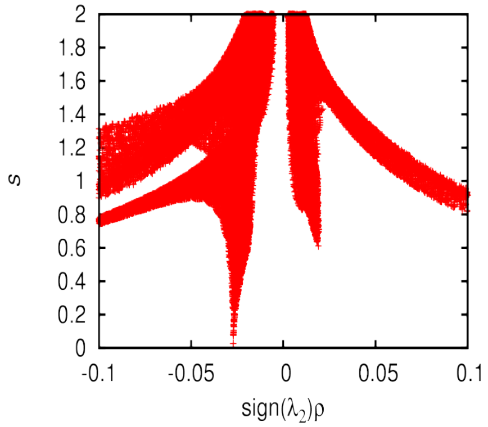

(ix) [emim][Br](**B2**)

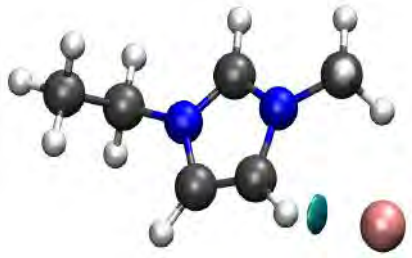

(x) [emim][Br](**B2**)

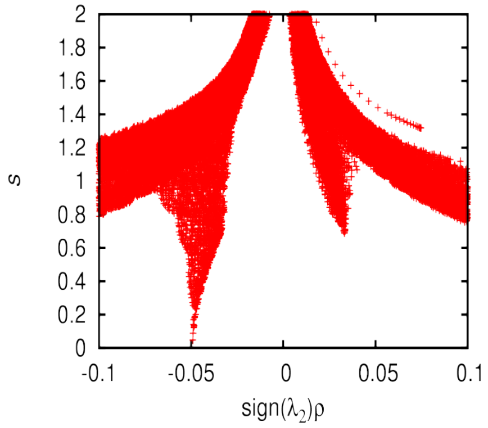

(xi) [emim][$MeCO_2$](**B**)

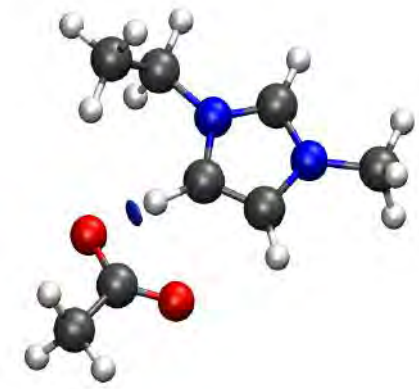

(xii) [emim][$MeCO_2$](**B**)

Fig. 3.16: The 2D and 3D NCI diagrams of the isolated hydrogen surfaces

Tab. 3.8: NCI properties of the hydrogen bond in the ion-pairs where the volume is in units $a_0{}^3$ and q_{att}, q_{rep}, q_{bind} and ρ_{bind} are in atomic units.

Complex	Volume	ρ_{att}	ρ_{rep}	ρ_{bind}	$\overline{\rho}_{bind}$
[emim][Cl](**F**)	0.659	-26.61	0.06	-26.28	-0.0397
[emim][Cl](**B2**)	0.595	-18.68	0.19	-17.64	-0.0286
[emim][Br](**F**)	0.767	-23.21	0.18	-22.22	-0.0282
[emim][Br](**B2**)	0.716	-17.33	0.09	-16.84	-0.0232
[emim][$MeCO_2$](**F**)	0.331	-12.79	0.18	-11.80	-0.0348
[emim][$MeCO_2$](**B**)	0.332	-15.40	0.00	-15.40	-0.0442

dent on the contribution of the attractive component of the density in the NCI framework. Surfaces involving the [emim][Br] ion-pair are larger than the other ion-pairs, followed by [emim][Cl] and then [emim][$MeCO_2$].

Figure 3.17 shows how the parameters correlate to certain QTAIM properties. ρ_{bind} is found to be solely dependent on ρ_{att} and the volume of the isosurface generally does not predict the strength of the interaction or the amount of charge enclosed for the ion-pairs that form hydrogen bonds. ρ_{bind}, which is expected to describe the relative strength of hydrogen bond, performs poorly in doing so.

From the QTAIM analysis, it is shown that the electron density at the bond critical point does well in estimating the potential energy of a hydrogen bond (E_{HB}), the same is attempted for the enclosed density. When the average density is plotted against the potential energy at the bond critical point, a strong trend is found with an R value of -0.94 and an even stronger correlation of 0.97 is found between the average density and the density at the bond critical point.

Using the integrated density we find that the strength of the hydrogen bond decreases as follows $MeCO_2$(**B**) > Cl(**F**) > $MeCO_2$(**F**) > Cl(**B2**) > Br(**F**) > Br(**B2**) whereas for QTAIM the ranking is $MeCO_2$(**B**) > $MeCO_2$(**F**) > Cl(**F**) > Cl(**B2**) > Br(**F**) > Br(**B2**). They differ only in the order of the strength of $MeCO_2$(**F**) and Cl(**F**) with NCI predicting that $MeCO_2$(**F**) would form a weaker

Fig. 3.17: Correlation plot of NCI and QTAIM properties.

hydrogen bond.

This is an important result because the easily accessible electron density can be used to describe hydrogen bonding directly both through visualisation of surfaces and through integration of the surfaces. With the NCI being a non-catastrophic method, depleting gradually as interactions range from bonding to non-bonding and being a more broad descriptor of interactions over space than QTAIM. The strength of the hydrogen bonds for the three ion-pairs was determined successfully, but the difficulty in finding hydrogen bonding conformers for the other ion-pairs limits the scope for investigating these specific interactions.

3.7 Conclusion

The electrostatic interactions are the most dominant interactions, greater than the dispersion and hydrogen bonding interactions by approximately an order of magnitude and the distributed multipole analysis (DMA) is the most accurate method for describing these interactions. Electrostatic interactions calculated using point charges were found to be more than half as weak as that described by the DMA. The result raises questions on the issue of charge scaling, which further reduces the electrostatic interactions and may cause significant errors in the local behaviour of ionic liquids. The dispersion and the hydrogen bonding interactions have a significant contribution to the total interaction and are of the same order. The D3 dispersion falls within the correlation energy limits and the classical force field was found to overestimate the dispersion strength, but the discrepancy is smaller than the difference between DMA and point charges in the electrostatic case.

The hydrogen bond is important in the stabilisation of three ion-pairs, which are [emim][$MeCO_2$], [emim][Br] and [emim][Cl] in the **F** and **B**/**B2** conformers. The NBO method was found to be useful in identifying hydrogen bonds by simply finding a significant amount of stabilisation through the donation of electrons from the hydrogen bond acceptor into the σ^* anti-bonding orbital. The potential energy density at the bond critical point using QTAIM was used as an estimate of the hydrogen bond energy. However, the restrictions to particular conformers was a limiting factor in determining the role of hydrogen bonding for all ion-pairs.

The NCI procedure was introduced as a method to visualise non-covalent interactions between the ion-pairs in both 2D and 3D plots. Both plots allow for the visualisation of weak disperse interactions and strong localised interactions. With the method able to characterise between these differences and also having reproduced potential energy profiles for small hydrogen bonded dimers (as reported by Yang et al.[54]) the properties of the NCI surfaces were calculated, beginning with

the volumes. It was found that the larger volumes are indicative of van der Waals interactions and ρ_{bind} was found to be small positive values. The hydrogen bond surfaces were isolated and it was found that $\overline{\rho}_{bind}$ is a good indicator of hydrogen bond strength as it correlates well the electron density at the bond critical point (ρ_C) and the potential energy at the bond critical point.

Balance of Interactions

Table 3.9 shows the combined interaction types used to estimate the total interaction energy. First the electrostatic interaction, calculated using the distributed multipole analysis, and the dispersion interaction calculated using the D3 correction are combined for the estimate of the total interaction. The hydrogen bond is then included and a mean absolute standard error (MASE) is calculated and shown.

The combined contribution of the electrostatic and dispersion interaction energies as an estimate of the total interaction energy results in a MASE of 4.94%, whilst the introduction of hydrogen bonding produces a MASE of 6.76%. The overall trend for both including and excluding hydrogen bonding results in interactions that are too strong. This is shown by a plot of the trend lines in figure 3.18. The red line is the target. The two trend lines show that the calculated estimates describe an over-binding of the complexes, with the hydrogen bonding making this effect more severe.

Missing Interactions

Exchange is not explicitly calculated and may be a contributor in the description of over-binding because attractive components are only considered. The description of the intermolecular interactions is thus incomplete. The induction or polarisation energy is also not introduced and may affect the overall results, although it may have a very limited impact.[56] These are available in SAPT but are computationally

Tab. 3.9: The energetic contributions to the total interactions

Ion-pair	E^{Total}	$E^{elst+disp}$	$E^{elst+disp+HB}$	$error^{elst+disp}$	$error^{elst+disp+HB}$
[emim][$MeCO_2$] (F)	-105.32	-104.43	-117.53	0.85	11.59
[emim][$MeCO_2$] (T)	-105.98	-109.89	-109.89	3.69	3.69
[emim][$MeCO_2$] (B)	-89.65	-89.09	-103.63	0.62	15.59
[emim][$MeSO_3$]	-101.02	-110.41	-110.41	9.30	9.30
[emim][Cl] (F)	-98.36	-93.74	-105.63	4.70	7.39
[emim][Cl] (T)	-99.93	-100.92	-100.92	0.99	0.99
[emim][Cl] (B)	-76.55	-82.74	-82.74	8.09	8.09
[emim][Cl] (B2)	-79.01	-73.25	-81.67	7.29	3.37
[emim][CF_3CO_2]	-94.95	-99.34	-99.34	4.62	4.62
[emim][BF_4]	-93.25	-92.17	-92.17	1.16	1.16
[emim][Br] (F)	-91.96	-90.66	-97.81	1.41	6.36
[emim][Br] (T)	-88.19	-99.48	-99.48	12.80	12.80
[emim][Br] (B)	-74.24	-78.21	-78.21	5.35	5.35
[emim][Br] (B2)	-82.80	-76.78	-85.47	3.64	3.22
[emim][CF_3SO_3]	-88.50	-93.71	-93.71	5.89	5.89
[emim][PF_6]	-87.61	-95.24	-95.24	8.71	6.76
MASE				4.94%	6.76%

expensive even at the size of the systems studied here. With the hydrogen bond increasing the MASE, its introduction in calculating it as a part in the total interaction energy must be questioned.

Hydrogen Bonding: Distinct or Excluded?

Can the hydrogen bond reasonably be described as a separate or unique interaction type that is not already included within the dispersion, electrostatic and induction interactions? The results appear to refute this because the hydrogen bond potential significantly raises the error for hydrogen bonded conformations of [emim][$MeCO_2$].

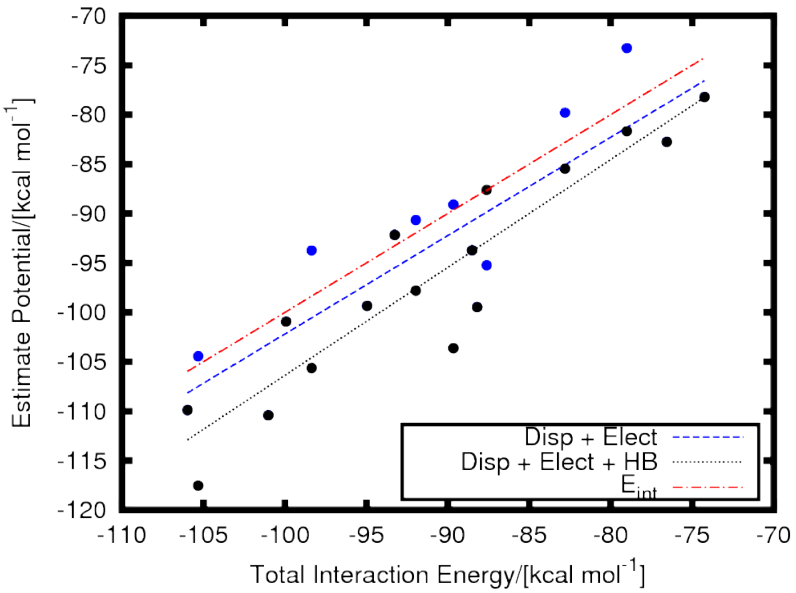

Fig. 3.18: Estimates of the total interaction energy

Hydrogen bonding from a chemist's perspective is very important and the ability to determine hydrogen bond strength may not be relevant in being included as part of the total interaction energy but is relevant in studying its effect on the properties of ILs. Geometry optimisations of the ion-pairs do not produce hydrogen bonding conformations for all pairs, thus a different method for finding these conformers from the condensed phase is presented in 4.

Bibliography

[1] Matthews, R. P.; Ashworth, C.; Welton, T.; Hunt, P. A. *J. Phys.:Condens. Matter* **2014**, *26*.

[2] Izgorodina, E. I.; Golze, D.; Maganti, R.; Armel, V.; Taige, T. J. S., M. amd Schubert; MacFarlane, D. R. *Phys. Chem. Chem. Phys.* **2014**, *16*, 7209–7221.

[3] Izgorodina, E. I.; MacFarlane, D. R. *J. Phys. Chem. B* **2011**, *115*, 14659–14667.

[4] Köckerling, M.; Ludwig, R.; Roth, C.; Pepperl, T.; Fumino, K.; Paschek, D. *Angew. Chem. Int. Ed.* **2011**, *50*, 6661–6665.

[5] Frisch, M. J. et al. Gaussian09 Revision D.01. Gaussian Inc. Wallingford CT 2009.

[6] Zhao, Y.; Truhlar, D. G. *Theor. Chem. Acc.* **2008**, *120*, 21–241.

[7] Sherrill, C. D.; Hohenstein, E. G.; Chill, S. T. *J. Chem. Theory Comput.* **2008**, *12*, 1996–2000.

[8] Weigend, F.; Ahlrichs, R. *J. Am. Chem. Soc* **1976**, *98*, 377–383.

[9] Zheng, J.; Xu, X.; Truhlar, D. G. *Theo. Chem. Acc.* **2011**, *128*, 295–305.

[10] Frontera, A.; Bauzá, A.; Quiñonero, D.; Deyá, P. M. *J. Am. Chem. Soc* **1976**, *98*, 377–383.

[11] Izgorodina, E. I.; MacFarlane, D. R.; Bernard, U. L. *J. Phys. Chem. C* **2010**, *114*, 20472–20478.

[12] Hunt, P. A.; Kirchner, B.; Welton, T. *Chem. Eur. J.* **2006**, *12*, 6762–6775.

[13] Keith, T. A. AIMAll (Version 14.06.21). Overland Park KS, USA, 2014 (aim.tkgristmill.com).

[14] Stone, A. J. *J. Chem. Theory Comput.* **2005**, *1*, 1128–1132.

[15] Kisiel, Z. PROSPE—Programs for ROtational SPEctroscopy. http://info.ifpan.edu.pl/ kisiel/prospe.htm.

[16] Spherical Coordinates. `http://en.wikipedia.org/wiki/Spherical_coordinate_system#mediaviewer/File:3D_Spherical.svg`, Accessed: 2014-10-13.

[17] Boys, S. F.; Bernadi, F. *Mol. Phys.* **1970**, *19*, 553.

[18] Maginn, E. J.; Morrow, T. I. *J. Phys. Chem. B* **2002**, *106*, 12807–12813.

[19] Bühl, M.; Chaumont, A.; Schurhammer, R.; Wipff, G. *J. Phys. Chem. B* **2005**, *109*, 18591–18599.

[20] Schröder, C. *Phys. Chem. Chem. Phys.* **2012**, *14*, 3089–3102.

[21] Cremer, T.; Kolbeck, C.; Lovelock, K.; Paape, N.; Wlfel, R.; Schulz, P.; Wasserscheid, P.; Weber, H.; Thar, J.; Kirchner, B.; Maier, F.; Steinrck, H.-P. *Chem. Eur. J.* **2010**, *16*, 9018–9033.

[22] Young, T. G. A.; Hardacre, C. *ChemPhysChem* **2008**, *9*, 1548–1558.

[23] Yan, T.; Wang, Y.; Knox, C. *J. Phys. Chem. B* **2010**, *114*, 6886–6904.

[24] Izgorodina, E. I.; Rigby, J. *Phys. Chem. Chem. Phys.* **2013**, *15*, 1632–1646.

[25] Mondal, A.; Balasubramanian, S. *J. Phys. Chem. B.* **2014**, *118*, 3409–3422.

[26] Maginn, E. J.; Zhang, Y. *J. Phys. Chem. B.* **2012**, *118*, 3409–3422.

[27] Bonhôte, P.; Dias, A.; Papageogiou, N.; Kalyanasundaram, K.; Grätzel, M. *Inorg. Chem.* **1996**, *35*, 1168–1178.

[28] Magill, B. F., A. M.and Yates *Aust. J. Chem.* **2004**, *57*, 1205–1210.

[29] Buckingham, A. D.; Fowler, P. W.; Hutson, J. M. *Chem. Rev.* **1988**, *88*, 963–988.

[30] Stone, A. J.; Aldertone, M. *Mol. Phys.* **2002**, *100*, 221–233.

[31] R Core Team, R: A Language and Environment for Statistical Computing. R Foundation for Statistical Computing: Vienna, Austria, 2013; ISBN 3-900051-07-0.

[32] Wei, T. corrplot: Visualization of a correlation matrix. 2013; R package version 0.73.

[33] Grimme, S.; Hujo, W.; Kirchner, B. *Phys. Chem. Chem. Phys.* **2012**, *14*, 4875–4883.

[34] Koopmans, T. *Physica* **1934**, *1*, 104–113.

[35] Israelachvili, J. *Intermolecular and Surface Forces*, third edition ed.; Academic Press, 2011.

[36] Liu, Z.; Huang, S.; Wang, W. *J. Phys. Chem. B* **2004**, *108*, 12978–12989.

[37] Wang, J.; Wolf, R. M.; Caldwell, J. W.; Kollman, P. A.; Case, D. A. *J. Comp. Chem.* **2004**, *25*, 1157–1174.

[38] Lopes, C.; José, N.; Pádua, A. H. *J. Phys. Chem. B* **2004**, *108*, 16893–16898.

[39] Canongia Lopes, J. N.; Pádua, A. A. H.; Shimizu, K. *J. Phys. Chem. B* **2008**, *112*, 5039–5046.

[40] Grimme, S.; Antony, J.; Ehrlich, S.; Krieg, H. *J. Chem. Phys.* **2010**, *132*, 154104–1–18.

[41] Wang, S. P.; Sun, I.; Chen, P.; Huang, J. *Inorg. Chim. Acta.* **2001**, *320*, 7–11.

[42] Lehman, S. B.; Roatsch, M.; Schöppke, M.; Kirchner, B. *Phys. Chem. Chem. Phys.* **2010**, *12*, 7473–7486.

[43] Fumino, K.; Peppel, T.; Geppert-Rybczyńska, M.; Zaitsau, D. H.; Lehman, J.; Verevkin, S. P.; Köckerling, M.; Ludwig, R. *Phys. Chem. Chem. Phys.* **2011**, *13*, 14064–14075.

[44] Dong, K.; Zhang, S. *Chem. Eur. J.* **2012**, *18*, 2748–2761.

[45] Kirchner, B.; Kohagen, M.; Brehm, M.; Lingscheid, Y.; Giemoth, R.; Sangoro, J.; Kremer, F.; Naumov, S.; Iacob, S.; Körger, J.; Valiuliln, R. *J. Phys. Chem. B.* **2011**, *115*, 15280–15288.

[46] Weinhold, F. *J. Comp. Chem* **2012**, *33*, 2363–2379.

[47] Bader, R. F. W. *Atoms in Molecules - A Quantum Theory*; Oxford University Press: Oxford, UK, 1990.

[48] Koch, U.; Popelier, P. L. A. *J. Phys. Chem.* **1995**, *99*, 9747–9754.

[49] Rozas, I.; Alkorta, I.; Elguero, J. *J. Am. Chem. Soc.* **2000**, *122*, 1154–11161.

[50] Parthasarathi, R.; Subramanian, V.; Sathyamurthy, N. *J. Phy. Chem. A* **2006**, *110*, 3349–3351.

[51] Espinosa, E.; Molins, E.; Lecomte, C. *Chem. Phys. Lett.* **1998**, *285*, 170–173.

[52] Katsyuba, S. A.; Vener, M. V.; Zvereva, E. E.; Fei, Z.; Scopelliti, R.; Laurenczy, G.; Yan, N.; Paunescu, E.; Dyson, P. J. *J. Phys. Chem. B.* **2013**, *117*, 9094–9105.

[53] Johnson, E.; Keinan, S.; Paula, M.; Julia, C.; Cohen, A.; Yang, W. *J. Am. Chem. Soc.* **2010**, *132*, 6498–6506.

[54] Julia, C.; Yang, W.; Johnson, E. *J. Phys. Chem. A.* **2011**, *115*, 12983–12990.

[55] Chaudret, R.; de Courcy, B.; Contreras-Garcia, J.; Gloaguen, E.; Zehnacker-Rentien, A.; Mons, M.; Piquemal, J.-P. *Phys. Chem. Chem. Phys.* **2014**, *16*, 9876–9891.

[56] Schmidt, J. R.; Choi, E.; McDaniel, J. G.; Yethiraj, A. *J. Phys. Chem. Lett.* **2014**, *5*, 2670–2674.

4

Analysis From the Condensed Phase

Integrating the NCI surface for its enclosed electron density is useful because it can be linked to the potential energy density at a bond critical point, which is used to estimate the strength of the hydrogen bond. The difficulty in obtaining conformers that undergo hydrogen bonding for anions other than the halogens and acetate is a large impediment in determining hydrogen bond strength. To remedy this, molecular dynamics simulations of the ionic liquids are run to produce an ensemble of configurations. From the trajectories, ion-pairs that fit a geometric criteria for the formation of a hydrogen bond are extracted. Once extracted, the average electron density and its gradient are calculated to produce an averaged reduced density gradient. The average reduced density gradient is used for the integration of the electron density and used to estimate the strength of the hydrogen bond. A similar approach has been used by Yang.[1]

4.1 Molecular Dynamics Simulations

Molecular dynamics simulations were run for 1-ethyl-3-methylimidazolium based ionic liquids. Parameters used were the same as those used in the previous chapter (see table 3.4 on page 88). Four systems are chosen for the molecular dynamics simulations, which are [emim][BF_4], [emim][Cl], [emim][$MeCO_2$] and [emim][CF_3SO_3].

Simulation Details

All simulations were performed at constant temperature and pressure using the Berendsen thermostat[2] using the DL_POLY 2.20 simulation code.[3] The simula-

tions were run at 400 K, a temperature higher than all the melting points.[4,5] The simulations were carried out using 500 pairs of cations and anions in the central simulation box. Starting structures were obtained from the Packmol programme,[6] which generates starting configurations for molecular dynamics simulations. 1 ns simulations were generated and the equations of motion integrated using a Leap-frog algorithm with the time step set to 1 fs. The SHAKE algorithm was used to constrain the intramolecular geometries for the covalent bonds involving hydrogen atoms.[7] Frames were saved every 100 steps. A cut-off radius of 12 Å was applied for the Lennard-Jones interactions. Long range electrostatics were accounted for by using the Ewald summation technique[8] with a precision of 1×10^{-8}.

Geometric Analysis

Hydrogen bonding statistics were produced by constructing histograms where the angle and distance between hydrogen bond donor (C2) and acceptor (X) were binned and plotted in figure 4.1. The binned distances range from 1 to 8 Å and the angles from 0 to 180°. The histograms were then used to define the geometric criteria from which ion-pairs were extracted in order to analyse the hydrogen bond.

All the histograms in figure 4.1 show that there are high counts around 2 Å and 120°, this is the region of interest from which we base our criteria for the extraction of the ion-pairs. It is also clear that the most dominant conformer in all the histograms lies at a distance from C2–H of 5 and 6 Å at an angle around 20°, this is the hydrogen bond acceptor at the back of the ring. Magnifying the region between 1 and 3 Å and angles between 90 and 180° (shown by the boxes in the figures) and remapping the colour scale produces figure 4.2.

4.2 Extraction of the Ion-Pair

The geometric criteria for extracting ion-pairs are shown in table 4.1. The selections are made such that the same ion-pair is not selected twice and all selections

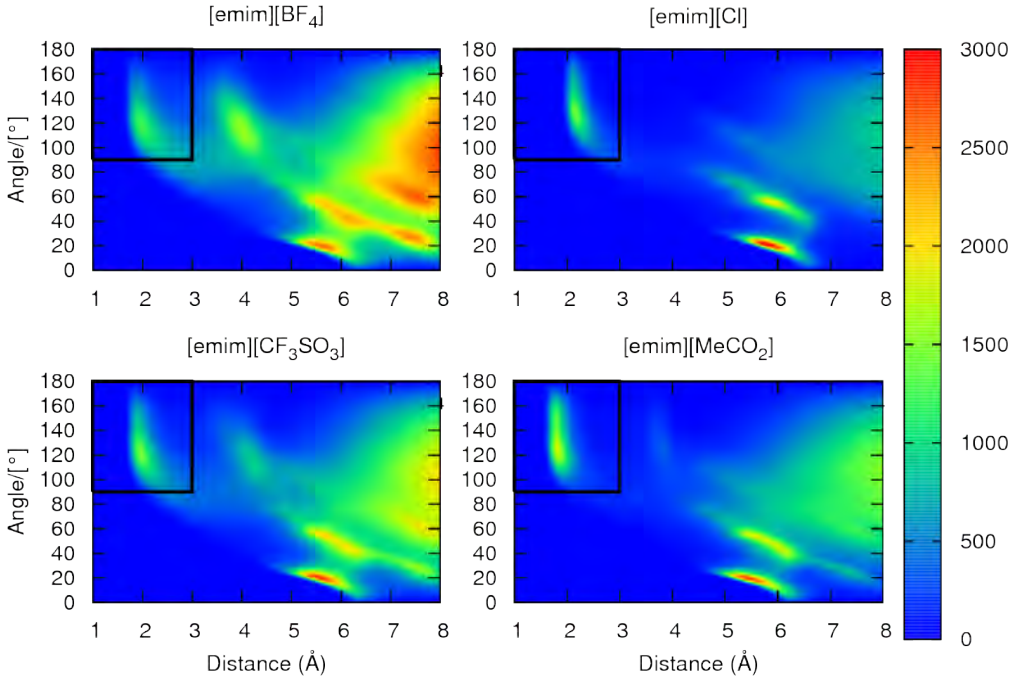

Fig. 4.1: Combined distribution functions (CDFs)

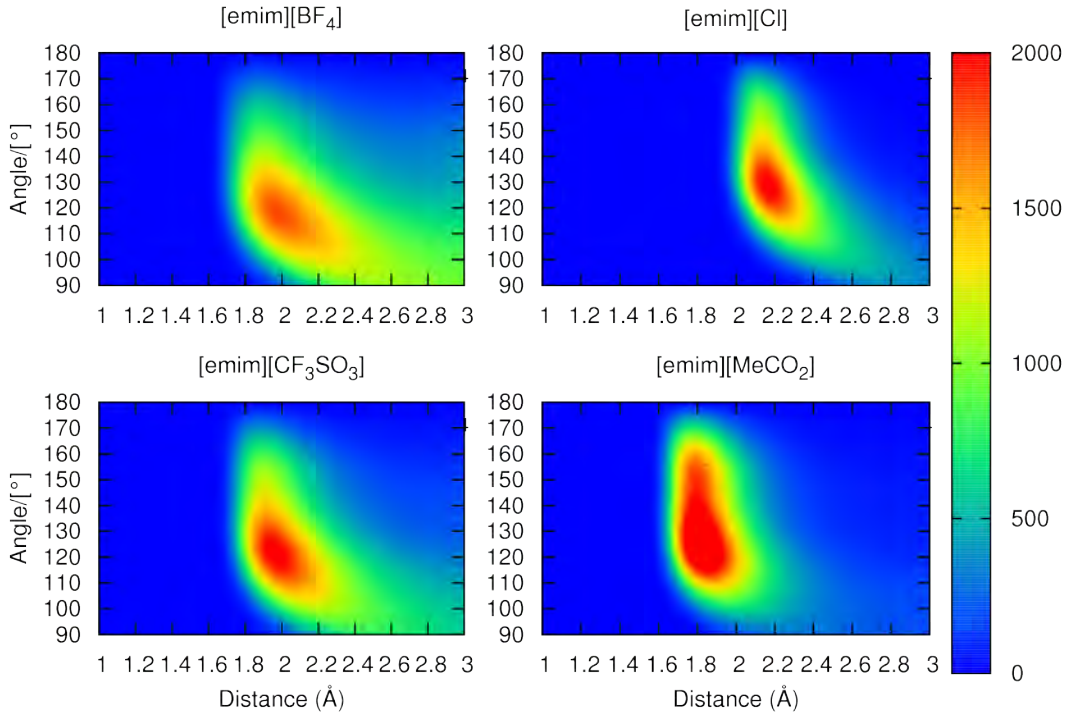

Fig. 4.2: Hydrogen Bond regions in the CDFs

are made from different frames. The ion-pair was then chosen as the QM layer in an ONIOM (Our Own N-layer Integrated molecular Orbital molecular Mechanics)[9] calculation and the 100 closest neighbouring anions and cations were taken as the local environment, which is the MM layer. The MM layer is modelled using the Amber force field with parameters from table 3.4; it remains fixed/static and provides a polarising environment that restricts the optimization of the ion-pair to hydrogen bonding conformations. The QM calculation is done using M06-2x/def2-TZVP with electronic embedding. The geometry optimization is done to improve on the description of the ion-pair interaction resulting from possible deficiencies in the force field. Between 70 and 100 frames were extracted for each ionic liquid.

Figure 4.4iii shows an example selection for [emim][$MeCO_2$]. The ball and stick representation shows the QM layer and the line representations show the local environment.

4.3 Average Reduced Density Gradient

Each of the optimised structures was reoriented such that the atoms in the ring of the imidazolium were aligned using the Kabsch algorithm, which generates the optimal rotation matrix for each set of geometries. All grid-points in each of the cube files must coincide if a reasonable average of the density around the cation is to be calculated. A set of atoms that remains fixed must be present as a reference for reorientation.

Tab. 4.1: The geometric criteria for the selection of hydrogen bonding geometries. Distances are reported in Å and angles in *ĉirc*

IL	Distance	Angle
[emim][BF_4]	1.90 – 2.10	119.0 – 121.0
[emim][Cl]	2.10 – 2.30	134.0 – 135.0
[emim][$MeCO_2$]	1.70 – 1.90	129.0 – 131.0
[emim][$MeSO_3$]	1.80 – 1.20	118.0 – 122.0

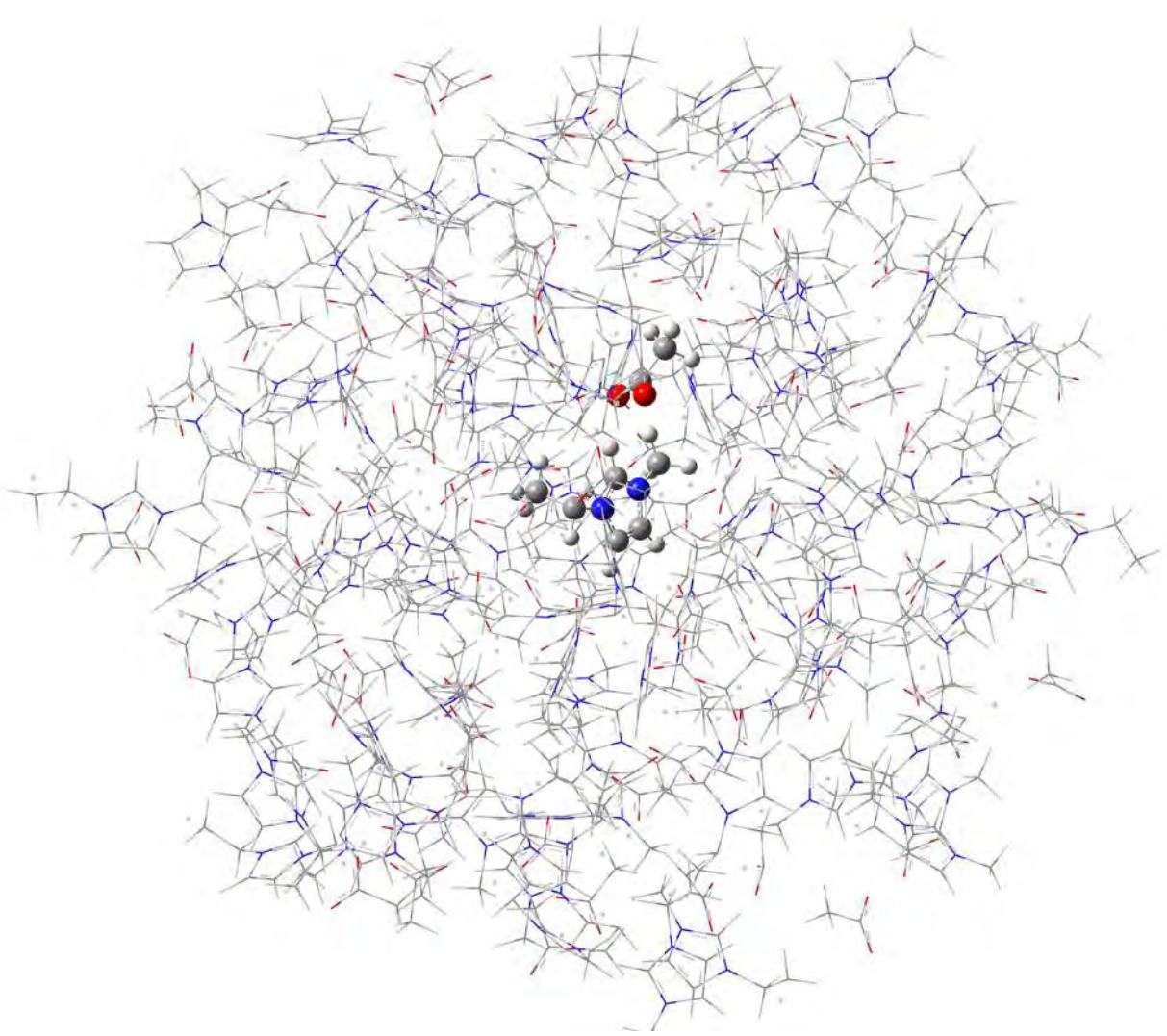

Fig. 4.3: An example of a single selection from a trajectory of [emim][$MeCO_2$] in a hydrogen bonding conformation. The ball and stick representation shows the QM layer and the line representation shows the MM layer

The merged structures of the ion-pairs are shown in figure 4.4, showing the ring atoms aligned. The anions $[BF_4]^-$, Cl^- and $[MeSO_3]^-$ group to occupy a band above, in front and below the the ring around C2. The $[MeCO_2]^-$ anions group more in front of the ring. The figure also illustrates that although similar selection criteria were used for the initial conformations, the ONIOM calculation results in a wider spatial distribution for the [emim][BF_4], [emim][Cl] and [emim][CF_3SO_3] ion-pairs. This could be an indication that the force field might not be adequate in describing ion-pairs for these systems.

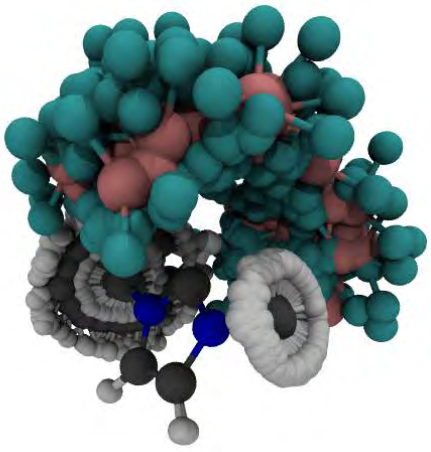

(i) [emim][BF_4] frames

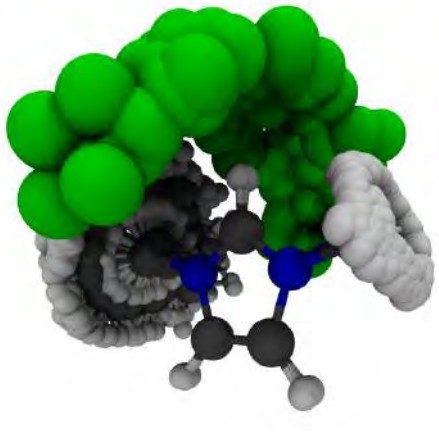

(ii) [emim][Cl] frames

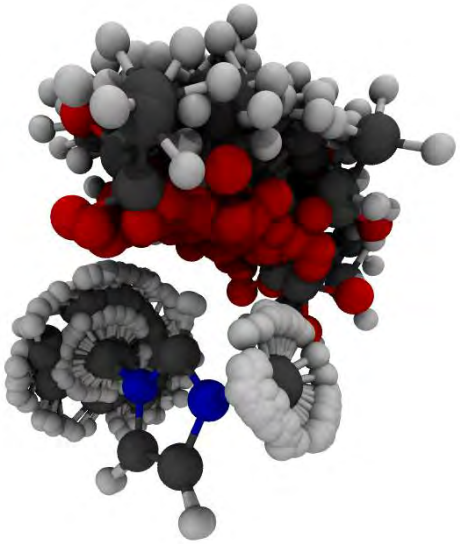

(iii) [emim][$MeCO_2$] frames

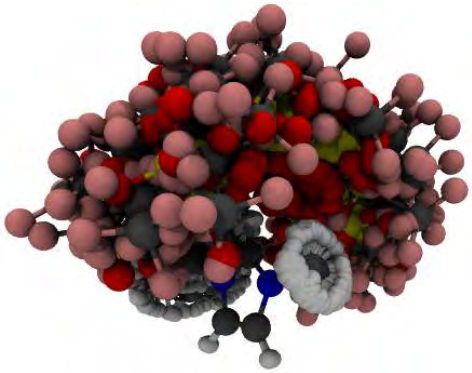

(iv) [emim][CF_3SO_3] frames

Fig. 4.4: Superposition of extracted ion-pairs in separate frames

Once aligned, the electron density and its gradient was calculated and the average RDG (aRDG) obtained from equation 4.1

$$\overline{s(r)} = \frac{1}{2(3\pi^2)^{1/3}} \frac{|\overline{\nabla\rho(r)}|}{\overline{\rho(r)}^{4/3}} \tag{4.1}$$

where $\overline{\rho(r)}$ is the average electron density and $\overline{\nabla\rho(r)}$ is the average gradient of the electron density. The 2D profiles of the aRDGs are shown in figure 4.5.

Peaks are present for all the profiles. [emim][BF_4] and [emim][$MeSO_3$] have similar profiles with very broad peaks around zero of $sign(\lambda_2)\rho$. [emim][Cl] has

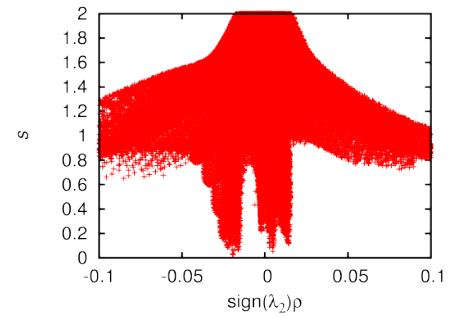

(i) average 2D NCI [emim][Cl]

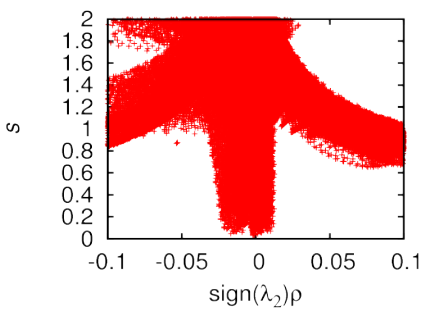

(ii) average 2D NCI [emim][BF_4]

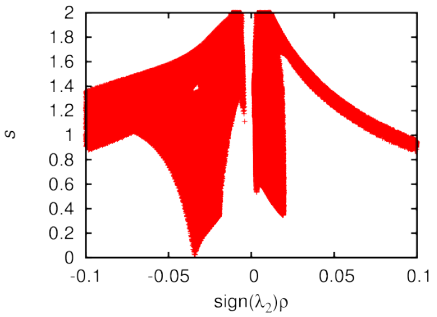

(iii) average 2D NCI [emim][$MeCO_2$]

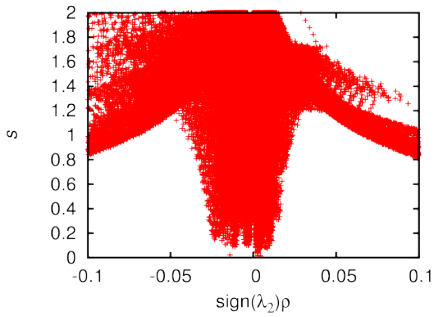

(iv) average 2D NCI [emim][$MeSO_3$]

Fig. 4.5: 2D average NCI

broad peaks in both the attractive and repulsive regions. Unlike [emim][$MeSO_3$] and [emim][BF_4], the attractive peak of [emim][Cl] is separate from the repulsive peak but is not deeper in the attractive region than the former. [emim][$MeCO_2$] has a sharp peak in the attractive region, similar to the hydrogen bond profile for the isolated ion-pair.

The 3D average NCI in figure 4.6 reflects the 2D profiles in real space. [emim][BF_4], [emim][Cl] and [emim][$MeSO_3$] have large delocalised green surfaces, which are typical of van der Waals interactions. The NCI surfaces of [emim][BF_4] and [emim][$MeSO_3$] ion-pairs have faint blue marks, which are possibly hydrogen bonds that are masked by the dispersion interactions.

With the surfaces being delocalised for these ionic liquids, obtaining the average hydrogen bond surfaces was not successful. However, the average reduced density surface for the hydrogen bond is found for [emim][$MeCO_2$] with a rounded surface that is blue in the middle and green on the edges. The method for generating an

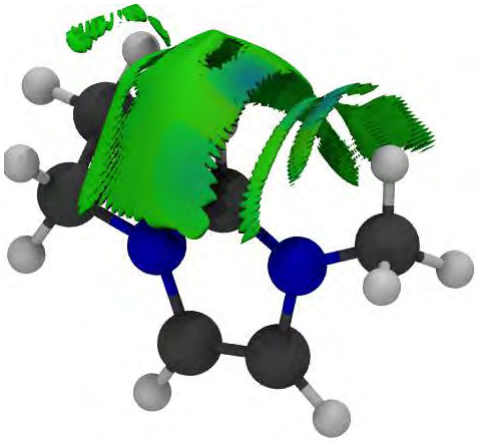

(i) [emim][BF_4]

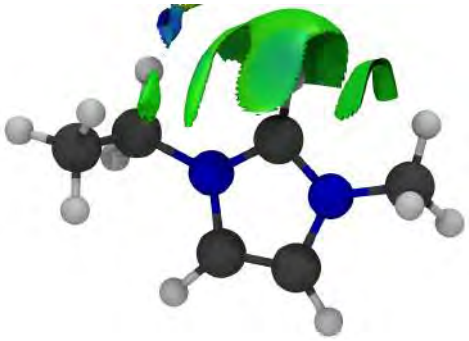

(ii) [emim][Cl]

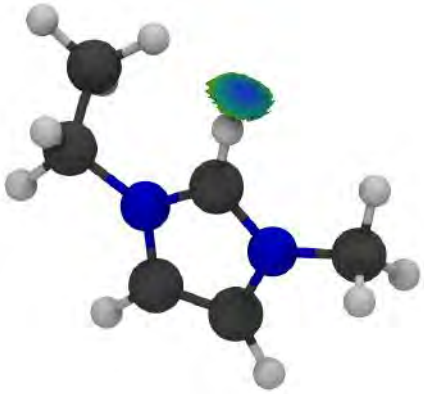

(iii) [emim][$MeCO_2$]

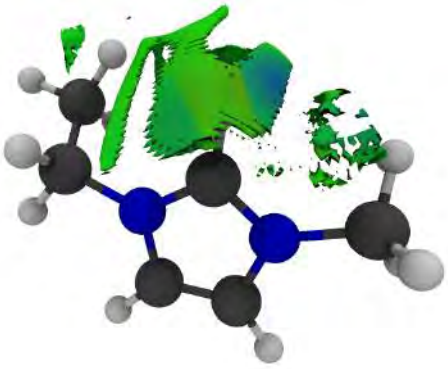

(iv) [emim][$MeSO_3$]

Fig. 4.6: aRDG isosurface plotted in real space for hydrogen bonding conformers extracted from the condensed phase at an isovalue of 0.5

average reduced density gradient shown in figure 4.10 is thus partially successful and can only be done for very strong hydrogen bonds.

4.3.1 Strength of the Hydrogen Bond in Bulk [emim][$MeCO_2$]

With the hydrogen bond surfaces found, the effect of the environment on hydrogen bond strength can be studied by simply removing the environment and calculating the average density and gradient. The properties of the RDG are reported in table 4.2 for the polarised and non-polarised ion-pair extracted from the molecular dynamics simulation and the gas phase ion-pair in the **F** conformation.

ρ_{att} suggests that the polarising environment reduces the attractive component of the hydrogen bond but ρ_{rep} suggests that the environment weakens the repulsive

Tab. 4.2: NCI Properties of the imidazolium acetate where the volume in units $\mathring{A}^3$ and ρ_{att}, ρ_{rep}, ρ_{bind} and $\overline{\rho}_{\text{bind}}$ are in atomic units ($\frac{e}{a_0^3}$) and the estimated potential (E) is in $\text{kcal} \cdot \text{mol}^{-1}$

Complex	ρ_{att}	ρ_{rep}	ρ_{bind}	$\overline{\rho}_{\text{bind}}$	E
[emim][$MeCO_2$](**pol**)	-11.08	2.05	-9.03	-0.0167	-3.13
[emim][$MeCO_2$](**nopol**)	-11.80	2.13	-9.67	-0.0240	-3.46
[emim][$MeCO_2$](**F**)	-12.79	0.18	-11.80	-0.0348	-10.83

pol = atomic charges of the environment polarising the ion-pair.
nopol = condensed phase ion-pair with atomic charges removed in the calculation

contribution when compared to the non-polarised ion-pair. This is shown by the estimate of the hydrogen bonding potential when polarised at -3.13 $\text{kcal} \cdot \text{mol}^{-1}$ and the non-polarised at -3.46 $\text{kcal} \cdot \text{mol}^{-1}$. The estimated hydrogen bond potential using NCI of the gas phase ion-pair is -10.83 $\text{kcal} \cdot \text{mol}^{-1}$. Overall, $\overline{\rho}_{\text{bind}}$ suggests that polarising the environment slightly weakens the hydrogen bond and that hydrogen bonding in the gas phase is approximately three times stronger than hydrogen bonding in the condensed phase. The weakening of the hydrogen bond may be attributed to two factors, the major factor is the difference in the hydrogen bonding geometry as a result of interactions with the other species in the liquid and the minor factor is the polarising effect of the environment.

The study of hydrogen bonding in ionic liquids by Kutsyuba et al. showed that hydrogen bonding for the isolated ion-pairs of 1-(2'-hydroxylethyl)-3-methylimidazolium ($[C_2OHmim]^+$) based ionic liquids with $[PF_6]^-$, $[BF_4]^-$ and $[CF_3SO_3]^-$ as the anions is twice as strong as hydrogen bonding in bulk because of multiple secondary interactions in the bulk.[10] The results in this study support the conclusion that the presence of the local environment reduces the hydrogen bond strength.

4.3.2 Effect of Polarisation on the Cation

To visualise the effects of polarisation on the cation, a difference density plot is shown in figure 4.7 at an isosurface of 0.002 a.u. The colour red in the figure represents regions where the density is higher for the polarised ion-pair and blue represents regions where the density is higher for the non-polarised ion-pair. Mov-

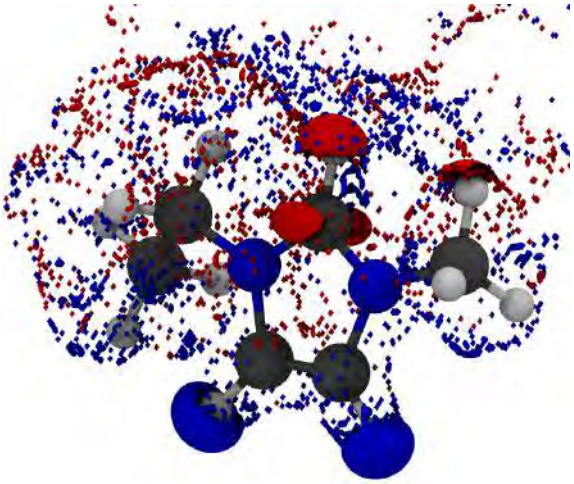

Fig. 4.7: Difference density plot of [emim][$MeCO_2$]. Red represents regions where the density is higher for the polarised ion-pair and blue represents regions where the density is higher for the non-polarised ion-pair.

ing from non-polarised to polarised ion-pairs, the electron density is moved from the blue region to the red region. This can be used to rationalise the reduction in hydrogen bond strength. From the figure, the density moves away from the hydrogen atoms in the 4 and 5-position toward the hydrogen in the 2-position and around the carbon in the 2-position. The polarising environment thus increases the acidity of the hydrogen atoms at the back of the ring and decreases the acidity of the hydrogen in the 2-position. This effectively reduces the hydrogen bond donor strength of the cation, making the hydrogen bond weaker.

The average Mulliken charges on the cation in the high layer of the ONIOM calculations are found and compared to the same cations when the polarising environment is removed, calculations are conducted with all the cations paired with their hydrogen bond acceptor partners in the higher layer. The average charges of the ring atoms are shown in table 4.3 Atoms C2 and H2 become less positive when the electronic effect of the environment is included. Atoms N1, N3, C4 and C5 become more negative. Atoms H4 and H5 become more positive. With respect to H2, the polarising environment has an anti-cooperative effect on the hydrogen bond, shifting electrons from the back of the ring to the front making the the cation a weaker hydrogen bond donor at C2. Results from the average NCI, difference density and average Mulliken charges support the conclusion that the

Tab. 4.3: Average Mulliken charges of the ring atoms in atomic units (e).

Atom	Polarised	Nonpolarised
C2	0.062	0.0854
H2	0.248	0.279
C4	-0.164	-0.104
H4	0.298	0.191
C5	-0.119	-0.091
H5	0.279	0.189
N1	-0.061	-0.050
N3	-0.063	-0.061

addition of the local environment to an ion-pair weakens the C2–H$\cdots$O hydrogen bond in [emim][$MeCO_2$]

4.4 Analysis of a Single Frame

The challenge of identifying the hydrogen bond in the gas-phase lead to an attempt to find it in the condensed phase. The condensed phase also gives a more physically reasonable description of the conformation that the ion-pairs would adopt when undergoing hydrogen bonding. The main challenge would be finding the hydrogen bond, which was attempted by specifying geometric criteria that is used to extract the ion-pairs. After the aRDG was plotted in real space and the visualisation of the superimposed images of the ion-pairs, it was evident that non-hydrogen bonding conformations were possibly produced, which overshadow the hydrogen bond surfaces with large surfaces and broad peaks. This forces the use of a single frame that represents a hydrogen bond for a single pair in a particular conformation at a point in the simulation. Although these pairs may not present themselves to statistical rigour, they can be used as an initial indicator of the behaviour of the hydrogen bond in the condensed phase (which must be considered anecdotal) and the effect of the local environment on its strength. For the first time in this report, a hydrogen bond for [emim][BF_4] and [emim][CF_3SO_3] is found.

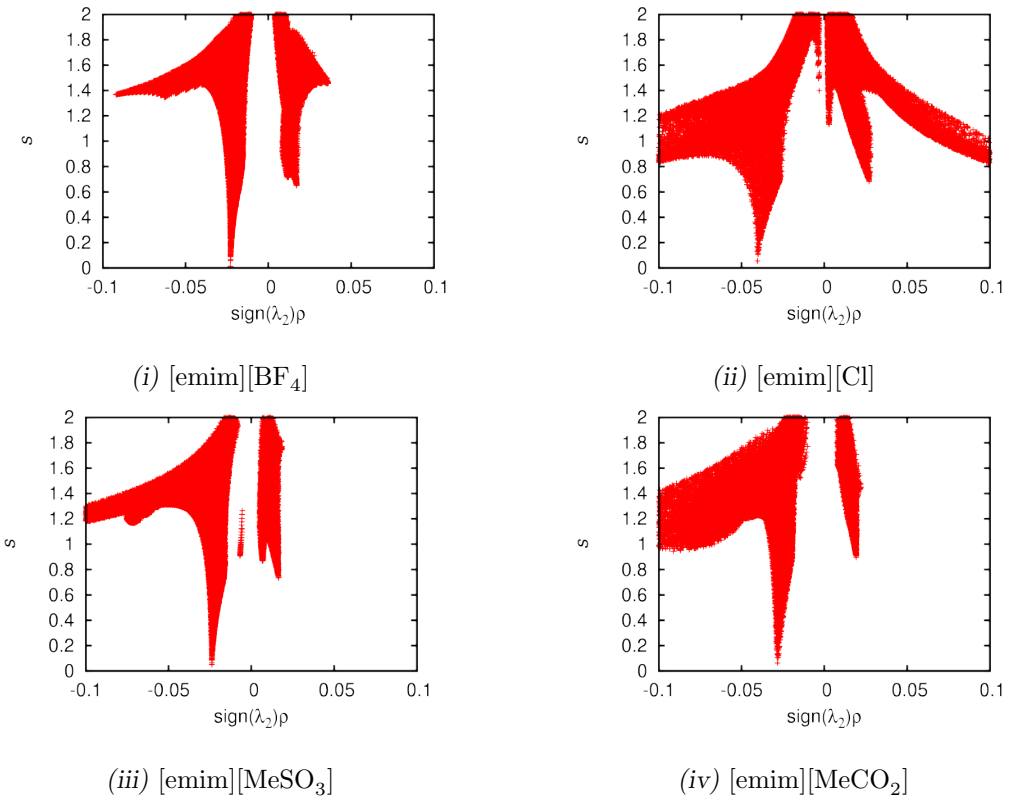

(i) [emim][BF_4] *(ii)* [emim][Cl]

(iii) [emim][$MeSO_3$] *(iv)* [emim][$MeCO_2$]

Fig. 4.8: Single frame NCI

The hydrogen bonding surfaces were isolated and NCI plots and surfaces were produces and shown in figures 4.8 and 4.9. The NCI plots share the same characteristics as those of the gas phase ion-pairs that undergo hydrogen bonding. There is a sharp peak in the attractive region, which corresponds to hydrogen bonding and a short repulsive peak. All hydrogen bonds are characterised by small pellet-shaped volumes between the hydrogen bond acceptor and H2. The positions of the peaks and the colours of the surfaces can be used as initial indicators of the strength of the hydrogen bond. [emim][Cl] forms the strongest hydrogen bond of all the pairs with its attractive peak being more to the left of the plot and having the surface coloured by a deeper shade of blue. [emim][BF_4] and [emim][CF_3SO_3] form the weakest hydrogen bonds.

The properties of the NCI surfaces, including the estimated potential (E) of the hydrogen bond, are shown in table 4.4. ρ_{rep} is 0 for all hydrogen bonds, consistent with the gas phase calculations where $\rho_{\text{rep}} \leq 0.19$ for all the ion-pairs, ρ_{bind} is thus solely dependent on ρ_{att}. $\overline{\rho}_{\text{bind}}$ is used to find E as good correlation between

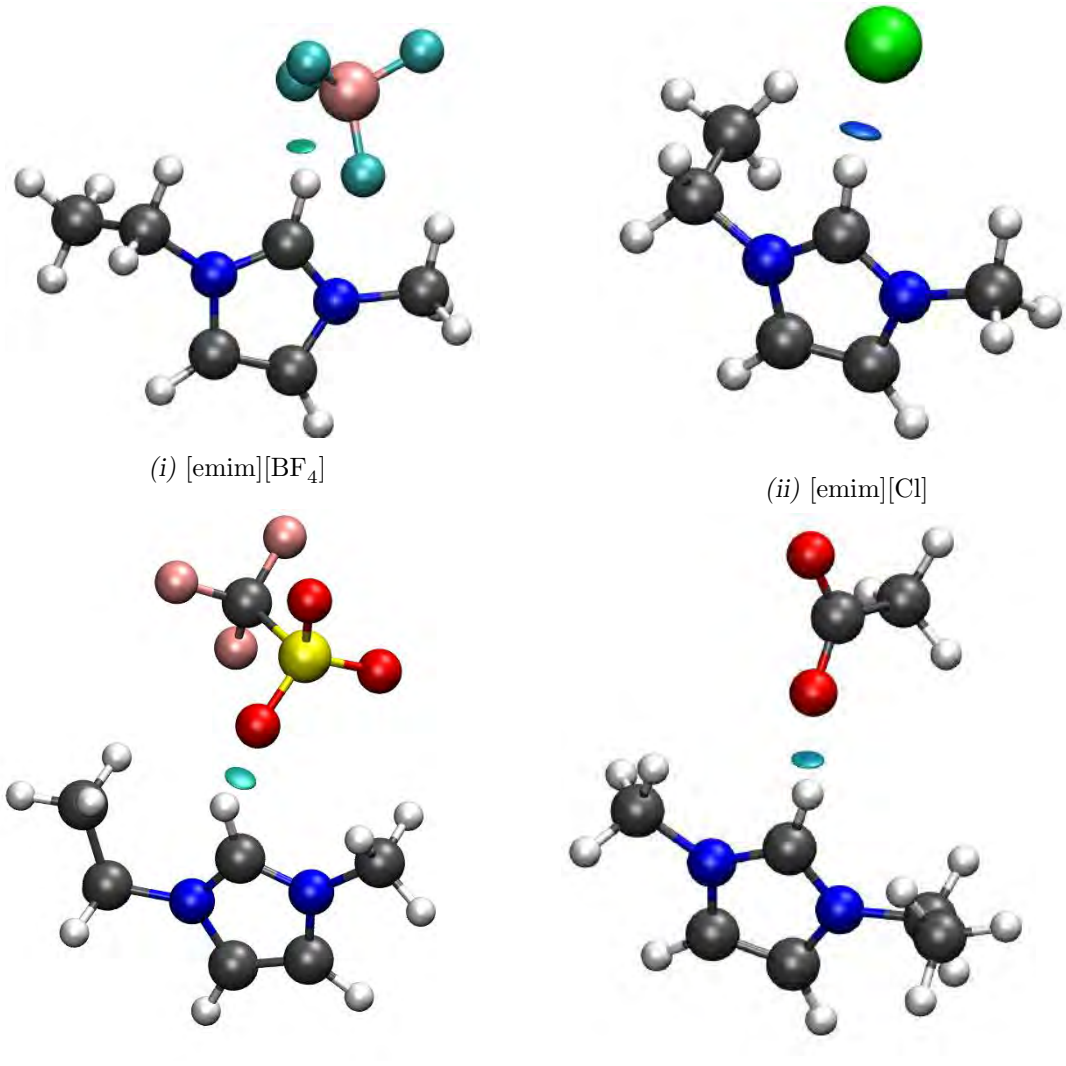

(i) [emim][BF_4] *(ii)* [emim][Cl]

(iii) [emim][$MeSO_3$] *(iv)* [emim][$MeCO_2$]

Fig. 4.9: RDG isosurface plotted in real space for hydrogen bonding conformers extracted from the condensed phase for one snapshot at an isovalue of 0.5.

these two quantities was found earlier (see section 3.6.2). The angles and distances reported are all within an acceptable geometric range for hydrogen bonding, all distances are less than or equal to 2 Å and the angle furthest from linearity is [emim][CF_3SO_3] at 147.92°. The inclusion of the polarising environment leads to a slight decrease in hydrogen bond strength for all hydrogen bonds.

[emim][Cl] has the strongest hydrogen bond whether the polarised environment is included (-12.00 kcal $\cdot$ mol^{-1}) or not (12.62 kcal $\cdot$ mol^{-1}). The hydrogen bond is as strong in the condensed phase conformation as it is in the gas phase. The hydrogen bond distance is approximately the same for both gas phase and con-

Tab. 4.4: NCI Properties of the ion-pairs where ρ_{att}, ρ_{rep}, ρ_{bind} and $\overline{\rho}_{\text{bind}}$ are in atomic units ($\frac{\text{e}}{\text{a}_0^3}$) and the estimated potential (E) is in kcal $\cdot$ mol^{-1}

Complex	ρ_{att}	ρ_{rep}	ρ_{bind}	Distance	Angle	$\overline{\rho}_{\text{bind}}$	E
[emim][BF_4](**pol**)	-14.31	0.0	-14.31	1.93	157.76	-0.02168	-5.28
[emim][BF_4](**nopol**)	-14.45	0.0	-14.45	1.93	157.76	-0.02183	-5.34
[emim][Cl](**pol**)	-9.31	0.0	-9.31	2.00	164.72	-0.03756	-12.00
[emim][Cl](**nopol**)	-10.69	0.0	-10.69	2.00	164.72	-0.03903	-12.62
[emim][CF_3SO_3](**pol**)	-18.23	0.0	-18.23	1.98	147.92	-0.02193	-5.39
[emim][CF_3SO_3](**nopol)**	-19.88	0.0	-19.87	1.98	147.92	-0.02259	-5.66
[emim][$MeCO_2$](**pol**)	-9.38	0.0	-9.38	1.98	166.93	-0.02759	-7.78
[emim][$MeCO_2$](**nopol**)	-27.19	0.0	-27.19	1.98	166.93	-0.02806	-7.98

The estimated potential of the hydrogen bond is determined by using the equation of the line of best fit that was obtained through a correlation between $\overline{\rho}_{\text{bind}}$ and the potential energy density at the bond critical point. $\text{E} = 423.01\text{kcal}\cdot\text{mol}^{-1}a_0^3\text{e}^{-1} \times \overline{\rho}_{\text{bind}} + 3.89\text{kcal}\cdot\text{mol}^{-1}$

densed phase but the angle of the latter is more linear, thus the hydrogen bond interaction is maximised in this particular snapshot. The hydrogen bond strength of [emim][$MeCO_2$] more than half that of the gas phase with the greater distance of 0.2 Å but a more linear angle. This is a more dramatic decrease in strength than that shown for [emim][Cl], which suggests that $[MeCO_2]^-$ is more prone to secondary interactions in the condensed phase, weakening the hydrogen bond. [emim][BF_4] and [emim][CF_3SO_3] have relatively weak hydrogen bonds at $\approx -5\text{kcal}\cdot\text{mol}^{-1}$. These hydrogen bonds are weaker than all other hydrogen bonds found in both the gas phase and the condensed phase and would probably be weaker if averages were taken.

4.5 Conclusion

Ion-pairs are extracted from the condensed phase to obtain hydrogen bonding conformers of the ILs $[MeCO_2]^-$, $[CF_3SO_3]^-$, Cl^- and $[BF_4]^-$. ONIOM calculations are performed and the QM region is optimised keeping the MM layer fixed. The average reduced density gradient (aRDG) is then calculated and shown in real space. It was shown that only the aRDG of $[MeCO_2]^-$ result in an average localised hydrogen bonding surface whilst the other ion-pairs have their hydrogen bond surfaces masked by large dispersion surfaces. The average hydrogen bond strength is calculated for $[MeCO_2]^-$ and it was found that the hydrogen bond is approximately 3 times weaker in the condensed phase than in the gas phase. A single snapshot of the remaining ion-pairs undergoing hydrogen bonding were found in order to calculate the RDG. This gives anecdotal evidence of hydrogen bond strength in the condensed phase. Chloride forms the strongest hydrogen bond, approximately the same as it is in the gas phase. The hydrogen bond strength of $[CF_3SO_3]^-$ and $[BF_4]^-$ are close in value and form the weakest hydrogen bond of all ion-pairs, approximately the same strength as bromide in the **B2** conformer. The effect of polarisation on the hydrogen bond decrease its strength slightly. It was found that the polarising environment shifts the electron density from the back of the ring toward C2 and H2.

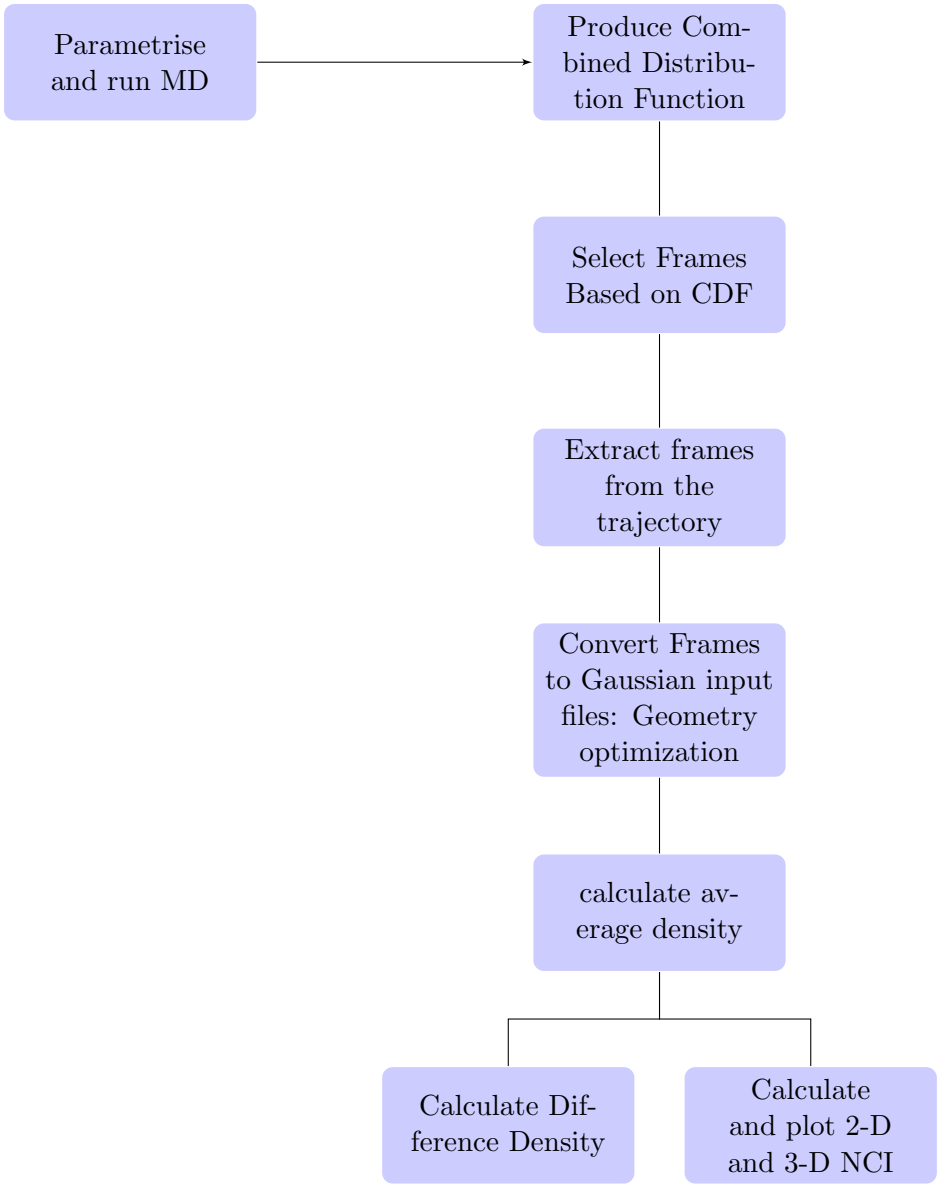

Fig. 4.10: The procedure of generating average NCIs

Bibliography

[1] Wu, P.; Chaudret, R.; Hu, X.; Yang, W. *J. Chem. Theory Comput.* **2013**, *9*, 2226–2234.

[2] Berendsen, H. J. C.; Postma, J. P. M.; van Gunsteren, W. F.; DiNola, A.; Haak, J. R. *J. Chem. Phys.* **1984**, *81*, 3684–3690.

[3] Smith, W.; Forester, T. *J. Mol. Graphics* **1996**, *14*, 136–141.

[4] Ngo, H. L.; LeCompte, K.; Hargens, L.; McEwen, A. B. *Thermochim. Acta* **2000**, *357358*, 97–102.

[5] Zhang, S.; Sun, N.; He, X.; Lu, X.; Zhang, X. *J. Phys. Chem. Ref. Data* **2006**, *35*, 1475–1517.

[6] Martínez, L.; Andrade, R.; Birgin, E. G.; Martínez, J. M. *J. Comp. Chem* **2009**, *30*, 2157–2164.

[7] Ryckaert, J.-P.; Ciccotti, G.; Berendsen, H. J. *J. Comp. Phys.* **1977**, *23*, 327–341.

[8] Darden, T.; York, D.; Pedersen, L. *J. Chem.l Phys.* **1993**, *98*, 10089–10092.

[9] Svensson, M.; Humbel, S.; Froese, R. D. J.; Matsubara, T.; Sieber, S.; Morokuma, K. *J. Phys. Chem.* **1996**, *100*, 19357–19363.

[10] Katsyuba, S. A.; Vener, M. V.; Zvereva, E. E.; Fei, Z.; Scopelliti, R.; Laurenczy, G.; Yan, N.; Paunescu, E.; Dyson, P. J. *J. Phys. Chem. B.* **2013**, *117*, 9094–9105.

5

Closing Remarks

The nature of the interactions has been studied in both the gas phase and the condensed phase. All interaction types were not studied (e.g. polarisation, induction and exchange was not explicitly quantified), but the most important component with respect to the ion-pair have been determined. A SAPT analysis would be ideal but was not possible over the course of the investigation. An advantage of the methods utilised is that they calculate the interaction types explicitly and allow us to critique the methods. For future work the following must be done:

- calculate the exchange energy to determine the repulsive contribution to the total interaction energy,
- calculate the polarisation energy to quantify its contribution to the total interaction energy,
- calculate the NBO stabilisation energies for extracted pairs to determine the presence of the hydrogen bond, which is relatively cheap calculation with respect to the geometry optimisation,
- recalculate the average reduced density gradient from the frames where NBO has determined the presence of the hydrogen bond,
- test the potential energy density as hydrogen bond strength indicator and
- calculate the interaction types in the condensed phase and compare to the gas phase interactions.